DEVICE PHYSICS FOR ENGINEERING DESIGN OF HEAVILY DOPED REGIONS IN PN-JUNCTION SILICON SOLAR CELLS

By

MUHAMMED AYMAN SHIBIB

A DISSERTATION PRESENTED TO THE GRADUATE COUNCIL OF
THE UNIVERSITY OF FLORIDA
IN PARTIAL FULFILLMENT OF THE REQUIREMENTS FOR THE
DEGREE OF DOCTOR OF PHILOSOPHY

UNIVERSITY OF FLORIDA

1979

To My Parents:

Subhi and Loutfieh Shibib

ACKNOWLEDGMENTS

I am indebted to my family for their encouragement and parental support that helped me pursue my graduate studies.

I want to express my deep appreciation to the chairman of my supervisory committee, Professor Fredrik A. Lindholm, for his guidance, encouragement, and support. His research insight and excellent tutoring in physical electronics have been invaluable for developing and guiding my research interests.

I extend my gratitude to Professor Jerry G. Fossum, the co-chairman of my supervisory committee, for guiding the development of this research and contributing significantly to its completion.

Thanks are due to Professor Arnost Neugroschel and Sheng S. Li for helpful discussions and for their participation on my committee. I am also grateful to Professor Charles F. Hooper, Jr., for serving on my committee.

Helpful discussions in solid-state physics with the late Thomas A. Scott, Professor of Physics, are most appreciated.

I thank professors Allan H. Marshak and H. P. D. Lanyon for their helpful comments.

The support of NASA and DOE is gratefully acknowledged.

I also thank my typist Sofia Kohli for her excellent work.

TABLE OF CONTENTS

		Page
ACKNOWLEDGMENTS		iii
ABSTRACT		vii
CHAPTER		
I.	INTRODUCTION	1
II.	AUGER RECOMBINATION IN HEAVILY DOPED SHALLOW-EMITTER SILICON PN-JUNCTION SOLAR CELLS, DIODES, AND TRANSISTORS	10
	2.1 Introduction	10
	2.2 Derivation	11
	2.3 Discussion	15
	2.4 Conclusion	20
III.	RECOMBINATION THROUGH DEFECTS IN HEAVILY DOPED SHALLOW-EMITTER SILICON PN-JUNCTION DEVICES	23
	3.1 Introduction	23
	3.2 Importance of Surface Recombination	24
	3.3 Shockley-Read-Hall Recombination via Defects	25
	3.4 The Excess Minority-Carrier Charge Storage in Heavily Doped Regions	30
IV.	ON THE DEIONIZATION OF IMPURITIES AS AN EXPLANATION FOR EXCESS INTRINSIC CARRIER DENSITY IN HEAVILY DOPED SILICON	34
V.	HEAVILY DOPED TRANSPARENT-EMITTER REGIONS IN SILICON JUNCTION SOLAR CELLS, DIODES, AND TRANSISTORS	44
	5.1 Introduction	44
	5.2 Derivation	46
	5.3 Heavy Doping Effects	49
	5.4 Discussion	54

TABLE OF CONTENTS--Continued

CHAPTER		Page
	5.5 Application to pn-Junction Silicon Solar Cells	60
	5.6 Perspective	68
VI.	A FIRST-ORDER ENGINEERING-DESIGN MODEL FOR HEAVILY DOPED SILICON DEVICES	70
	6.1 Introduction	70
	6.2 Modeling Approach	71
	6.3 Development of the Model	74
	6.4 Relating Device Design Parameters to the First-Order Model's Parameters	75
	6.5 Verification of First-Order Model by Computer Analysis	76
	6.6 Experimental Support	89
	6.7 Summary and Conclusions	89
VII.	COMPUTER-AIDED STUDY OF V_{OC} IN N^+P AND P^+N SILICON SOLAR CELLS	91
	7.1 Introduction	91
	7.2 Dependence of V_{OC} on the Emitter Design Parameters N^+P and P^+N Silicon Solar Cells	91
	7.2A Dependence of V_{OC} on W_E	92
	7.2B Dependence of V_{OC} on N_S	102
	7.2C Dependence of V_{OC} on S	102
	7.3 Discussion	109
	7.4 Experimental Support	112
	7.5 Conclusions	112
VIII.	SUMMARY, CONCLUSIONS, AND RECOMMENDATIONS	114
	8.1 Summary	114
	8.2 Accomplishments	116
	8.3 Scope and Limitations	118
	8.4 Recommendations for Future Research	119
APPENDICES		
A.	EXTENSION OF SHOCKLEY'S AUXILIARY RELATIONS FOR HEAVILY DOPED PN-JUNCTION DEVICES	124

TABLE OF CONTENTS--Continued

APPENDICES

Page

B. QUASI-ELECTRIC FIELDS IN HEAVILY DOPED SEMICONDUCTORS 135

C. INCLUSION OF DEGENERACY IN THE ANALYSIS OF HEAVILY DOPED SEMICONDUCTOR DEVICES 138

D. LISTING OF THE COMPUTER PROGRAM 146

E. CHARACTERIZATION OF THE EMITTER CURRENT IN HEAVILY DOPED SILICON DEVICES BY COMPUTER-AIDED NUMERICAL ANALYSIS 165

F. ON THE PARABOLIC DENSITY OF STATES IN HEAVILY DOPED SILICON 183

REFERENCES 185

BIOGRAPHICAL SKETCH 193

Abstract of Dissertation Presented to the Graduate Council of the University of Florida in Partial Fulfillment of the Requirements for the Degree of Doctor of Philosophy

DEVICE PHYSICS FOR ENGINEERING DESIGN OF HEAVILY DOPED REGIONS IN PN-JUNCTION SILICON SOLAR CELLS

By

Muhammed Ayman Shibib

December 1979

Chairman: Fredrik A. Lindholm
Co-Chairman: Jerry G. Fossum
Major Department: Electrical Engineering

This dissertation presents a quantitative study of the physical mechanisms underlying the anomolously large recombination current experimentally observed in heavily doped regions of silicon pn-junction solar cells and bipolar transistors. The study includes a comparison of theoretical predictions with a variety of experimental observations in heavily doped silicon and silicon devices.

A major conclusion is that the simplest physical model that adequately describes the heavily doped regions must include Fermi-Dirac statistics, a phenomenological excess intrinsic carrier density (or deficit impurity concentration), Auger recombination in the bulk, and recombination at the surface. These mechanisms are incorporated in a first-order model useful in the design of silicon pn-junction solar cells. The accuracy of the first-order model is supported by comparing its results with the results of more detailed models and of a numerical

analysis of the problem. Experimental data are presented that are consistent with the predictions of the first-order model and of the numerical solution.

CHAPTER I

INTRODUCTION

Heavily doped regions of silicon pn-junction devices show experimentally a larger recombination current than is predicted by classical pn-junction theory [1,2]. This large recombination current in heavily doped regions is responsible for the low values of the open-circuit voltage V_{OC} of silicon solar cells [3] and the common-emitter current gain h_{FE} in silicon bipolar transistors [4,5].

The main objective of this dissertation is to study quantitatively large recombination currents in heavily doped regions and to describe the fundamental limitations imposed by heavy doping on the performance of silicon pn-junction solar cells and bipolar transistors. The achievement of this objective involves:

A. Identifying physical mechanisms associated with heavy doping.

B. Determining the dominant heavy-doping mechanisms that affect the device performance.

C. Including the dominant heavy-doping mechanisms in analytic and computer-aided analysis of heavily doped regions in silicon devices.

D. Establishing accurate and simple first-order engineering design models based on device physics.

From charge-control theory [6-10], the recombination current in any heavily doped region, for example, the minority-carrier emitter current J_E, can be expressed by

$$J_E = \frac{Q_E}{\tau_E} \tag{1.1}$$

where Q_E is the minority-carrier charge storage and τ_E is the effective lifetime in the emitter. From classical pn-junction theory [11], Q_E increases with decreasing bandgap and decreases with increasing majority carrier density. The effective lifetime τ_E may be the average bulk lifetime of the minority carriers or their transit time, defined as the average time needed by a minority carrier to cross the semiconductor region without recombining in the bulk, or a combination of the two. From (1.1) we can see that an excessive emitter current is due to (a) a large minority-carrier charge, (b) a short effective lifetime, and (c) a combination of (a) and (b).

Various physical mechanisms associated with heavy doping in semiconductors can give rise to (a), (b), or (c). These heavy-doping mechanisms are outlined, in Table I, and contrasted to corresponding mechanisms in lightly doped semiconductors. We will describe briefly some of the fundamental heavy-doping mechanisms outlined in Table I.

One of the fundamental heavy-doping mechanisms that yields a large minority-carrier charge, and consequently a large current by (1.1), is energy-bandgap narrowing. From a theoretical standpoint, various mechanisms exist that lead to bandgap narrowing [12-19]. Moreover, electrical measurements in heavily doped single-crystal silicon

TABLE I

COMPARISON BETWEEN A LOW IMPURITY CONCENTRATION SEMICONDUCTOR (LESS THAN $\simeq 10^{16}/CM^3$) AND A HIGH IMPURITY CONCENTRATION SEMICONDUCTOR (MORE THAN $\simeq 10^{18}/CM^3$)

Low Impurity Concentration	High Impurity Concentration
Effective bandgap = Intrinsic bandgap $(\Delta E_G = 0)$	Effective bandgap < Intrinsic bandgap $(\Delta E_G \neq 0)$
Maxwell-Boltzmann statistics for the majority and minority carriers	Maxwell-Boltzmann statistics for minority carriers; Fermi-Dirac statistics for majority carriers
Simple Law of Mass Action valid $P_0 N_0 = n_i^2(T)$	Generalized Law of Mass Action $P_0 N_0 = n_{ie}^2(T,x)$
All impurity atoms ionized (at room temperature)	Some impurity atoms deionized (at room temperature)
μ_N, μ_P, D_P and D_N constant (independent of impurity concentration)	μ_N, μ_P, D_P and D_N dependent on impurity concentration
Einstein's relation valid $\frac{D}{\mu} = \frac{kT}{q}$	Einstein's relation not valid; modified relation: $\frac{D}{\mu} = \frac{kT}{q} \cdot \frac{F_{1/2}(\eta)}{F_{-1/2}(\eta)}$
Built-in electric field in QNR is same for majority and minority carriers $E_{maj} = E_{min}$	Effective drift field in QNR is not same for majority and minority carriers $E_{maj} \neq E_{min}$

TABLE I--Continued

Low Impurity Concentration	High Impurity Concentration
Recombination of excess minority carriers via defects, (Shockley-Read-Hall)	Recombination of excess minority carriers via (a) fundamental band-to-band Auger process, (b) position-dependent recombination centers or defects (Shockley-Read-Hall)

materials and devices indicate that the forbidden energy gap may be smaller than the intrinsic energy gap of pure silicon. These experimental measurements are:

A. Measurements of the temperature dependence of the current gain in silicon bipolar transistors [4,5]

B. Measurements of the collector current and its temperature dependence in silicon bipolar transistors [20]

C. Measurements of the temperature dependence of the photoresponse of silicon pn-junctions and transistors [21]

D. Measurements of the temperature dependence of the emitter current in silicon solar cells (in the dark condition) and bipolar transistors [22]

E. Measurements of the emitter current in different pn-junction structures [23]

Rather than providing a direct measurement of the bandgap, the above measurements yield an excess effective intrinsic carrier density n_{ie}^2, defined as the thermal equilibrium pn-product in heavily doped silicon [24]. The measured values of n_{ie}^2 are considerably larger than n_i^2 for pure silicon.

Another mechanism that can provide an excess intrinsic carrier density, and a large minority-carrier charge in the heavily doped region, is deionization of impurities at high doping concentrations [25]. For low concentrations of shallow impurities in silicon at room temperature, all impurity atoms are essentially ionized. This is so

because the Fermi level is well below the impurity levels. As the impurity concentration increases (above 10^{16} cm^{-3}) some deionization of impurities occur. The degree of ionization of impurity atoms depends on the density and position of localized energy levels in the bandgap and on the position of the Fermi level relative to these levels.

Another fundamental heavy-doping mechanism that must be considered is the degeneracy of the majority carriers in heavily doped semiconductors. Majority-carrier concentrations in heavily doped semiconductors are high enough that the carriers can interact with each other via the Pauli Exclusion Principle. Thus Maxwell-Boltzmann statistics are no longer applicable and Fermi-Dirac statistics must be used instead.

We consider now two other fundamental heavy-doping mechanisms that can increase J_E in (1.1) by decreasing τ_E. The first mechanism is Auger band-to-band recombination [26]. It is fundamental in the sense that it sets an upper bound on the minority-carrier lifetimes in these regions. The second mechanism is Schockley-Read-Hall recombination [27-28] via position-dependent defect densities.

We have discussed the fundamental heavy-doping mechanisms that can limit the performance of heavily doped silicon pn-junction devices such as solar cells and bipolar transistors. We outline now our approach in assessing the relative importance of these heavy-doping mechanisms to the performance of silicon devices.

Our approach in assessing the importance of heavy-doping effects is to include each of these effects separately in a simple yet

accurate model for the heavily doped region. We first include Auger recombination alone, neglecting other heavy-doping effects, in a rigorous analytic model for the emitter region of silicon solar cells and bipolar transistors. The model includes also a finite surface recombination velocity at the emitter surface. We find, in Chapter II, that values of V_{OC} in silicon solar cells, predicted by this model, are considerably higher than those experimentally observed. So Auger recombination is not the dominant mechanism that yields the large emitter current in bipolar devices.

Next, we consider recombination via defects, in Chapter III. Using a previous detailed study of defect recombination [9], we argue that if recombination via defects is the main mechanism underlying the large emitter current, then surface recombination should not influence the device performance. This implication is inconsistent with recent experimental data [29] showing the sensitivity of V_{OC} in typical silicon solar cells to surface treatment. These experimental data emphasize the importance of surface recombination and an excess intrinsic carrier density in heavily doped silicon (i.e., $n_{ie}^2 > n_i^2$).

The importance of deionization in heavily doped silicon is assessed in Chapter IV. We investigate whether deionization can be the main mechanism underlying the experimentally observed effective intrinsic carrier density in heavily doped silicon. By using a variety of experimental data, we infer that deionization in heavily doped silicon at room temperature is not an important mechanism, at least not in accordance with the recent models of Popovic and Heasell.

Having established the important fundamental heavy-doping mechanisms, we proceed to develop engineering design models for heavily doped regions.

Energy-bandgap narrowing, Fermi-Dirac statistics, and a finite surface recombination velocity are included in a rigorous analytic model of the heavily doped emitter of silicon devices in Chapter V. The emitter is assumed to be transparent to the injected minority carriers, that is, most of the injected minority carriers can cross the quasi-neutral emitter region and recombine mainly at the surface rather than in the bulk. The transparency assumption can be tested for self-consistency for any given device. We show, in Chapter V, that the transparent emitter model can explain the experimentally observed values of V_{OC} in silicon solar cells if the surface recombination velocity is high and energy-bandgap narrowing and Fermi-Dirac statistics are included. In agreement with other experimental data, we also show that reducing the front surface recombination velocity increases V_{OC} in silicon solar cells.

In Chapter VI, we develop a simple first-order model for the emitter that includes energy-bandgap narrowing, Fermi-Dirac statistics, Auger recombination, and a finite surface recombination velocity. The first-order model is useful as a design tool particularly for silicon solar cells. The accuracy of the model is checked by a rigorous computer-aided numerical analysis of the problem. The model is found to be accurate if the surface impurity concentration is less than 4×10^{20} cm^{-3}.

To compare the limitations imposed by heavy doping on N^+P and P^+N cells, we present, in Chapter VII, the results of a quantitative parametric study of the dependence of V_{OC} in N^+P and P^+N silicon solar cells. These design parameters considered are the surface impurity concentration, the width of the quasi-neutral emitter region, and the emitter surface recombination velocity. We show, based on our computer-aided analysis, that it is more beneficial to have a P^+ emitter than an N^+ emitter to achieve large V_{OC} in silicon solar cells.

Finally, we summarize our studies and review the main conclusions and accomplishments of this dissertation in Chapter VIII. We also discuss the scope and limitations of this work and provide suggestions for future research.

CHAPTER II

AUGER RECOMBINATION IN HEAVILY DOPED SHALLOW-EMITTER SILICON PN-JUNCTION SOLAR CELLS, DIODES, AND TRANSISTORS

2.1 Introduction

Because the recombination current occurring in the quasi-neutral emitter can limit the current gain of silicon junction transistors and the open-circuit voltage of pn-junction silicon solar cells, the physical origin of this current is of interest. In an attempt to develop a simple physical model that is consistent with experimental data, a recent study [30] asserted that the inclusion of Auger recombination in the heavily doped regions of the emitter is alone sufficient to explain the data, and that it is unnecessary to include the heavy-doping effect of bandgap narrowing [19]. This conclusion is questionable since Auger recombination was accounted for qualitatively in the study [30], rather than by a rigorous quantitative treatment.

To remove this uncertainty, we present in this chapter a rigorous analytic evaluation of a model for the emitter region that includes Auger recombination but excludes bandgap narrowing and degeneracy of the charge carriers. We show that for silicon pn-junction solar cells this model cannot explain the experimentally observed values of V_{OC} [3,31] and the observed dependence of V_{OC}

on surface treatment [29]. It follows that for bipolar transistors, the model cannot explain the measured values of the common-emitter current gain. Inclusion of Fermi-Dirac statistics would worsen the discrepancy between theory and experiment. Our conclusions are contrary to the assertions of [30] but are consistent with previous numerical treatments of the problem [32-35]. Our analysis, therefore, reinforces the importance of bandgap narrowing in silicon devices.

2.2 Derivation

We consider an N-type, heavily doped, inhomogeneous emitter region having a Gaussian net impurity profile:

$$N_{DD}(x) = N_S \exp\left[-\left(\frac{W_E - x}{2L}\right)^2\right] \tag{2.1}$$

where N_S is the surface impurity concentration and W_E is the width of the quasi-neutral emitter region in thermal equilibrium. The Auger recombination lifetime (assuming full ionization of impurity atoms) is

$$\tau_A(x) = \frac{1}{C_A N_{DD}^2(x)} \tag{2.2}$$

where C_A is the Auger coefficient [36]. The relationships (2.1) and (2.2) are used in the hole continuity equation (for the dark condition),

$$-\frac{1}{q}\frac{dJ_p(x)}{dx} = \frac{\Delta P(x)}{\tau_A(x)} \tag{2.3}$$

where ΔP is the excess hole density. If we let

$$y(x) = N_{DD}(x) \cdot \Delta P(x) \tag{2.4}$$

and use the general expression for the hole current density, including both drift and diffusion components, then, for the usual low-injection conditions, (2.3) becomes

$$\frac{d^2y}{dx^2} - \left[\frac{W_E - x}{2L^2}\right]\frac{dy}{dx} - \frac{\exp\left[2\left(\frac{W_E - x}{2L}\right)^2\right]}{L_A^2}\, y = 0 \tag{2.5}$$

where

$$L_A^2 \equiv \frac{D_P}{C_A N_S^2} \tag{2.6}$$

is the square of the hole diffusion length at the emitter surface. In (2.6), D_P is an average value for the hole diffusion coefficient in the emitter. The solution of the differential equation (2.5) is similar to that given in [37]:

$$y = A \sinh\left[\frac{\sqrt{\pi}\, L}{L_A} \operatorname{erf}\left(\frac{W_E - x}{2L}\right)\right] + B \cosh\left[\frac{\sqrt{\pi}\, L}{L_A} \operatorname{erf}\left(\frac{W_E - x}{2L}\right)\right] \tag{2.7}$$

The coefficients A and B are determined by the boundary conditions [11],

$$\Delta P(0) = \frac{n_i^2}{N_{DD}(0)}\left[\exp\left(\frac{qV}{kT}\right) - 1\right] \tag{2.8}$$

and

$$J_P(W_E) = q \cdot S_P \cdot \Delta P(W_E) \tag{2.9}$$

In (2.9), S_p is the hole recombination velocity at the emitter surface.

The minority-carrier current can be written (for low-level injection) as

$$J_p(x) = - \frac{qD_p}{N_{DD}(x)} \cdot \frac{dy}{dx} \tag{2.10}$$

Substitution of the expressions obtained for A and B into (2.10) yields the following expression for the emitter saturation current density:

$$J_{PO} = \frac{q D_p n_i^2}{N_S L_A} \frac{\cosh\left[\frac{\sqrt{\pi}\, L}{L_A} \operatorname{erf}\left(\frac{W_E}{2L}\right)\right] + (D_p/S_p L_A) \sinh\left[\frac{\sqrt{\pi}\, L}{L_A} \operatorname{erf}\left(\frac{W_E}{2L}\right)\right]}{\sinh\left[\frac{\sqrt{\pi}\, L}{L_A} \operatorname{erf}\left(\frac{W_E}{2L}\right)\right] + (D_p/S_p L_A) \cosh\left[\frac{\sqrt{\pi}\, L}{L_A} \operatorname{erf}\left(\frac{W_E}{2L}\right)\right]} \tag{2.11}$$

Equation (2.11) reduces to:

$$J_{PO} = \frac{q D_p n_i^2}{N_S L_A} \cdot \coth\left[\frac{\sqrt{\pi}\, L}{L_A} \operatorname{erf}\left(\frac{W_E}{2L}\right)\right] \tag{2.12}$$

as $S_p \longrightarrow \infty$, and to the familiar expression:

$$J_{PO} = \frac{q D_p n_i^2}{N_S L_A} \cdot \coth\left(\frac{W_E}{L_A}\right) \tag{2.13}$$

as $S_p \longrightarrow \infty$ and $L \longrightarrow \infty$ ($L \longrightarrow \infty$ corresponds to a flat impurity profile with $N_{DD}(x) = N_S$).

With the charge-control relation,

$$J_p(0) \equiv \frac{Q_p}{\bar{\tau}_p} \tag{2.14}$$

we can evaluate $\bar{\tau}_p$, the effective hole lifetime in the emitter. The charge storage in the emitter is

$$Q_p = q \int_0^{W_E} \Delta P(x)\, dx \tag{2.15}$$

The contribution to $J_p(0)$ due to surface recombination, J_{PS}, and due to Auger recombination, J_{PA}, can be determined by integrating (2.3) over the quasi-neutral emitter region:

$$J_p(0) = J_p(W_E) + q \int_0^{W_E} \frac{\Delta P(x)}{\tau_A(x)}\, dx \tag{2.16}$$

$$= J_{PS} + J_{PA}$$

Using the mean-value theorem, we can write

$$q \int_0^{W_E} \frac{\Delta P(x)}{\tau_A(x)}\, dx = \frac{Q_p}{\bar{\tau}_A} \tag{2.17}$$

Thus, from (2.14), (2.16), and (2.17), we obtain

$$\frac{1}{\bar{\tau}_p} = \frac{1}{\bar{\tau}_A} + \frac{1}{\tau_t} \tag{2.18}$$

where

$$\tau_t \equiv \frac{Q_P}{J_{PS}} \tag{2.19}$$

defines the hole transit time, the average time required for a hole to cross the quasi-neutral emitter region and recombine at the surface. In the limiting case of negligible bulk recombination ($\overline{\tau}_A \longrightarrow \infty$), $\overline{\tau}_P$ is equal to τ_t.

To summarize the analysis, we have obtained a closed-form solution of the continuity equation, and have derived an expression for the hole current density when Auger recombination is the dominant bulk recombination mechanism in a heavily doped N-type emitter. Bandgap narrowing and Fermi-Dirac statistics have not been included. The surface and Auger components of the emitter recombination current and the associated hole transport parameters in the emitter can be easily obtained form (2.14), (2.15), (2.16), (2.17), and (2.19).

2.3 Discussion

The preceding development is then an analytic treatment of the minority-carrier transport in the emitter of pn-junction devices for the case in which Auger recombination is included but bandgap narrowing is neglected. In this treatment a Gaussian impurity profile is assumed, and a finite surface recombination velocity S_p is included. Inclusion of a finite S_p is particularly important for solar cells [29].

To illustrate quantitative results of this model, we apply it to an N^+P silicon solar cell with a base doping density

$N_{AA} = 5 \times 10^{17}\ cm^{-3}$. We let $N_S = 10^{20}\ cm^{-3}$ and $W_E = 0.25\ \mu m$. The electron diffusion length L_n in the base is assumed to be $\simeq 80\ \mu m$, consistent with experimental data [1]. In Figure 2-1, we plot J_{PO} and its two components, J_{PSO} and J_{PAO}, as functions of S_p. For low values of S_p (about 10^3 cm/sec), $J_{PSO} << J_{PAO}$. For the high values of S_p (above 10^6 cm/sec) $J_{PSO} \simeq 2J_{PAO}$. As Figure 2-1 shows, the two components of J_{PO} are equal when $S_p \simeq 10^5$ cm/sec. When the emitter current is due mainly to Auger recombination ($S_p \simeq 10^3$ cm/sec or lower), for an assumed short-circuit-current density of 23 mA/cm^2 [1], we get $V_{OC} \simeq 680$ mV. This voltage disagrees markedly with the corresponding maximum observed V_{OC} of 610 mV. The disagreement corresponds to a discrepancy in J_{PO} of about a factor of 15.

We consider now the variations of J_{PO} as a function of W_E, with N_S fixed at $10^{20}\ cm^{-3}$. In Figure 2-2, we plot J_{PO} versus W_E for $S_p = 10^2$ cm/sec and $S_p = 10^8$ cm/sec. The figure shows the dominance of bulk Auger recombination for large W_E, independent of the value of S_p, and the dominance of surface recombination for small W_E and large S_p. For low values of S_p ($S_p = 10^2$ cm/sec in Figure 2-2) the emitter current is due mainly to Auger recombination ($J_{PO} \simeq J_{PAO}$) and it decreases slightly for small W_E. The largest value of the Auger recombination current is about 3×10^{-14} A/cm^2, corresponding to $V_{OC} \simeq 680$ mV. Again, this voltage disagrees appreciably with the 610 mV value that is observed experimentally.

The dominance of the surface recombination is emphasized in Figure 2-3, where we let $S_p = 10^8$ cm/sec and plot the resulting

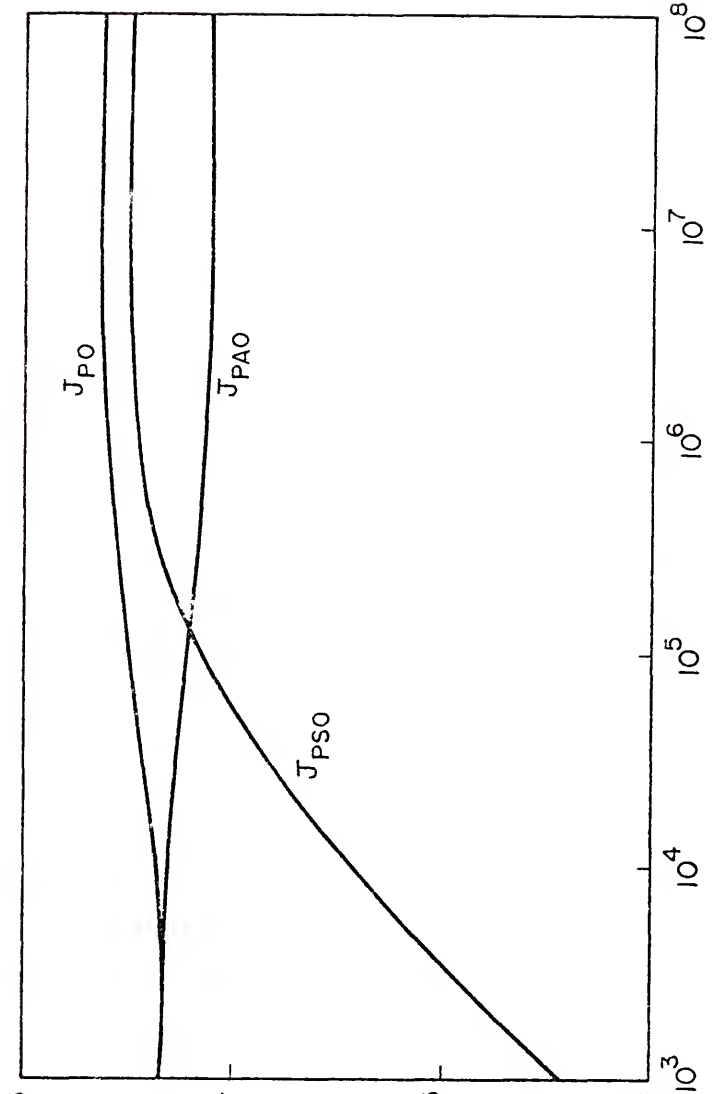

Figure 2.1 The emitter saturation current J_{PO} and its surface-recombination component J_{PSO} and Auger-recombination component J_{PAO} versus the surface recombination velocity S_P

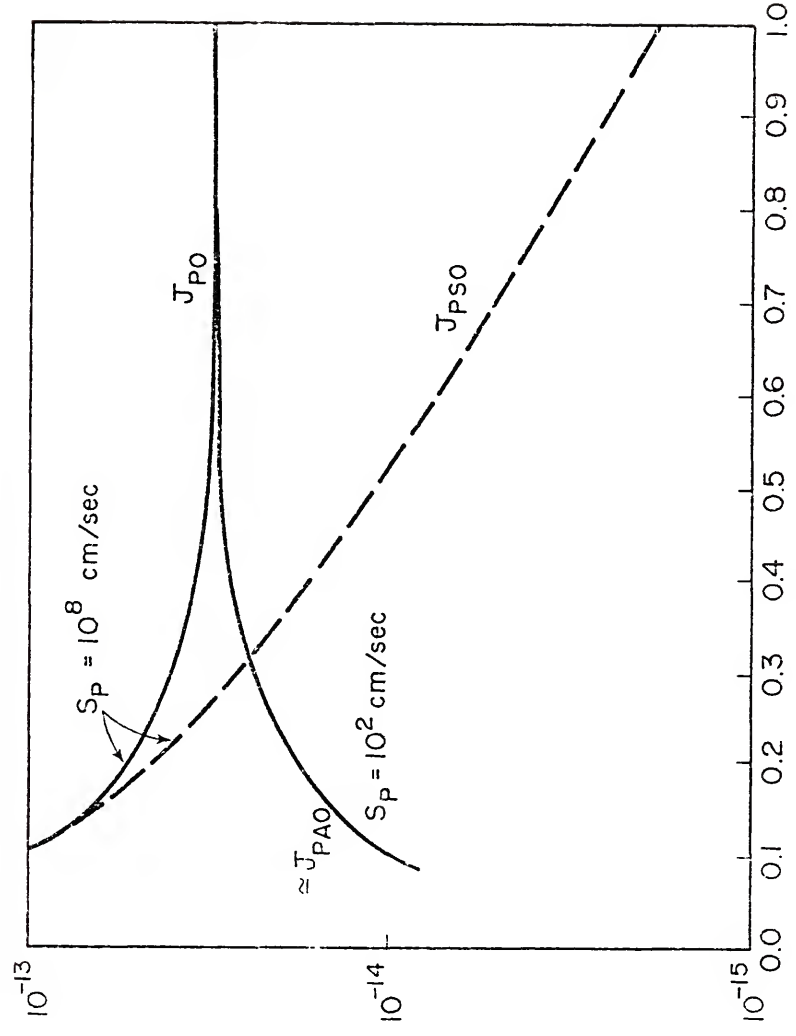

Figure 2.2 J_{PO} versus W_E for $S_P = 10^2$ cm/sec and $S_P = 10^8$ cm/sec; J_{PSO} is the surface-recombination component of J_{PO} and J_{PAO} is the Auger-recombination component

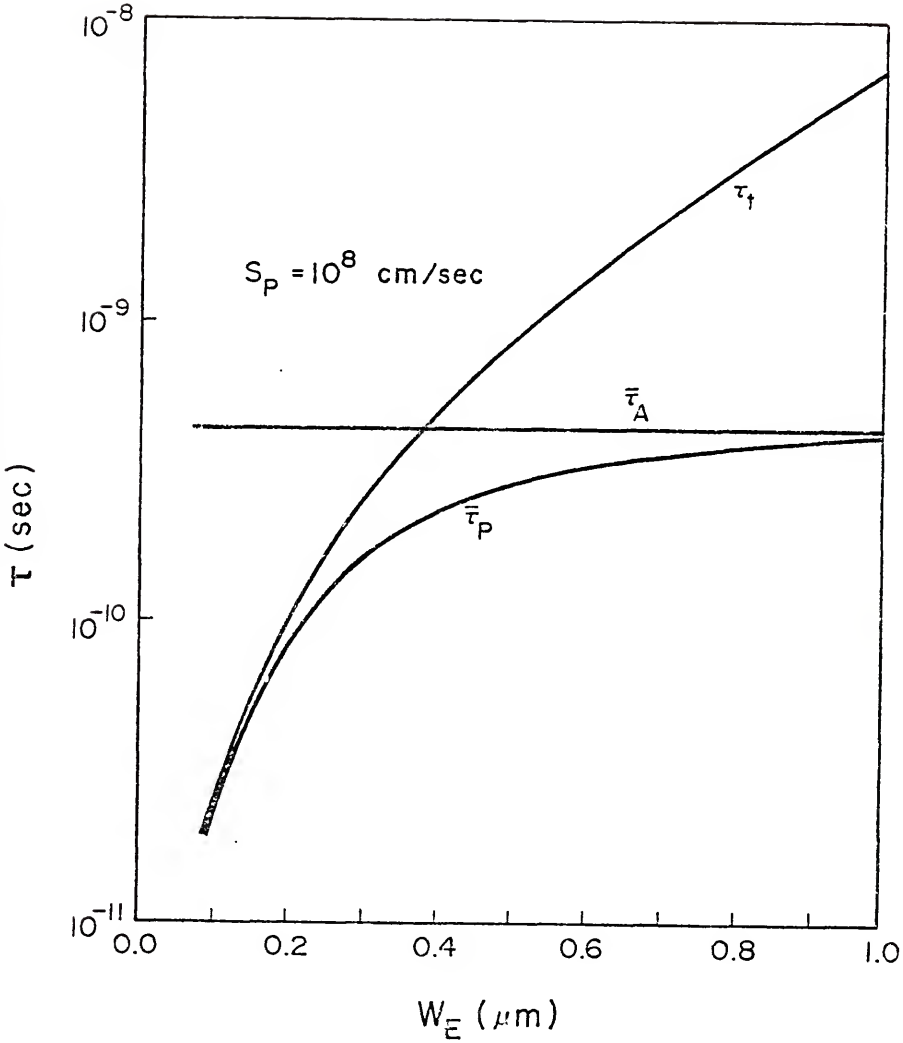

Figure 2.3 The effective hole lifetime $\bar{\tau}_p$ and its two components, the transit time τ_t and the average Auger lifetime $\bar{\tau}_A$, versus W_E for $S_p = 10^8$ cm/sec

effective hole lifetime and its components as functions of W_E. The surface concentration N_S is 10^{20} cm^{-3}. Note that the transit time essentially determines the emitter recombination current for $W_E < 0.3$ μm. This corresponds to a transparent emitter [24] in which the minority carriers recombine mainly at the emitter surface. The transparent-emitter model is consistent with experimental observations in conventional pn-junction silicon solar cells [29], and, because of high recombination velocity at an ohmic contact, the model can be expected to apply also to shallow-emitter silicon transistors. For larger W_E, the average Auger lifetime is smaller than the transit time and Auger recombination becomes important.

Finally, Figure 2-4 shows the dependence of V_{OC} on the surface concentration N_S for different values of S_P with W_E = 0.25 μm. When N_S is relatively small (about 10^{19} cm^{-3}), surface recombination is the dominant recombination mechanism in the emitter, and V_{OC} is very sensitive to S_P. As N_S increases toward 10^{21} cm^{-3}, V_{OC} is eventually limited by Auger recombination. The value of V_{OC} that results when the emitter current is dominated by Auger recombination (N_S larger than 2 x 10^{20} cm^{-3}) is about 680 mV. Once again, this result corresponds to a discrepancy with experiment of about a factor of 15 in emitter recombination current.

2.4 Conclusion

The analytic results we have presented demonstrate that a model for the emitter of silicon pn-junction devices based on Auger

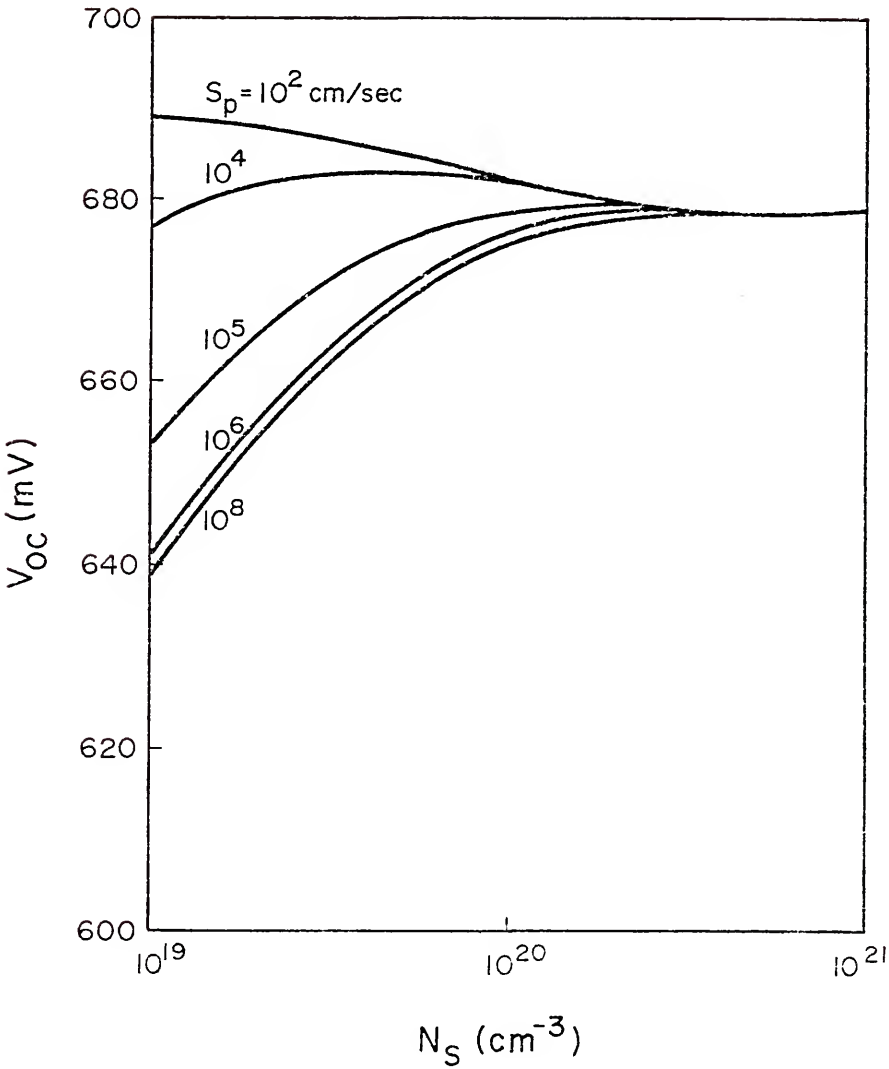

Figure 2.4 V_{OC} versus the surface concentration N_S for different values of S_p with W_E = 0.25 μm

recombination without bandgap narrowing cannot explain experimental values of V_{OC} in pn-junction solar cells. It follows that this model also cannot explain the low values of the common-emitter current gain measured in bipolar transistors. In this demonstration, we have used Maxwell-Boltzmann statistics. Use of Fermi-Dirac statistics would worsen the discrepancies between the model and experimental measurements [1]. Contrary to the conclusions of [30], therefore, we must conclude that physical mechanisms, e.g., bandgap narrowing, in addition to Auger recombination are responsible for the large emitter recombination currents observed in pn-junction devices.

CHAPTER III

RECOMBINATION THROUGH DEFECTS IN HEAVILY DOPED SHALLOW-EMITTER SILICON PN-JUNCTION DEVICES

3.1 Introduction

Having established in Chapter II that Auger recombination alone cannot explain the observed experimental values of V_{OC} in silicon solar cells, we must consider other heavy-doping mechanisms that will bring theory and experiment into agreement.

In this chapter, we consider recombination mechanisms, other than the Auger process, that can possibly occur in heavily doped shallow-emitter regions. These mechanisms are recombination via defects and surface recombination. We compare the effects of these two mechanisms with recent experimental observations showing the sensitivity of the open-circuit voltage in silicon pn-junction solar cells to surface treatment. These experiments are discussed briefly in Section 3.2.

In Section 3.3, we discuss Shockley-Read-Hall recombination via defects. We argue that recombination via defects alone yields results that are inconsistent with experimental observations of V_{OC} in silicon solar cells. If the Shockley-Read-Hall lifetime is very short (in the order of picoseconds), it will yield a low value of V_{OC}, as observed experimentally. However, in that case, V_{OC} will be insensitive

to surface treatment (i.e., surface recombination velocity) contrary to the experimental observations discussed in Section 3.2. For larger Shockley-Read-Hall lifetimes, which will yield a V_{OC} that is sensitive to variations in the surface recombination velocity, the calculated V_{OC} is larger than the experimentally observed values.

From Section 3.3 and Chapter II, we conclude in Section 3.4 that a short minority-carrier lifetime cannot yield an excessive recombination current that agrees with experiment, and at the same time be consistent with the recent experimental observations discussed in Section 3.2. Therefore, other heavy-doping mechanisms that can provide a large minority-carrier charge storage must be considered. This conclusion is corroborated by recent experimental measurements of the short-wavelength quantum efficiency of silicon solar cells [38]. Excessive charge storage in heavily doped semiconductor regions is attributed to either an effective excess intrinsic carrier density or an effective deficit majority-carrier density.

3.2 Importance of Surface Recombination

Fossum et al. [29] recently reported a considerable improvement in the open-circuit voltage in a variety of silicon solar cells by reducing the recombination velocity at the emitter surface. These solar cells include diffused, implanted, back-surface-field (BSF), and high-low-emitter (HLE) structures, of both N-on-P and P-on-N types [29].

It was observed that the growth of a thin thermal SiO_2 layer on the front (emitter) surface increased V_{OC} by about 20 mV in some

cells [29]. Table II, taken from [29], shows the improvement attained in V_{OC} in the solar cells described above by growing thermal SiO_2 on the emitter surface.

Other experiments, reported in [29], indicate that the thermal growth of SiO_2 reduced the surface recombination velocity rather than improved the bulk minority-carrier lifetime in the emitter. The reduction of the surface recombination velocity by thermal SiO_2 was observed for both N^+- and P^+-emitters. These experiments indicating the sensitivity of V_{OC} to the emitter surface condition imply that the emitter region is at least partially transparent to minority carriers. That is, a significant portion of the emitter recombination current occurs at the surface (prior to the surface passivation).

3.3 Shockley-Read-Hall Recombination via Defects

Defects in doped silicon can result from the diffusion of impurities and the subsequent heat treatment of pn-junction devices. These defects are due primarily to vacancies and vacancy complexes near the surface region of the device [39].

Lindmayer and Allison [40] suggested a dead-layer model for the emitter of thin diffused silicon solar cells in which the thin surface layer is strongly damaged by the diffusion of impurities. In this surface layer, there are large defect densities that result in very short minority-carrier lifetimes (in the picosecond range). The short lifetimes yield a large (dark) emitter recombination current that limits the open-circuit voltage of solar cells to values lower than those predicted by classical pn-junction theory.

In a treatment of recombination via defects and other heavy-doping effects, Lindholm et al. [9] studied the effect on the dark emitter current of process-induced defects in the emitter of silicon junction solar cells. They derived an impurity-concentration-dependent defect density N_{TT} [9]:

$$N_{TT}(x) = K[N_{DD}(x) + N_{AA}]^m \tag{3.1}$$

for an N^+-region. The integer m can vary from 1 to 4 depending on the type of vacancy in the semiconductor. In (3.1), $N_{DD}(x)$ is the impurity concentration in an N^+-emitter, N_{AA} is the P-type base impurity concentration, and K is a constant. For an assumed linear impurity profile near the junction, that is, an impurity concentration that depends linearly on distance, they found, for an emitter junction depth of 0.25 μm, that the excess minority carriers are packed in a very thin layer (about 200 Å in width) next to the space-charge region. This situation, illustrated in Figure 3.1, means that most of the minority carriers could not reach the surface.

The above conclusion is similar to earlier bipolar-transistor studies [41,42] of the effect of a built-in electric field in a diffused quasi-neutral emitter region, having a constant minority-carrier lifetime. In [9], the position-dependent minority-carrier lifetime, due to the position dependence of the defect density, enhanced the confinement of the excess injected minority carriers to a region near the junction.

We consider now the position-dependent defect density model of Lindholm et al. [9] in which the defect density is proportional

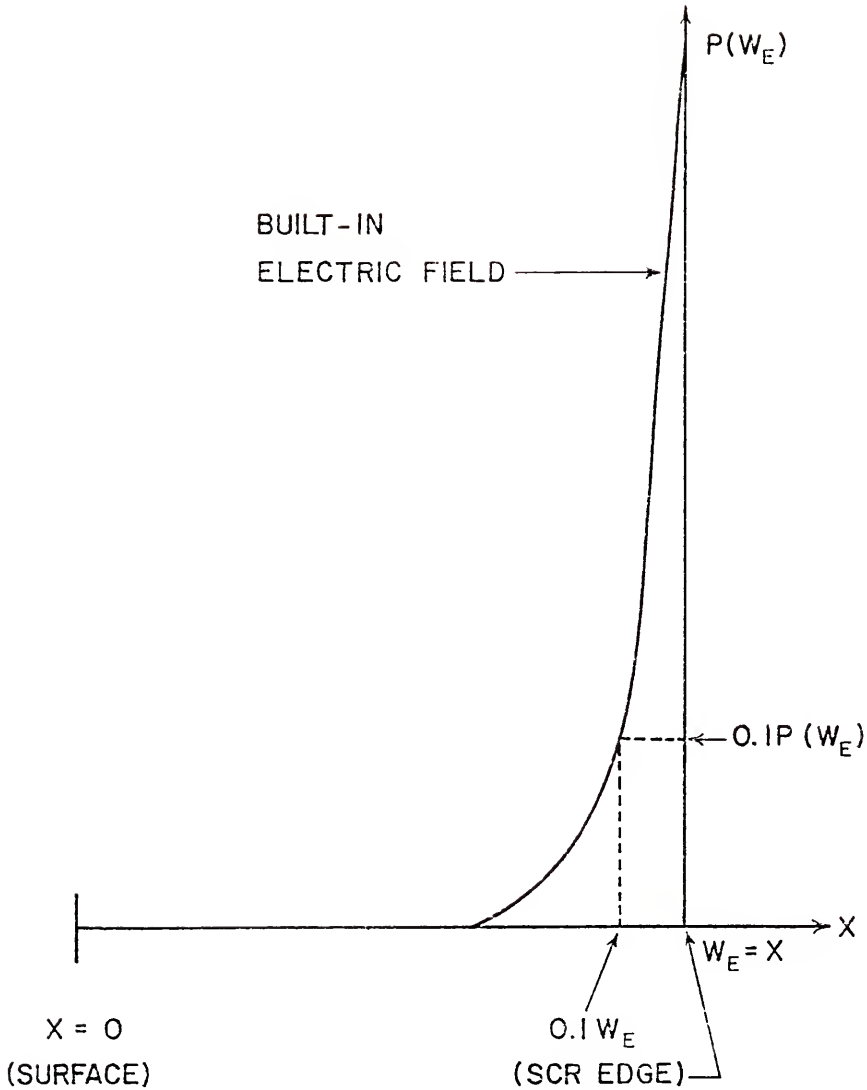

Figure 3.1 Sketch of minority-carrier concentration in a heavily doped emitter having a graded impurity profile and a large defect density, after [9]

to an integer power of the doping density as in (3.1). We assess the importance of defect recombination by determining if recombination via defects is alone sufficient to explain the experimentally low values of V_{OC} and its observed sensitivity to surface treatment. We consider three cases for the integer m in (3.1): m = 1, m = 2, and m > 2.

If m = 1, the Shockley-Read-Hall lifetime for low-level injection is

$$\tau_{SRH} \cong \frac{1}{C_{SRH}\, N(x)} \tag{3.2}$$

where C_{SRH} is a constant. Fossum [43] considered this case in a detailed numerical study of silicon solar cells. He showed that in order to predict a value of V_{OC} comparable to experimentally observed values in silicon solar cells, very short minority-carrier lifetimes in the emitter region (~ 1 nsec) are needed. Such short lifetimes yielded a V_{OC} that was insensitive to variations in the surface recombination velocity at the emitter surface [43], contrary to experimental observations [29]. Therefore, although short Shockley-Read-Hall lifetimes that vary inversely with N(x) can yield V_{OC} in the range of experimental values, they cannot account for the sensitivity of V_{OC} to the surface treatment.

For m = 2, the Shockley-Read-Hall lifetime has the same dependence on the doping density N(x) as for Auger recombination, except that the coefficient C_{SRH} is different than C_A:

$$\tau_{SRH} \cong \frac{1}{C_{SRH}\,[N(x)]^2} \tag{3.3}$$

In this case, for Shockley-Read-Hall recombination to dominate over Auger recombination, C_{SRH} must be larger than the Auger coefficient C_A. This yields $\tau_{SRH} < \tau_A$.

We used the analytic model of Chapter II to calculate V_{OC}, the transit time, and the average bulk lifetime for this case (with $m = 2$). We found that for $C_A \leq C_{SRH} \leq 4C_A$, the transit time is smaller than the average bulk lifetime for high values of surface recombination velocity S (about 10^8 cm/sec), and consequently V_{OC} is sensitive to variations in S. However, the magnitude of V_{OC} we obtained (> 670 mV) was considerably higher than the experimentally observed value of about 600 mV. For $C_{SRH} > 4C_A$, our calculations yielded a bulk lifetime in the order of a fraction of a nanosecond, which is much smaller than the transit time. Hence, although the short lifetimes yield lower values of V_{OC} (< 670 mV), they result in a V_{OC} that is insensitive to variations in S.

For basically the same reason discussed above, we infer that for $m > 2$ in (3.1), the emitter is expected to be insensitive to surface recombination. As the lifetime varies faster than $[N(x)]^{-2}$, the injected minority-carrier concentration falls sharply with increasing distance away from the junction. Thus, most of the injected minority carriers cannot reach the emitter surface before they recombine in the bulk via defect centers.

3.4 The Excess Minority-Carrier Charge Storage in Heavily Doped Regions

We discussed Shockley-Read-Hall recombination via defects in the last section and showed that for Shockley-Read-Hall lifetimes that have an inverse-power functional dependence on the doping density, recombination via defects cannot alone be the dominant mechanism limiting V_{OC} in silicon solar cells. This is because such a recombination mechanism cannot yield results that are simultaneously in agreement with the low values of V_{OC} observed in silicon solar cells and with the sensitivity of V_{OC} to surface treatment. Furthermore, recent experimental investigation of the short wavelength spectral response of silicon solar cells indicates that heavy-doping effects, other than short lifetimes, are required to obtain agreement between experimental and theoretical results [38].

Combining the above conclusion with the conclusion of Chapter II, we deduce that short minority-carrier lifetimes cannot be the only cause of the large emitter current in silicon solar cells. A similar conclusion is anticipated for bipolar transistors. From Equation (1.1), we infer that the minority-carrier charge storage in heavily doped regions must then be large to account for the large current.

We now show qualitatively that a large minority-carrier charge storage is due either to an excess intrinsic carrier density or to a deficit majority-carrier concentration.

The minority-carrier charge storage Q_p, in an N-type region for example, is

$$Q_p = q \int_0^{W_E} \Delta P(x)\, dx \tag{3.4}$$

where $\Delta P(x)$ is the excess minority-carrier (hole) concentration. For non-equilibrium conditions in a non-degenerate semiconductor,

$$PN = n_i^2 \exp\left[\frac{E_{FN} - E_{FP}}{kT}\right] \tag{3.5}$$

where E_{FP} and E_{FN} are the hole and electron quasi-Fermi levels. From (3.5), the condition of low-injection,

$$N \simeq N_0 \tag{3.6}$$

and the fact that

$$P \simeq \Delta P \tag{3.7}$$

we get

$$\Delta P \propto \frac{n_i^2}{N_0} \tag{3.8}$$

If we assume full ionization of impurities,

$$N_0 \simeq N_{DD} \tag{3.9}$$

and (3.8) becomes

$$\Delta P \propto \frac{n_i^2}{N_{DD}} \tag{3.10}$$

If, because of some physical mechanism, e.g., energy-bandgap narrowing, n_i^2 is larger than its intrinsic value (in pure silicon), or N_0 is smaller than the doping concentration because of, e.g., incomplete ionization of the impurity atoms, then ΔP, and consequently Q_p in (3.4), will be larger than anticipated, and thus, by (1.1), the emitter current will be excessively large.

The two effects mentioned above, n_i^2 larger than its intrinsic value and $N_0 < N_{DD}$, can be phenomenologically incorporated into an effective excess intrinsic carrier density n_{ie}^2 such that (3.10) can be written as

$$\Delta P \propto \frac{n_{ie}^2}{N_{DD}} \tag{3.11}$$

for a non-degenerate N-type semiconductor. For a degenerate semiconductor, we show later that n_{ie}^2 can include the effects of Fermi-Dirac statistics, and hence (3.11) is still applicable. Note that, in this way, heavy-doping effects can be incorporated in a single parameter, n_{ie}^2.

In the next chapter, we will consider deionization of impurities, as discussed by the recent papers of Heasell [25,44] and Popovic [45], as a possible mechanism that results in $n_{ie}^2 > n_i^2$.

TABLE II

MEASURED V_{OC} OF A VARIETY OF SILICON SOLAR CELLS WITH AND WITHOUT A FRONT-SURFACE THERMAL SiO_2 LAYER (T = 25°C)

Cell Designation	Cell Description	(V_{OC}) without SiO_2	(V_{OC}) with SiO_2
A	N^+-P (diffused)	596 mV	605 mV
B	N^+-N-P HLE	599 mV	619 mV
C	N^+-P (implanted)	625 mV[a]	644mV[a]
D	P^+-N-N^+ BSF	594 mV	626 mV

[a]Measurements for cell C were made at AMO whereas those for the other cells were made at AM1.

Source: [29]

CHAPTER IV

ON THE DEIONIZATION OF IMPURITIES AS AN EXPLANATION FOR EXCESS INTRINSIC CARRIER DENSITY IN HEAVILY DOPED SILICON

Experimental measurements of the collector currents in silicon bipolar transistors [20] have indicated that n_{ie}^2, the square of the effective intrinsic carrier concentration, increases to values well above n_i^2, the classical intrinsic carrier concentration, as the doping level in the quasi-neutral base region increases. This was interpreted by Slotboom and DeGraaff to be due to energy-bandgap narrowing in the quasi-neutral base region, which was heavily doped in the devices used for their study [20].

Recently, Popovic [45] presented an alternate interpretation for the increase of n_{ie}^2 with the doping level. He argued that, in the range of impurity concentrations of 10^{17} cm^{-3} to 10^{19} cm^{-3} in silicon, the increase of n_{ie}^2 can be attributed to a Fermi energy difference ΔE corresponding to different density-of-states models, whose physical significance will be discussed later. In recent papers [25, 44], Heasell gave another interpretation based on the assumption of a constant impurity activation energy at high doping levels. The models of Popovic and Heasell resemble each other in that they both emphasize the importance of deionization of impurity levels, which results in the majority carrier density being substantially lower than the net doping density.

We discuss here in detail the models of Popovic and Heasell, and show that their underlying assumptions are inconsistent with a variety of experimental observations in heavily doped silicon. Hence we conclude that these interpretations do not dislodge energy-bandgap narrowing as a possible mechanism underlying the increase in n_{ie}^2 in heavily doped silicon.

As the basis for his model, Heasell assumed (a) that the bandgap of silicon is not affected by heavy doping, and (b) that the impurity energy-levels in the bandgap due to the presence of shallow-level impurity atoms are independent of the impurity concentration. For heavily doped silicon, these assumptions lead to a small ionization ratio, which we define as the ratio of the concentration of ionized impurity atoms to the total concentration of impurity atoms. To show this, consider a donor energy level of E_D. Then the majority-carrier concentration N (electrons for an N^+ region), which equals the ionized impurity concentration, is related to the total donor concentration, N_{DD}, for uncompensated N^+ silicon by [46]

$$N = [N_{DD}N_C/g_D]^{1/2}\exp[-(E_C - E_D)/2kT] \qquad (4.1)$$

for $N_{DD} > 10^{18}$ cm^{-3}. Here g_D is the impurity energy-level degeneracy factor, N_C is the conduction-band effective density of states, and E_C is the conduction-band edge. Thus, in the Heasell model, where E_D does not depend on the impurity concentration, the majority-carrier concentration varies in proportion as the square root of the impurity concentration. If N_{DD} increases by two orders of magnitude, N increases

by only one order of magnitude. Hence, the NP (electron-hole) product (given, at equilibrium for low doping concentrations, by the law of mass action) implies a larger minority-carrier density than is predicted classically. This has the same effect in device analysis as would n_{ie}^2 being larger than n_i^2.

The above assumption of a fixed discrete impurity energy level disagrees with the experimental observations of Pearson and Bardeen [47] and Penin et al. [48]. They found that the ionization energy of the impurity atoms vanishes as the impurity concentration approaches about 3×10^{18} cm^{-3} for both n-type and p-type silicon. Therefore, Heasell's assumption of a fixed impurity energy level in the bandgap of heavily doped silicon conflicts with long established experimental findings.

To modify Heasell's approach to bring it into harmony with the results of these experiments, we have calculated the ionization ratio for heavily doped silicon using an impurity-concentration dependence of the ionization energy based on the experimental results of Pearson and Bardeen [47]. We found, in agreement with [49], that the lowest ionization ratio at room temperature is about 90% for phosphorus-doped silicon, and about 70% for boron-doped silicon. This difference in the degree of ionization arises from the difference in the effective density of states in the conduction and valance bands and in the degeneracy factors applying to the donor and acceptor impurity energy levels. This deionization of impurities, based on the experimental results of Pearson and Bardeen [47], is not large enough

to account for the experimentally observed values of n_{ie}^2 quoted by Heasell [25]. Thus Heasell's assertion that deionization is the first-order mechanism underlying the large values of n_{ie}^2 observed in heavily doped silicon is not justified.

We discuss now the treatment of Popovic [45]. Popovic related the increase of n_{ie}^2 observed in the base region of a bipolar transistor as the impurity concentration increases above 10^{17} cm^{-3} [20] to a difference in Fermi energy ΔE. The energy difference ΔE originates from calculations based on two different models for the density of states in heavily doped silicon.

The first (classical) model assumes parabolic conduction and valance bands; i.e., the density of states is assumed proportional to the square root of energy, and full impurity ionization is assumed. This model yields a Fermi energy E_F, calculated from the quasi-neutrality condition, that increases monotonically as the doping level increases. Above an impurity concentration of about 10^{19} cm^{-3}, E_F enters the conduction band (for n-type material) or the valance band (for p-type material).

The second model assumes that (a) the conduction-band and valance-band density of states have exponential tails that extend into the forbidden bandgap, (b) the impurity density of states has a Gaussian form, and (c) the total density of states is the envelope of the density of states in (a) and (b) [16]. When used with the quasi-neutrality condition in the base region, this model predicts a different Fermi energy E_F' than that (E_F) calculated from the classical

model. The Fermi energy E_F' saturates for high impurity concentrations at the low-impurity-concentration value of the impurity energy level in the bandgap [16].

Popovic claims that the energy difference,

$$\Delta E = E_F - E_F' \tag{4.2}$$

is an alternate interpretation to energy-bandgap narrowing in silicon in the doping range of 10^{17} to 10^{19} cm^{-3}, an interpretation that can account for the increase in n_{ie}^2 in the same way as bandgap narrowing, i.e.,

$$n_{ie}^2 = n_i^2 \exp(\Delta E/kT) \tag{4.3}$$

for Maxwell-Boltzmann statistics. The energy difference ΔE increases as the impurity concentration increases because, in the second model [16] for the density of states, E_F' saturates at the impurity energy level, while, according to the classical (first) model, E_F increases monotonically as the impurity concentration increases.

To estimate quantitatively the effect of ΔE on n_{ie}^2, we consider a concentration of 10^{19} cm^{-3} phosphorus atoms in silicon at room temperature. Then, $\Delta E \simeq 0.045$ eV since E_F is very close to the conduction band edge, while E_F' is nearly at the impurity energy level of phosphorus in silicon--0.045 eV below the conduction band edge. Using this value of ΔE, we obtain

$$n_{ie}^2 \simeq 6n_i^2 \tag{4.4}$$

Since 0.045 eV is the maximum value of ΔE in the range of doping considered (from 10^{17} cm^{-3} to 10^{19} cm^{-3}), the maximum value of n_{ie}^2 due to the difference in Fermi energy is less than an order of magnitude larger than n_i^2. If we use this value of n_{ie}^2, for the range of doping specified above, add the effect of the bandgap narrowing model of Vol'fson and Subashiev [50] (for $N_{DD} \geq 2 \times 10^{19}$ cm^{-3}), as suggested by Popovic, and include Fermi-Dirac statistics, we get values of the open-circuit voltage in silicon solar cells and the common-emitter gain in silicon bipolar transistors that are much higher than experimentally observed values. Thus the increase of n_{ie}^2 due to the saturation of E_F', assuming, in this part of the discussion, that it saturates, is too small to account for these experimental findings in silicon devices.

We now turn to the basic assumptions of Popovic's treatment: the saturation of the Fermi level E_F' and the resulting tacit assumption of impurity deionization in heavily doped silicon.

From a theoretical viewpoint, saturation of the Fermi level in the bandgap is due primarily to impurity band widening, that is, to the spread of impurity energy levels from discrete to quasi-continuous levels in the bandgap at high impurity concentrations (in the range of 10^{17} to 10^{19} cm^{-3}). Impurity band widening introduces a large number of energy levels in the bandgap that can be populated by the majority carriers. This lessens the density of carriers in the majority allowed band, and makes the Fermi level tend to saturate.

Deionization of impurities is tacitly assumed in Popovic's treatment because the charge carriers populating the impurity band

are regarded to be localized spatially. This is so because, if the carriers occupying the impurity band were not localized, i.e., if their wavefunctions were to extend all over the crystal, there would be, in effect, energy-bandgap narrowing since allowed band-like states would exist at lower energies (for N-type material) than those present in pure silicon. However, since Popovic asserts in his model that the bandgap does not change because of the presence of impurities in the doping range of 10^{17} to 10^{19} cm^{-3}, Popovic's model must assume that the impurity band states are localized spatially. Such localization results in a majority carrier concentration N that is considerably less than the impurity concentration N_{DD}. Thus, popovic's model leads to the deionization of impurity atoms, which was a central physical mechanism also in the Heasell model. In the Popovic model, impurity deionization and Fermi-level saturation go hand-in-hand.

But we now note that Fermi level saturation is <u>not</u> the trend observed experimentally in heavily doped silicon. A variety of experimental observations in heavily doped, single-crystal silicon indicates that the localization of charge carriers is greatly reduced by the increase in impurity concentration and the electrons (or holes) show, experimentally, physical properties that are in good agreement with the degenerate free-electron gas model in metals. These experimental observations in heavily doped silicon involve measurements of: resistivity and Hall effect [47-48, 51-55], electron spin resonance (ESR) [53], magneto-resistance [54], electronic specific heat [56], and nuclear magnetic resonance (NMR) [57-58]. A thorough discussion

of these mechanisms in group IV semi-conductors is given in [58]. We consider briefly here the implication of measurements of the electronic specific heat [56] and nuclear magnetic resonance [57-58] as they relate to the position of the Fermi level in heavily doped silicon.

Measurements of the electronic specific heat in phosphorus-doped silicon ($N_{DD} > 6 \times 10^{18}$ cm^{-3}) show that the electrons behave as a degenerate electron gas [56]. The electronic specific heat of the heavily doped silicon samples (a) has a linear dependence on temperature, (b) increases considerably as the impurity concentration increases, and (c) has an $N_{DD}^{1/3}$ dependence on the impurity concentration in agreement with the dependence predicted by the degenerate free-electron gas model for metals [59]. The above results indicate that, for $N_{DD} > 6 \times 10^{18}$, a parabolic density of states in the conduction band is probably a good approximation. Furthermore, although no quantitative estimates of the degree of ionization can be concluded from measurements of the electronic specific heat, these measurements do indicate that almost all donor electrons occupy delocalized states; otherwise the specific heat would not exhibit the metallic character described above.

Experimental determination of the position of the Fermi level and of the delocalization of donor electrons (that is, of the ionization of impurity atoms) is provided by nuclear magnetic resonance (NMR) experiments in phosphorus-doped silicon [57-58]. These experiments indicate, via the spin interactions of electrons and impurity nuclei, that, at an impurity concentration of about 3×10^{18} cm^{-3}, electrons in

heavily doped silicon are delocalized, in agreement with the results of Pearson and Bardeen [47]. Furthermore, at a phosphorus concentration of about 2×10^{19} cm^{-3}, the Fermi level in heavily doped silicon is <u>at</u> the conduction band edge of silicon [58], that is, the Fermi level <u>enters</u> the conduction band. Thus NMR experiments indicate that the Fermi level <u>does not</u> saturate in the bandgap of silicon [58]. They indicate also that at impurity concentrations above 2×10^{19} cm^{-3} the impurity band merges almost completely with the conduction band [58], resulting in a composite density of states having, to a good approximation, a parabolic dependence on energy ($E^{1/2}$) [57].

Therefore, we conclude that the basic assumptions of Popovic's treatment are not justified since experiments predict that the Fermi level does not saturate, and impurity deionization is not a first-order mechanism in heavily doped silicon.

Our approach has been to dispute the conclusions of Heasell and Popovic because their initial premises conflict with experimental observations. In the case of Heasell's model, we also showed that a version of it, modified to be consistent with experiment, still failed to explain the observed variation of n_{ie}^2 with doping level. In this chapter we have not discussed theoretical grounds for the model advanced earlier to explain the variation of n_{ie}^2, that is, the model of energy-bandgap narrowing. Our position is that bandgap narrowing is a possible valid mechanism influencing n_{ie}^2--and thus the common-emitter current gain of silicon transistors and the open-circuit voltage of silicon solar cells. But we believe that the stage now

reached in theoretical and experimental work on bandgap narrowing does not allow a consensus of agreement to be reached that it is the dominant mechanism underlying the observed variations in n_{ie}^2.

In accordance with the above comment, the expression "bandgap narrowing" will mean, in the following chapters, a phenomenological narrowing of the bandgap characterized by an excess intrinsic carrier concentration $n_{ie}^2 > n_i^2$. That is, our use of the term "bandgap narrowing" does not necessarily refer to the true shrinkage in the bandgap of the semiconductor. As shown in Chapter II and later in this dissertation, use of a phenomenological bandgap narrowing in the analysis of heavily doped silicon devices is important to bring theory and experiment into agreement.

In the next chapter, we incorporate bandgap narrowing into the analysis of heavily doped emitters of silicon pn-junction devices.

CHAPTER V

HEAVILY DOPED TRANSPARENT-EMITTER REGIONS IN SILICON JUNCTION SOLAR CELLS, DIODES, AND TRANSISTORS

5.1 Introduction

Excess minority carriers injected into the emitter of pn-junction devices recombine in the bulk and at the surface of the emitter. If the emitter junction is shallow enough, the minority carriers can cross the quasi-neutral emitter region without appreciable bulk ecombination. The minority carriers then recombine at the emitter surface. For this case the emitter is transparent to the injected minority carriers, and an important parameter then is the surface recombination velocity S at the emitter surface.

This parameter is particularly important for pn-junction silicon solar cells in which most of the illuminated surface is not covered by metal. In devices in which thermal SiO_2 covers this nonmetallized portion of the surface, experiments show that S can be less than 10^4 cm/sec for both P-cells (P-type substrate) [29] and N-cells [29]. This value of S is orders of magnitude less than that of an ohmic contact and is consistent with values determined earlier by different experimental methods [60]. Furthermore, recent experiments involving P-on-N and N-on-P cells without thermal SiO_2 demonstrate that the emitter can be completely transparent [29].

The purpose of this chapter is to provide an analytical treatment of transparent emitter devices, particularly solar cells, that is more complete than treatments previously available In this treatment, we include the effects of (a) bandgap narrowing [19,61], (b) Fermi-Dirac statistics, (c) built-in field due to the impurity profile, and (d) a finite surface recombination velocity S. Detailed numerical studies including these various effects have been done [32,62-63], but they have not treated the case of the transparent emitter.

A major result of this chapter is the demonstration that the transparent-emitter model can predict experimental values of V_{OC} observed on N^+P thin diffused junction silicon solar cells made on low-resistivity (0.1 Ω-cm) substrates. Thus, the transparent-emitter model is shown to provide an explanation for the discrepancy between the prediction of simple classical theory ($V_{OC} \cong 700$ mV) and the measured maximum value ($V_{OC} \cong 600$ mV). The transparent-emitter model gives $V_{OC} \cong 600$ mV for high values of S_p ($S_p > 10^4$ cm/sec) provided the effects of bandgap narrowing (modified by Fermi-Dirac statistics) are included. This result suggests that V_{OC} can be increased toward the classical value of 700 mV if S_p is decreased and the effects of bandgap narrowing are reduced. This is accomplished in the HLE solar cells, early verions of which have shown increases in V_{OC} to the 640-650 mV range [64-65].

In addition to the development of the theory for the transparent-emitter device, and its application to solar cells, this

chapter will include a test for the self-consistent validity of the transparent-emitter model. This test compares the calculated transit time of minority carriers across the emitter with the Auger-impact minority-carrier lifetime within the emitter region.

5.2 Derivation

We consider an N-type heavily doped quasi-neutral emitter region; analogous results apply to P-type emitters. The minority carrier current density in the N-type region is

$$J_p(x) = q\mu_p \Delta P(x)\, E(x) - qD_p \frac{d\Delta P(x)}{dx} \tag{5.1}$$

in which E(x) is the thermal equilibrium value of the effective field which, for low-level injection, is given by

$$E(x) = \frac{D_p}{\mu_p} \cdot \frac{1}{P_0(x)} \cdot \frac{dP_0(x)}{dx} \tag{5.2}$$

We now define an effective intrinsic density n_{ie} such that

$$n_{ie}^2(x) = P_0(x)\, N_0(x) \tag{5.3}$$

in which $P_0(x)$ and $N_0(x)$ are the hole and electron concentrations in thermal equilibrium. The parameter n_{ie}^2 depends on position for two reasons:

1. The influence of Fermi-Dirac statistics, and
2. The influence of bandgap narrowing

These influences are discussed in Section 5.3. For Maxwell-Boltzmann statistics and no bandgap narrowing, n_{ie}^2 is the square of

the intrinsic carrier concentration in silicon and is a function of temperature only.

If the expressions is (5.2) and (5.3) are used in (5.1), we get, after some manipulations,

$$J_p(x)\,\frac{N_0(x)}{n_{ie}^2(x)}\,dx = -qD_p d\left[\Delta P(x)\cdot\frac{N_0(x)}{n_{ie}^2(x)}\right] \tag{5.4}$$

If we integrate (5.4) over the quasi-neutral emitter region, we get

$$\int_0^{W_E} J_p(x)\cdot\frac{N_0(x)}{n_{ie}^2(x)}\,dx = -q\bar{D}_p\left[\Delta P(x)\cdot\frac{N_0(x)}{n_{ie}^2(x)}\right]_0^{W_E} \tag{5.5}$$

where $\bar{D}_p$ is some average value of D_p. If the emitter is transparent (transit-time limtied), that is, if the minority carrier transit time τ_t is much less than the minority carrier lifetime τ_p (for an N-type emitter), then J_p is constant independent of position in the emitter. Use of the minority carrier boundary conditions [11]

$$\Delta P(0) = P_0(0)(\exp(qV/kT) - 1) \tag{5.6}$$

at the edge of the emitter space charge region, and [11]

$$J_p(W_E) = q \cdot S_p \cdot \Delta P\,(W_E) \tag{5.7}$$

at the emitter surface, enable (5.5) to be expressed as

$$J_p = \frac{q\bar{D}_p\,(\exp(qV/kT) - 1)}{\displaystyle\int_0^{W_E}\frac{N_0(x)}{n_{ie}^2(x)}\,dx + \frac{\bar{D}_p \cdot N_0(W_E)}{S_p \cdot n_{ie}^2(W_E)}} \tag{5.8}$$

Equation (5.8) is the general experssion for the minority-carrier current in a transparent emitter.

To check the condition, $\tau_t << \tau_p$, required for transparancy, we must determine the steady-state transit time τ_t, which is defined by the charge control relation,

$$\tau_t = \frac{Q_p}{J_p} \tag{5.9}$$

Here Q_p is the excess minority carrier charge storage in the emitter:

$$Q_p = q \int_0^{W_E} \Delta P(x)\, dx \tag{5.10}$$

Using (5.4), (5.8), and (5.10) to express Q_p, and combining with (5.9), we find the following expression for the minority carrier transit time:

$$\tau_t = \left\{ \left[\frac{1}{\overline{D}_p} \int_0^{W_E} \frac{N_0(x)}{n_{ie}^2(x)}\, dx + \frac{N_0(W_E)}{S_p \cdot n_{ie}^2(W_E)} \right] \cdot \int_0^{W_E} \frac{n_{ie}^2(x)}{N_0(x)}\, dx \right.$$

$$\left. - \frac{1}{\overline{D}_p} \int_0^{W_E} \int_0^{x} \frac{N_0(x')}{N_0(x)} \cdot \frac{n_{ie}^2(x)}{n_{ie}^2(x')}\, dx'\, dx \right\} \tag{5.11}$$

Some special cases are of interest. For a flat impurity concentration profile, the above expression reduces to

$$\tau_t = \frac{W_E^2}{2\overline{D}_p} + \frac{W_E}{S_p} \tag{5.12}$$

If, furthermore, S_p is infinite, (5.12) reduces to the familiar expression,

$$\tau_t = \frac{W_E^2}{2\overline{D}_p} \tag{5.13}$$

5.3 Heavy-Doping Effects

In thermal equilibrium, heavy-doping concentrations of shallow level impurities affect the minority-carrier concentration in a quasi-neutral region by two mechanisms: bandgap narrowing and Fermi-Dirac statistics. These two mechanisms affect the minority-carrier concentration in opposite ways. For any given position of the Fermi level relative to the band edges, bandgap narrowing tends to increase the minority-carrier concentration, while inclusion of Fermi-Dirac statistics tends to decrease the minority-carrier concentration below the value calculated using Maxwell-Boltzmann statistics. The dominance of either of the two effects, at any specific impurity concentration, depends on the model of bandgap narrowing adopted.

In this treatment, we assume that bandgap narrowing occurs without changing the parabolic dependence on energy of the density of

states in the conduction and valance bands. This is the rigid-band approximation; it is discussed in Appendix F.

The effects of bandgap narrowing and Fermi-Dirac statistics can be lumped into a position-dependent effective intrinsic carrier concentration at thermal equilibrium given by

$$n_{ie}^2(x) = \frac{n_i^2 \exp(\Delta E_G(x)/kT)}{1 + C(\eta) \exp(\eta)} \tag{5.14}$$

where

$$\eta = \eta_C = (E_F - E_C)/kT \tag{5.15}$$

for N-type material, and

$$\eta = \eta_V = (E_V - E_F)/kT \tag{5.16}$$

for P-type material. The derivation of (5.14) appears in Appendix C. In (5.15) and (5.16), E_C and E_V are the edges of the conduction and valence bands, respectively, and E_F is the Fermi level. The factor $C(\eta)$ is a function of η, which, for $\eta \leq 4$ (e.g., $N_D \leq 2 \times 10^{20}$ cm^{-3} in N-type silicon), is [24]

$$C(\eta) \cong -0.04\eta + 0.3 \tag{5.17}$$

The above approximation of $C(\eta)$ gives values of the Fermi-Dirac integral of order 1/2 with less than 4% error.

In nonequilibrium conditions, bandgap narrowing increases the minority-carrier current by:

1. Increasing the minority-carrier concentration
2. Decreasing the retarding built-in electric field acting on the minority carriers

The increase in the minority-carrier concentration P results from the increase in $n_{ie}^2(x)$. The decrease of the built-in electric field is due to the position dependence of $n_{ie}^2(x)$ (and hence of the effective bandgap) in the inhomogeneously doped emitter.

To develop a simple expression illustrating the reduction of the electric field, we now include only bandgap narrowing excluding the effect of Fermi-Dirac statistics for the present. Then the effective electric field acting on the minority carriers, given in (5.2), can be expressed by using (5.3) and (5.14) as:

$$E(x) = R(N_0)\left[-\frac{D_P}{\mu_P}\cdot\frac{1}{N_0(x)}\cdot\frac{dN_0(x)}{dx}\right] \tag{5.18}$$

where

$$R(N_0) \equiv \left[1 - \frac{N_0(x)}{kT}\quad\frac{d\,\Delta E_G(x)}{dN_0(x)}\right] \tag{5.19}$$

The factor $R(N_0)$ measures the reduction of the built-in electric field due to bandgap narrowing. For any model of bandgap narrowing, $R(N_0)$ is always less than one. Figure 5.1 shows $R(N_0)$ as a function of the electron (majority carrier) concentration for three models of bandgap narrowing: Slotboom and DeGraaff [20], Hauser [12], and Lanyon and Tuft [13].

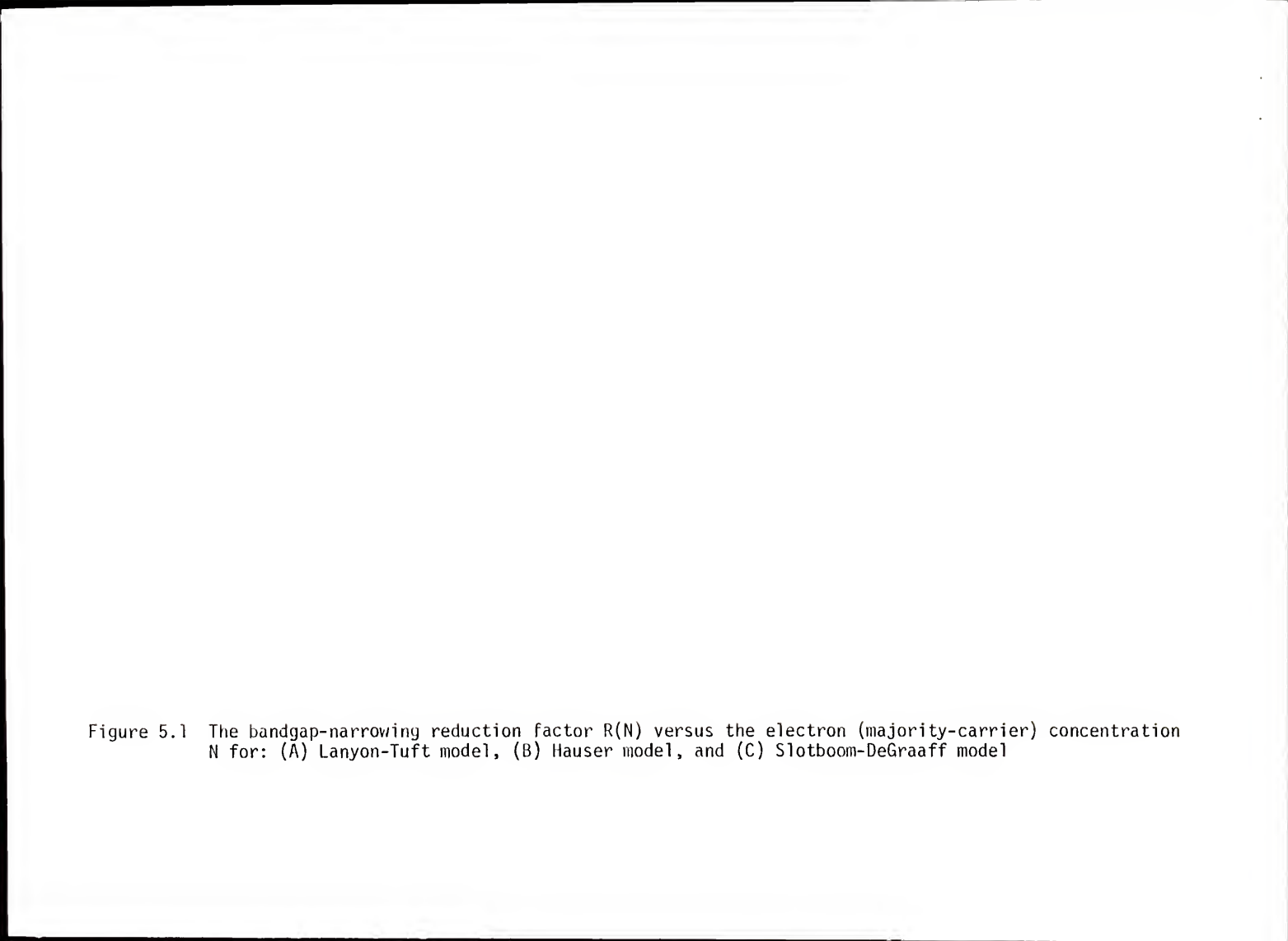

Figure 5.1 The bandgap-narrowing reduction factor R(N) versus the electron (majority-carrier) concentration N for: (A) Lanyon-Tuft model, (B) Hauser model, and (C) Slotboom-DeGraaff model

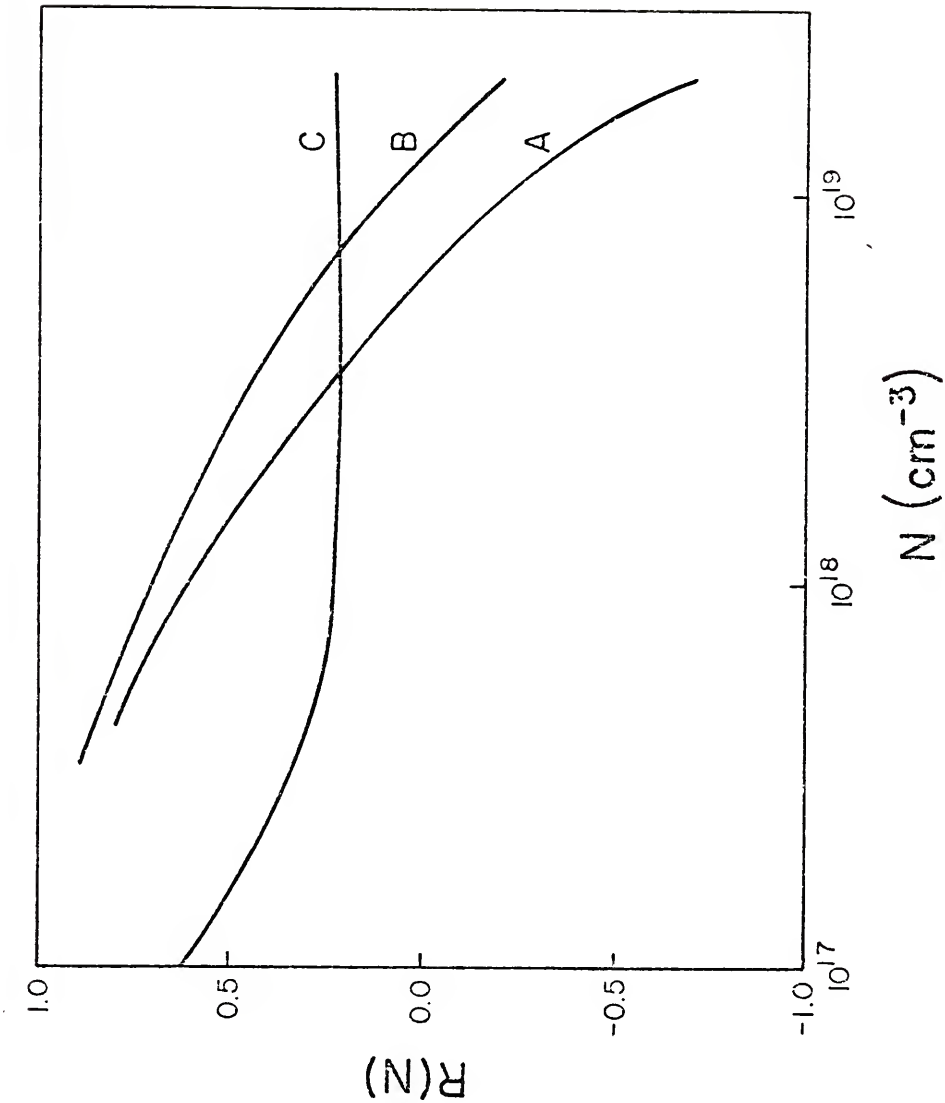
C
B
A
1.0
0.5
0.0
-0.5
-1.0
R(N)
10^{17}
10^{18}
10^{19}
N (cm^{-3})

In the absence of bandgap narrowing, the holes experience a retarding electric field in an N-type diffused emitter. Equations (5.18) and (5.19) indicate that the position dependence of the bandgap narrowing, in effect, decreases the retarding electric field. The more it is decreased the smaller is the transit time for a specific surface recombination velocity. In (5.11) the transit time is shown to be a function of n_{ie}^2. In Figure 5.2 the transit time is plotted as a function of W_E, the width of the quasi-neutral emitter region, in two cases: neglecting bandgap narrowing, and including bandgap narrowing (Slotboom and De Graaff model). Note that inclusion of bandgap narrowing makes the transit time close to the value it has if the impurity profile is flat. In general, bandgap narrowing decreases the transit time if the impurity profile is not flat.

Conversely, inclusion of Fermi-Dirac statistics increases the transit time as can be seen in Figure 5.2 Inclusion of Fermi-Dirac statistics shifts the value of the transit time closer to that calculated when heavy-doping effects are neglected.

5.4 Discussion

From (5.8), the minority-carrier saturation current for a transparent emitter is

$$J_{PO} = \frac{q\bar{D}_p}{\int_0^{W_E} \frac{N_D(x)}{n_{ie}^2(W_E)}\,dx + \frac{\bar{D}_p N_D(W_E)}{S_p n_{ie}^2(W_E)}} \qquad (5.20$$

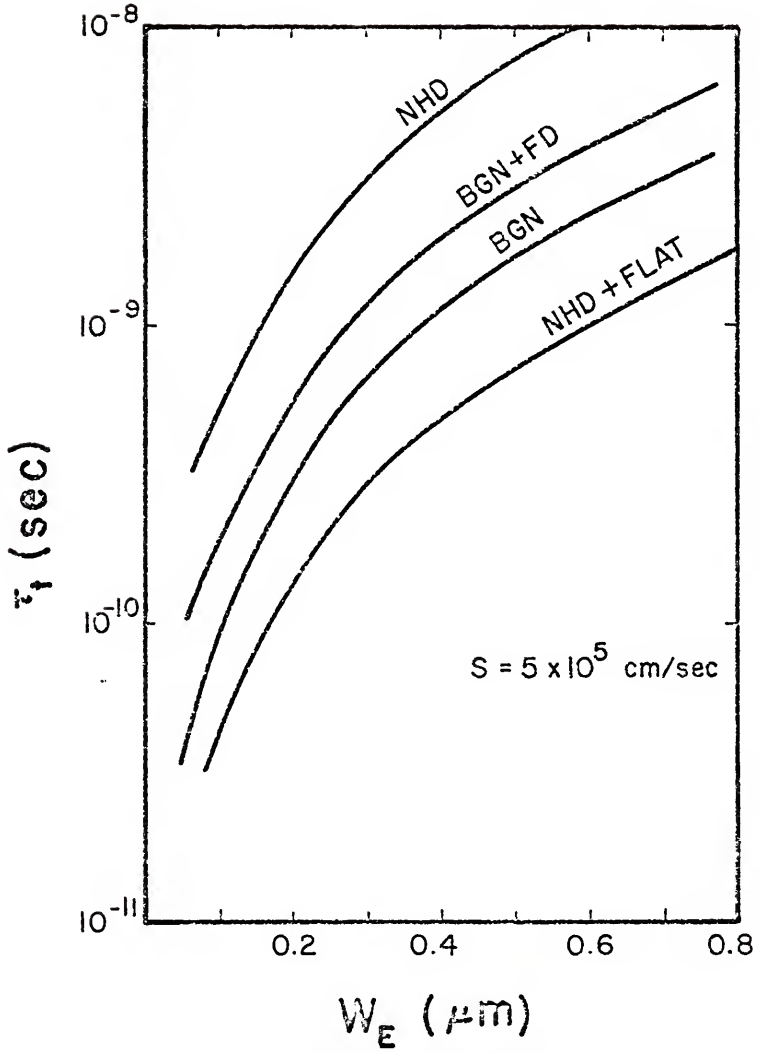

Figure 5.2 The transit time τ_t versus the width of the emitter region W_E for $S = 5 \times 10^5$ cm/sec and a Gaussian profile with: no heavy doping (NHD), bandgap narrowing (Slotboom-DeGraaff model) and Fermi Dirac statistics (BGN + FD), bandgap narrowing (Slotboom-DeGraaff model) only (BGN), and for a flat profile (NHD + flat)

If

$$S_P >> \frac{N_0(W_E)}{n_{ie}^2(W_E)} \cdot \frac{\bar{D}_P}{\int_0^{W_E} \frac{N_0(x)}{n_{ie}^2(x)}\, dx} \tag{5.21}$$

then (5.20) reduces to

$$J_{P0} \cong \frac{q\bar{D}_P}{\int_0^{W_E} \frac{N_0(x)}{n_{ie}^2(x)}\, dx} \tag{5.22}$$

which is the exact expression for an infinite surface recombination velocity. For

$$S_P << \frac{N_0(W_E)}{n_{ie}^2(W_E)} \cdot \frac{\bar{D}_P}{\int_0^{W_E} \frac{N_0(x)}{n_{ie}^2(x)}\, dx} \tag{5.23}$$

(5.20) reduces to

$$J_{P0} \cong \frac{qS_P n_{ie}^2(W_E)}{N_0(W_E)} \tag{5.24}$$

It is desirable to make J_{P0} small for the bipolar transistor. This results in a large emitter efficiency. For the pn-junction solar cell, if the emitter recombination current J_{P0} is small compared with

the base recombination current, the value of V_{OC} can approach the classical theoretical limit.

To illustrate the dependence of J_{P0} on S_p, consider the desirable case in the transparent-emitter model in which S_p is small enough to satisfy (5.23). Figures 5.3 and 5.4 show the variation of the emitter saturation current density, J_{P0}, and the transit time, τ_t, as a function of S_p for three models of bandgap narrowing: Slotboom and De Graaff [20], Hauser [12], and the recent model of Lanyon and Tuft [13], which has the form

$$\Delta E_G = 22.5 \times 10^{-3} \, (N/10^{18})^{1/2} \text{ eV}$$

for non-degenerately doped silicon, and (5.25)

$$\Delta E_G = 162. \times 10^{-3} \, (N/10^{20})^{1/6} \text{ eV}$$

for degenerately doped silicon. A Gaussian impurity profile is assumed with a surface impurtiy concentration of 10^{20} cm^{-3} and a junction depth of .25 μm. Full ionization of the impurity atoms is also assumed.

For values of S_p below 10^6 cm/sec, J_{P0} and τ_t vary rapidly with variations in S_p, while for values of S_p above 10^6 cm/sec, both J_{P0} and τ_t saturate. J_{P0} saturates to its largest value, and τ_t saturates to its lowest value. The largest value of J_{P0} at any S_p occurs for the Lanyon-Tuft model of bandgap narrowing.

The validity of the transparent-emitter model is based on the condition that the minority-carrier transit time is much smaller than the minority-carrier lifetime: $\tau_t << \tau_p$. To test this condition, τ_t

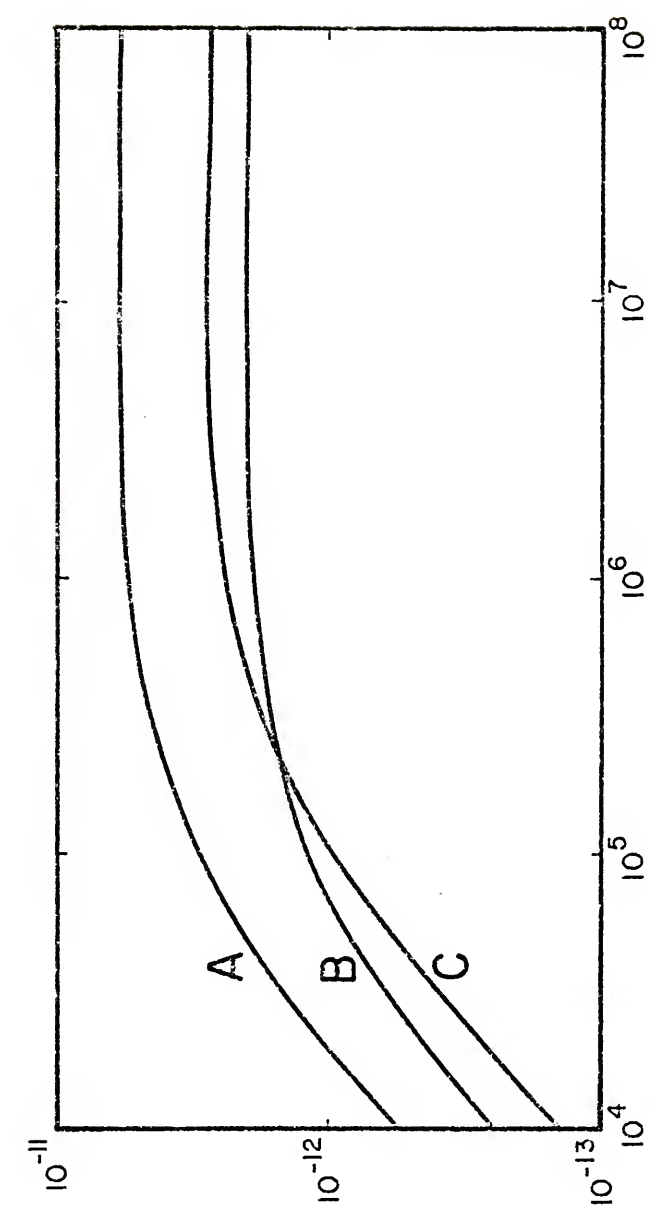

Figure 5.3 The emitter saturation current density J_{po} as a function of the surface recombination velocity S_p, for W_E = 0.25 μm, Fermi-Dirac statistics and bandgap narrowing included: (A) Lanyon-Tuft, (B) Hauser, and (C) Slotboom-DeGraaff. For low values of S_p (less than about 10^4 cm/sec) the self-consistency test yields $\tau_t > \tau_p$ so the emitter current is then due to Auger recombination and may be larger than values reported above.

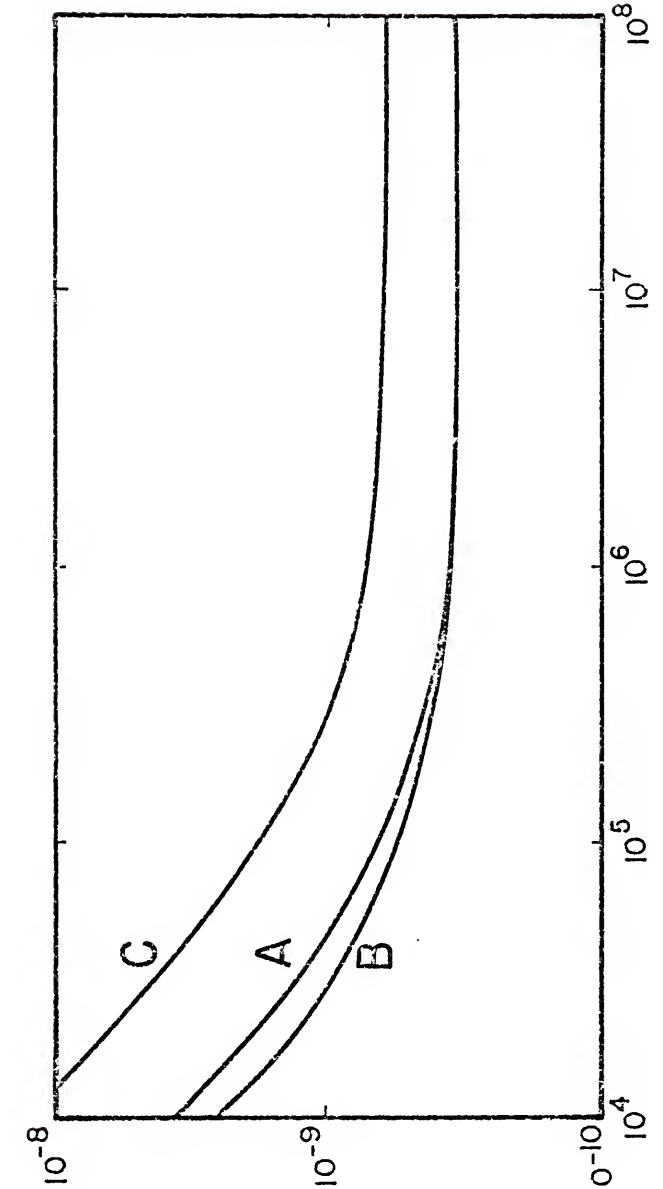

Figure 5.4 τ_t as a function of surface recombination velocity S_p for $W_E = 0.25\,\mu m$, Fermi-Dirac statistics and bandgap narrowing are included: (A) Lanyon-Tuft, (B) Hauser, and (C) Slotboom-DeGraaff

is calculated from (5.11). Values of τ_t are plotted in Figures 5.4 and 5.5. In Figure 5.4 τ_t is plotted as a function of S_p for the three models of bandgap narrowing (assuming W_E = .25 μm), while in Figure 5.5, values of τ_t are plotted as a function of the quasi-neutral emitter region width, W_E, for $S_p = 5 \times 10^5$ cm/sec. The recombination lifetime τ_p has an upper bound determined by the Auger band-to-band recombination at high impurity concentration.

To illustrate the self-consistency test for transparency, we assume the surface concentration of a diffused emitter to be 10^{20} cm^{-3}. With the impurity profile assumed Gaussian, this corresponds to an average Auger lifetime[1] of $\tau_A = 2.4 \times 10^{-9}$ sec. In Figures 5.4 and 5.5, we compare this lifetime with τ_t for each of the three bandgap narrowing models (assuming that W_E = 0.25 μm). Note that the emitter is completely transparent if S_p exceeds 10^5 cm/sec and is opaque if S_p is below 10^4 cm/sec.

5.5 Application to pn-Junction Silicon Solar Cells

In this section, we apply the transparent-emitter model to calculate the open-circuit voltage of silicon pn-junction solar cells having low substrate resistivity.

The open-circuit voltage is given by

$$V_{OC} \cong \frac{kT}{q} \ell n \frac{J_{SC}}{J_0} \tag{5.26}$$

---

[1]The average Auger recombination lifetime was calculated from a model similar to that of W. W. Sheng [37], in which the emitter is divided into two regions; one region has Shockley-Read-Hall recombination, and the surface region is dominated by Auger recombination.

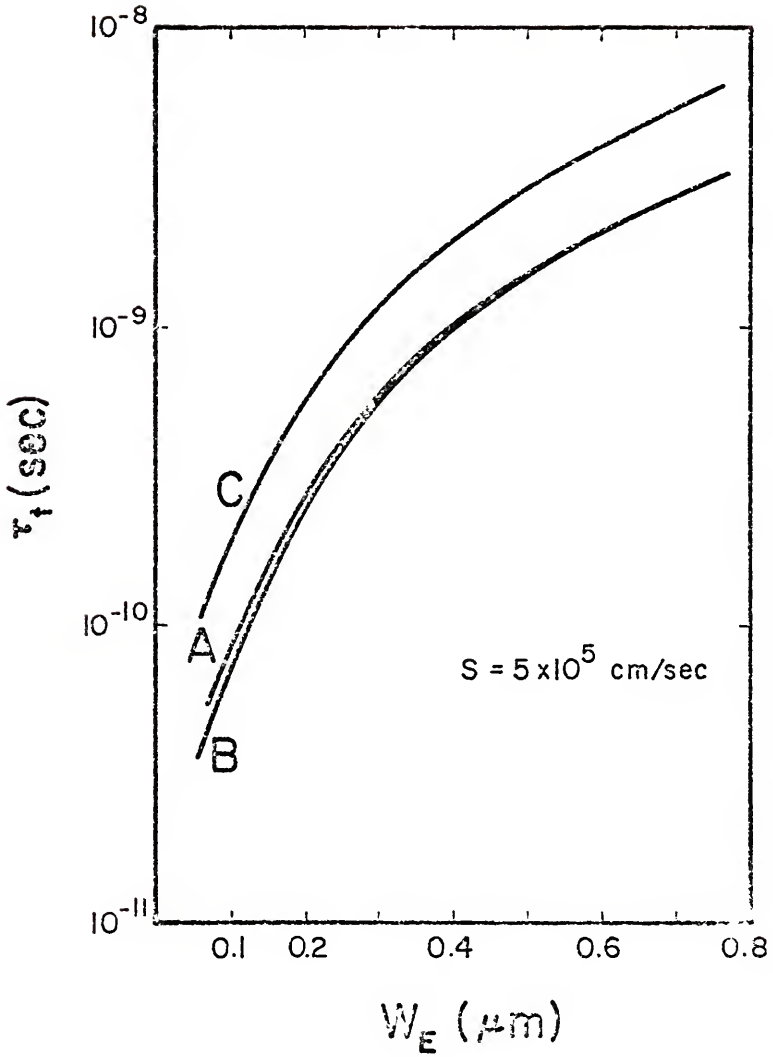

Figure 5.5 τ_t versus W_E for S = 5 x 10^5 cm/sec. Fermi-Dirac statistics and bandgap narrowing are included: (A) Lanyon-Tuft, (B) Hauser, and (C) Slotboom-DeGraaff

where J_{SC} is the short-circuit current density and J_0 is the saturation current of the solar cell in the dark. The saturation current density J_0 of the diode is

$$J_0 = J_{PO} + J_{NO} \tag{5.27}$$

where J_{PO} is the emitter minority-carrier saturation current density and J_{NO} is the base minority-carrier saturation current density.

The base saturation current density is

$$J_{NO} = \frac{qn_i^2 D_N}{N_{AA} L_N} \tag{5.28}$$

Consider low-resistivity silicon solar cells with base doping concentration of $N_{AA} = 5 \times 10^{17}$ cm^{-3}. Measurements made on such cells indicated the minority carrier diffusion length, L_N, to be 80 μm [66], corresponding to $J_{NO} \cong 6.2 \times 10^{-14}$ A/cm^2. The general expression for the transparent-emitter current density, given in (5.8), has yielded J_{PO} as a function of S_P, as shown in Figure 5.3.

Combining these characterizations for J_{NO} and J_{PO} with J_{SC} = 23 mA/cm^2 (AMO conditions) [1], we plot, in Figure 5.6, V_{OC} versus S_P. For low S_P (about 10^3 cm/sec), V_{OC} is limited by the base current, and for higher values of S_P, V_{OC} is limited by the emitter current, as has been observed experimentally [1]. Note that for $S_P > 10^5$ cm/sec, V_{OC} saturates to its lowest value. Note also that the Lanyon and Tuft model of bandgap narrowing gives lower values of V_{OC} (for any given value of S_P) than those given by the Slotboom and De Graaff and Hauser models.

Figure 5.6 V_{OC} versus S_P for W_E = 0.25 μm. Fermi-Dirac statistics and bandgap narrowing are included: (A) Lanyon-Tuft, (B) Hauser, and (C) Slotboom-DeGraaf. In (D) heavy-doping effects are not included. For low values of S_P (less than 10^4 cm/sec) V_{OC} is limited by the Auger-recombination current in the emitter because $\tau_t > \tau_p$ and V_{OC} may be lower than values suggested in this figure.

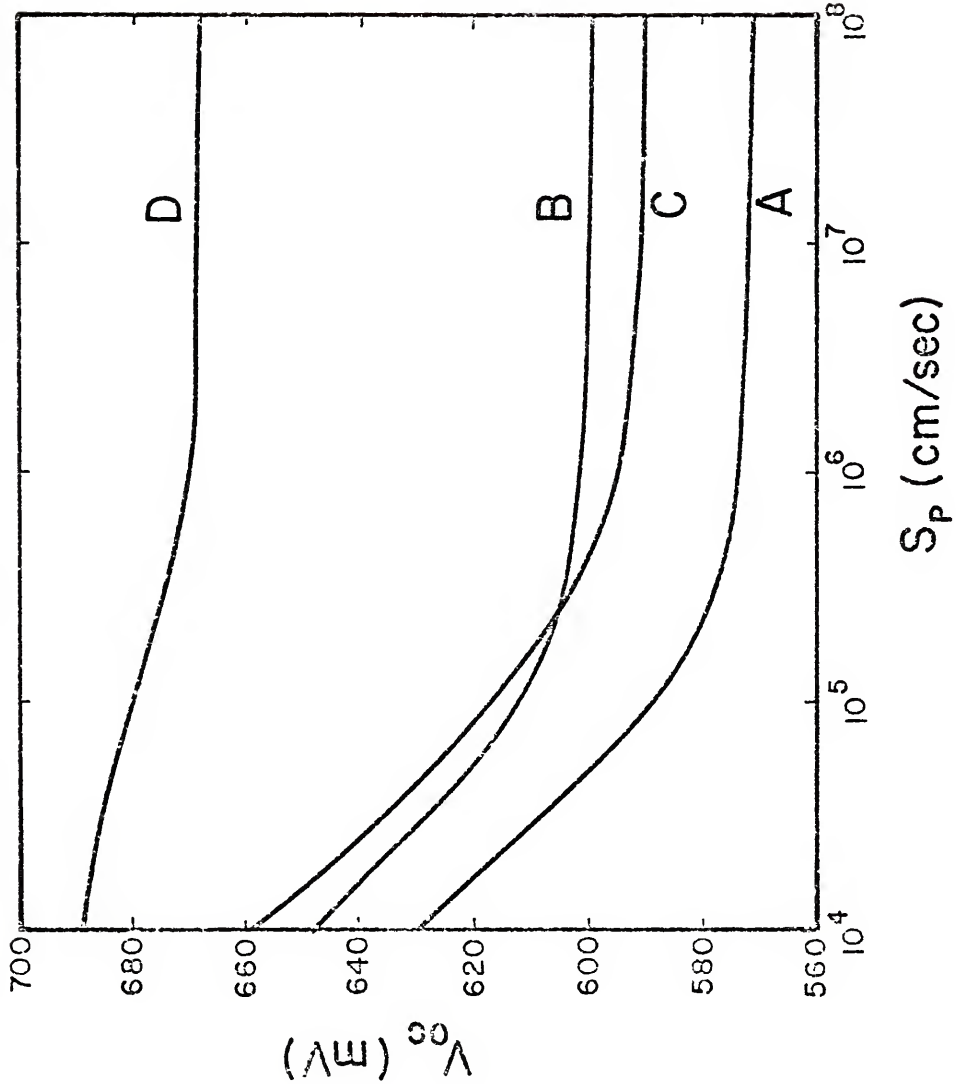
D
B
C
A
700
680
660
640
620
600
580
560
10^4
10^5
10^6
10^7
10^8
V_{oc} (mV)
S_p (cm/sec)

So far we have assumed, for simplicity, that all of the emitter surface is characterized by a single value of S_p. We now consider a more realistic structure of silicon solar cells, Figure 5.7. The emitter saturation current J_{P0} is the sum of three components from regions 1, 2, and 3 shown in Figure 5.7(b), [67]. The components of the current denisty from the metal-covered surface, region 1, and the nonmetal-covered surface, region 2, are given by (5.8). In region 3, the flow of minority carriers is two-dimensional since the minority carriers within about a diffusion length from region 1 are much more influenced by the high value of S_p of region 1 than they are by the relatively low value of S_p of region 2. To avoid the complexity of two-dimensional analysis, we make the first-order approximation that the component of J_{P0} from region 3 is essentially the same as that from region 1 ($J_{P3} \cong J_{P1}$) because S_p of the unmetallized surface can be made orders of magnitude smaller than S_p of the ohmic contact.

The emitter saturation is then

$$I_{P0} = (A_1 + A_3)\, J_{P01} + A_2 J_{P02} \tag{5.29}$$

where A_1 is the metallized surface area and $(A_2 + A_3)$ is the unmetallized surface area and J_{P01} and J_{P02} are the corresponding currents. The area A_3 is approximately equal to

$$A_3 \cong 2nL_G L_P \tag{5.30}$$

where n is the number of metal grid lines (or fingers), L_G is the length of the grid lines (see Figure 5.7), and $A_2 = A_T - (A_3 + A_1)$, A_T being the total area of the cell.

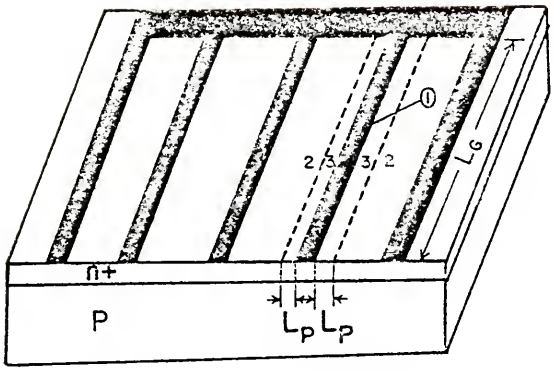

(a)

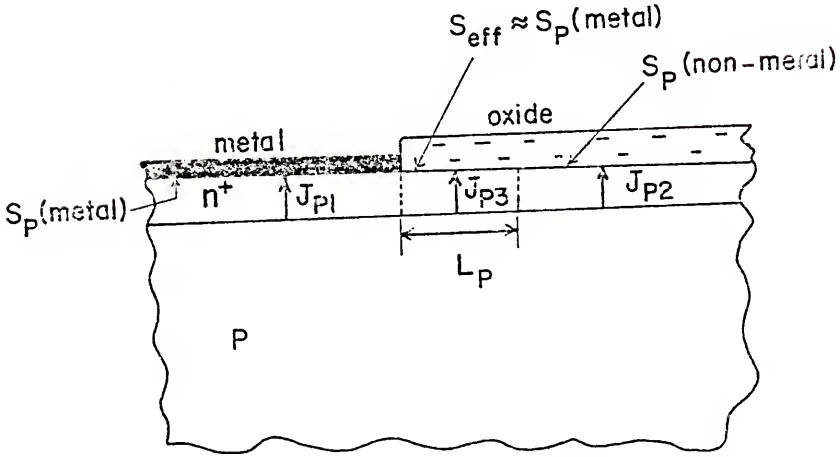

(b)

Figure 5.7 (a) The structure of a pn-junction solar cell
(b) The three components of the emitter current: J_{P1}, J_{P2}, and J_{P3}

As a numerical example, let $A_T = 4\ cm^2$, $L_G = 2$ cm, $n = 6$, $L_p \cong 1\ \mu m$, and assume 10% metal coverage. Then $A_1 \cong 0.4\ cm^2$, $A_2 \cong 3.59\ cm^2$, and $A_3 \cong 0.0024\ cm^2$. In this case, A_3 is negligible, and

$$V_{OC} = \frac{kT}{q} \ell n \frac{J_{SC}}{\frac{A_1}{A_T} \cdot J_{P01} + \frac{A_2}{A_T} \cdot J_{P02} + J_{NO}} \tag{5.31}$$

This expression can be used to estimate S_p of the nonmetallized surface from experimental values of V_{OC}. For diffused, thin-junction pn-junction solar cells made on low resistivity ($\cong 0.1\ \Omega$-cm) material, the maximum observed open-circuit voltage is about 600 mV [1]. As one example, if we consider the Lanyon-Tuft model of bandgap narrowing, and let S_p of the ohmic contact be 10^6 cm/sec, let the doping concentration be Gaussian with a surface concentration of $10^{20}\ cm^{-3}$. then by using (5.31), with $A_1/A_T = 0.1$ and $V_{OC} = 600$ mV, we get S_p (nonmetal) = 5×10^4 cm/sec. Thus the value for S_p could result in the low V_{OC} seen in conventional, diffused, thin-junction solar cells. Note that Figures 5.4 and 5.5 indicate the self-consistent validity of the transparency assumption for this device in the Lanyon-Tuft model which permits use of (5.20).

Although the preceding discussion has focused on the transparent-emitter model applied to N^+P silicon solar cells, the model can also be applied to P^+N cells. It is straightforward to show that heavy-doping effects (bandgap narrowing and Fermi-Dirac

statistics) degrade N^+P cell performance more than that of P^+N cells because the effective mass of electrons in silicon is greater than the effective mass of holes. The resulting different effective densities of states in the conduction and valence bands (N_C and N_V) cause the onset of degeneracy to occur at lower impurity concentrations in P-type material than in N-type material [32], if both N-type and P-type regions have the same bandgap narrowing. Thus the net effect of bandgap narrowing and Fermi-Dirac statistics is to degrade the N-type heavily doped region more than the P-type region with the same impurity concentration. This may, in part, be responsible for the high efficiency P^+NN^+ cells that have been observed experimentally [68-69].

5.6 Perspective

This chapter has dealt with the transparent-emitter model of a solar cell, which is defined by the condition that the minority carriers in the dark quasi-neutral emitter recombine mainly at the surface rather than in the bulk. Surface recombination can predominate over bulk recombination if the emitter junction depth is shallow enough and if the surface recombination velocity is high enough. In fact, this occurs in typical pn-junction silicon solar cells, as demonstrated by recent experiments showing the sensitivity of V_{OC} to the surface recombination velocity [29]. From a theoretical standpoint, the self-consistency test in Section 5.4 can determine the validity, for a given solar cell, of the transparent-emitter model, provided the emitter

recombination center density is low enough for the Auger process to dominate over the Shockley-Read-Hall process.

Although the transparent-emitter model may describe many conventional shallow pn-junction silicon solar cells, the high value of the surface recombination velocity S necessary to validate the transparent-emitter model is not necessarily desirable from a design point of view. Growth of a thermal SiO_2 layer on the emitter surface can substantially decrease S and increase V_{OC}. For such devices, the dark emitter recombination current is determined mainly by bulk recombination.

CHAPTER VI

A FIRST-ORDER ENGINEERING-DESIGN MODEL FOR HEAVILY DOPED SILICON DEVICES

6.1 Introduction

In the previous chapter, we presented a rigorous analytic model for the emitter that included bandgap narrowing, Fermi-Dirac statistics, and a finite surface recombination velocity at the emitter surface. The main assumption of that treatment is the transparency of the emitter to the injected minority carriers, that is, the transit time of the minority carriers is much less than their average bulk lifetime. This case can be physically realized if the emitter junction depth is shallow, and the surface recombination velocity is high.

In this chapter, we present a first-order engineering-design model that includes all the mechanisms of the transparent emitter model except that we relax, in this treatment, the transparency assumption and include a position-dependent Auger lifetime. Thus we provide a general first-order model that includes all the fundamental heavy-doping effects. This model can be easily used to characterize the minority-carrier current in the heavily doped emitter.

There is no analytic solution for the minority-carrier continuity equation when a position-dependent lifetime, impurity concentration, and $n_{ie}^2(x)$ are included. To provide a numerical solution, we developed a computer program that solves the continuity

equation. This computer solution serves two purposes. First, it provides information needed to characterize the first-order model. Second, it verifies the accuracy of the first-order model.

6.2 Modeling Approach

The key approximation of the first-order model is the assumption of a negligible net drift component in the minority-carrier current expression in the heavily doped emitter (see Equation (B.1) in Appendix B). The rationale for this approximation is discussed in [29].

To provide further justification, we note that the approximation is consistent with calculations, which include bandgap narrowing and Fermi-Dirac statistics, of the effective doping density, i.e., $(n_i^2/n_{ie}^2)N_{DD}$. Figures 6.1 and 6.2 show the effective doping densities for the Lanyon-Tuft model of bandgap narrowing [13] versus the actual doping densities N_{DD} and N_{AA}. Note that, in the range of doping from 10^{18} to about 10^{20} cm^{-3}, the effective doping density is nearly independent of the actual doping density, which corresponds to nearly zero net electric field for minority carriers.

In the first-order model, therefore, the minority carriers flow primarily by diffusion. We characterize the position-dependent diffusion length for minority carriers by an average value $\overline{L}_A$:

$$\overline{L}_A \equiv [\overline{D} \cdot \overline{\tau}_A]^{1/2} \tag{6.1}$$

where $\overline{D}$ is an average value for the diffusion coefficient and $\overline{\tau}_A$ is an average Auger lifetime for the minority carriers. We will later

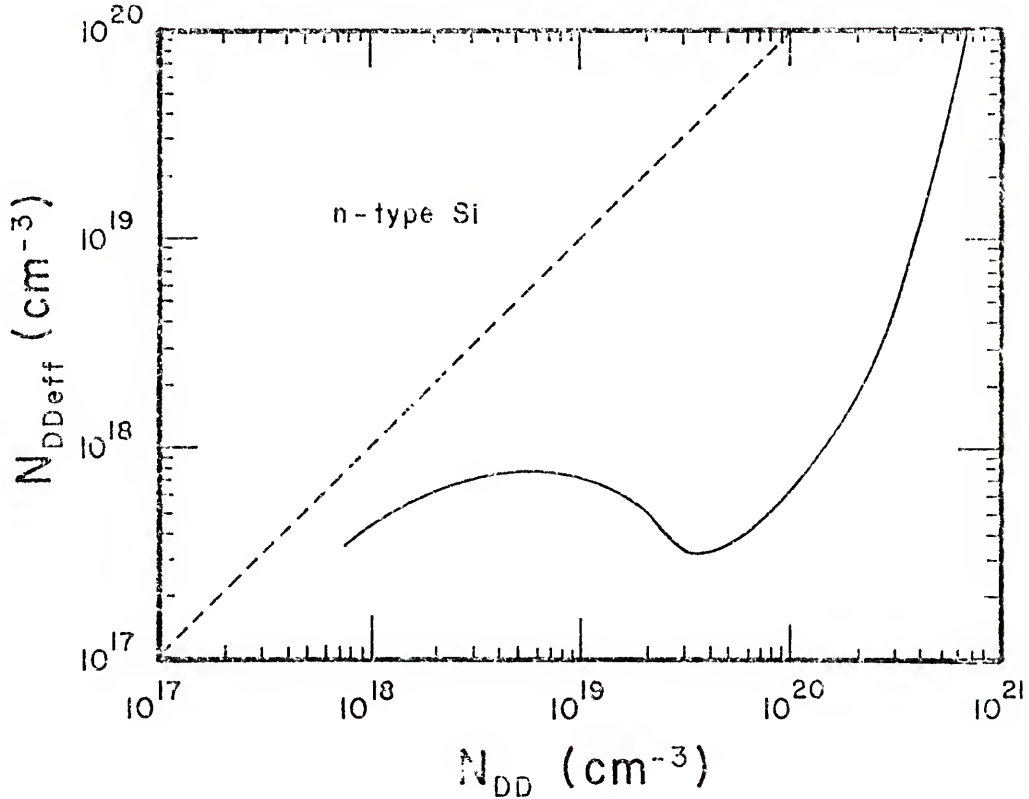

Figure 6.1 The effective doping density N_{DDeff} versus the actual doping density N_{DD} for N-type silicon. Lanyon-Tuft model of energy-bandgap narrowing and Fermi-Dirac statistics are included.

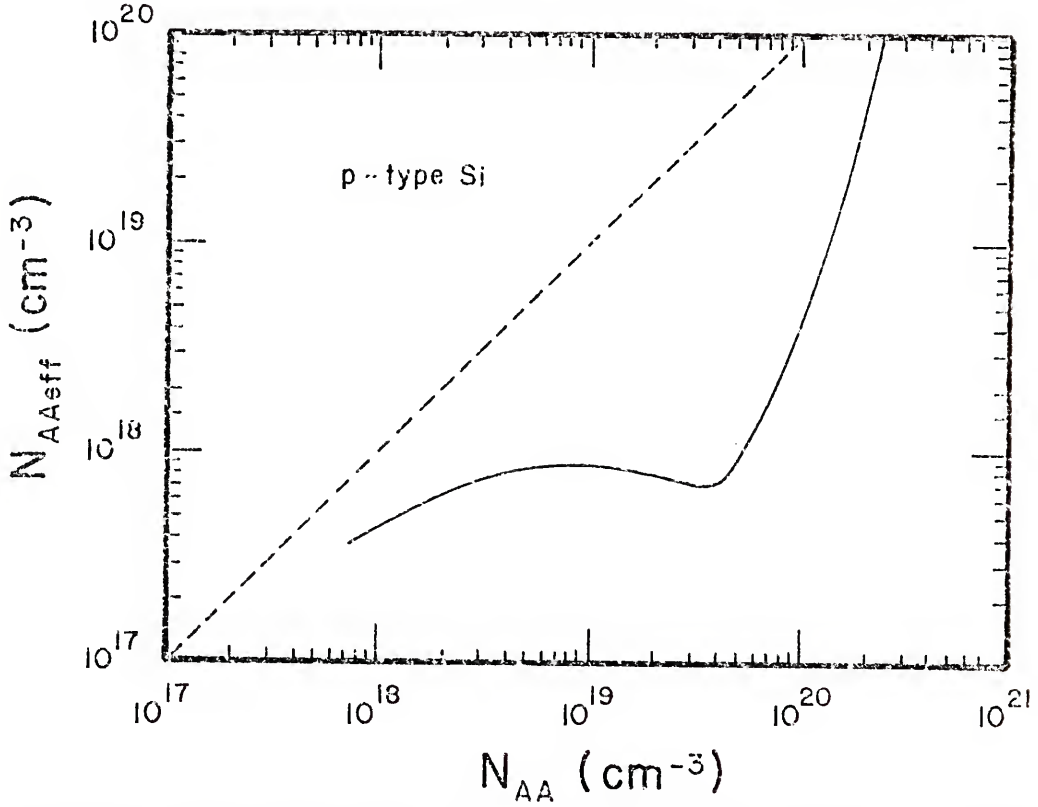

Figure 6.2 The effective doping density N_{AAeff} versus the actual doping density N_{AA} for P-type silicon. Lanyon-Tuft model of energy-bandgap narrowing and Fermi-Dirac statistics are included.

verify that the use of $\bar{L}_A$ is consistent with the results of the computer solution.

6.3 Development of the Model

Using the approximations of Section 6.2, we solve the minority-carrier continuity equation in the heavily doped emitter and obtain the following expression for the minority-carrier saturation current (J_{PO} in an N^+-emitter, for example):

$$J_{PO} = \frac{q\, n_i^2\, \bar{D}_P}{\bar{N}_{DDeff} \cdot \bar{L}_A} \cdot \frac{S_P \bar{L}_A + \bar{D}_P \tanh(W_E/\bar{L}_A)}{\bar{D}_P + S_P \bar{L}_A \tanh(W_E/\bar{L}_A)} \tag{6.2}$$

where S_P is the emitter surface recombination velocity for holes, W_E is the emitter quasi-neutral region width, and $\bar{N}_{DDeff}$ is an average effective doping density.

We can simplify (6.2) by considering the following special cases:

A. If $W_E \gg \bar{L}_A$, then (6.2) reduces to

$$J_{PO} \simeq \frac{q\, n_i^2\, \bar{D}_P}{\bar{N}_{DDeff} \cdot \bar{L}_A} \tag{6.3}$$

which is the familiar expression of the minority-carrier saturation current for a completely opaque emitter.

B. If $\bar{L}_A \gg W_E$, then (6.2) reduces to

$$J_{PO} \simeq \frac{q\, n_i^2}{\bar{N}_{DDeff}} \cdot \frac{[1 + W_E/\bar{\tau}_A S_P]}{[1/S_P + W_E/\bar{D}_P]} \tag{6.4}$$

We further simplify the expression in (6.4) by considering different values of S_p. If $S_p \approx 0$, then (6.4) reduces to

$$J_{PO} \approx \frac{q\, n_i^2}{\overline{N}_{DDeff}} \cdot \frac{W_E}{\overline{\tau}_A} \tag{6.5}$$

In this case J_{PO} is directly proportional to W_E. If S_p is very high ($S_p \rightarrow \infty$), then (6.4) reduces to

$$J_{PO} \approx \frac{q\, n_i^2}{\overline{N}_{DDeff}} \cdot \frac{\overline{D}_p}{W_E} \tag{6.6}$$

and J_{PO} is inversely proportional to W_E. For the case when

$$\overline{\tau}_A >> \frac{W_E}{S_p} \qquad \text{and} \qquad S_p << \frac{\overline{D}_p}{W_E}$$

then (6.4) reduces to

$$J_{PO} \approx \frac{q\, n_i^2}{\overline{N}_{DDeff}} \cdot S_p \tag{6.7}$$

and J_{PO} does not depend on W_E.

6.4 Relating Device Design Parameters to the First-Order Model's Parameters

In this section, we provide means for characterizing the parameters of the first-order model for any set of design parameters for the emitter. At least three design parameters need to be known to evaluate the recombination current of the emitter: the surface

impurity concentration N_S, the emitter quasi-neutral region width W_E, and the surface recombination velocity S. The parameters of the first-order model are $\overline{N}_{eff}$, $\overline{D}$, $\overline{\tau}_A$, W_E, and S.

We now describe how $\overline{N}_{eff}$, $\overline{D}$, and $\overline{\tau}_A$ are determined. We assume that the impurity profile is Gaussian. The parameter $\overline{N}_{eff}$ is obtained from a spatial average using Figures 6.1 and 6.2. In Figures 6.3 and 6.4, we plot average effective and actual doping densities, $\overline{N}_{DDeff}$ and $\overline{N}_{DD}$ for N-type and $\overline{N}_{AAeff}$ and $\overline{N}_{AA}$ for P-type, as functions of the surface impurity concentration N_S.

To find $\overline{D}$, we first evaluate the average doping density in the emitter (by averaging over the Gaussian profile), and find from tables the mobility of the minority carriers corresponding to $\overline{N}$. By using the Einstein relation in its non-degenerate or degenerate [70] form (depending on $\overline{N}$) we can calculate $\overline{D}$.

We characterize $\overline{\tau}_A$ as a function of N_S by Figures 6.5 and 6.6 for N-type and P-type silicon, respectively. These characterizations are derived from the rigorous computer-aided numerical solution.

6.5 Verification of First-Order Model by Computer Analysis

A computer program has been developed that solves the minority-carrier continuity equation with heavy-doping mechanisms such as energy-bandgap narrowing, Fermi-Dirac statistics, and a position-dependent lifetime included. This program (see Appendix D for a listing) is used to verify the accuracy of our first-order model and to characterize the average bulk Auger lifetime in the emitter

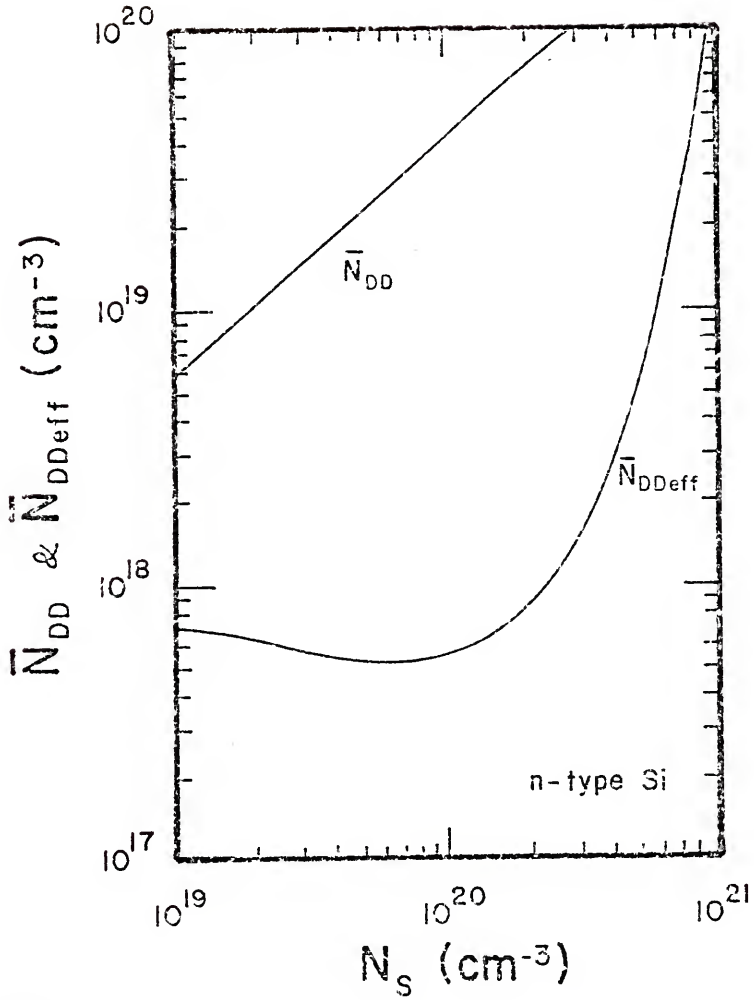

Figure 6.3 The average actual doping density $\bar{N}_{DD}$ and the average effective doping density $\bar{N}_{DDeff}$ versus the surface impurity concentration N_S for N-type silicon. Lanyon-Tuft model of energy bandgap narrowing and Fermi-Dirac statistics are included.

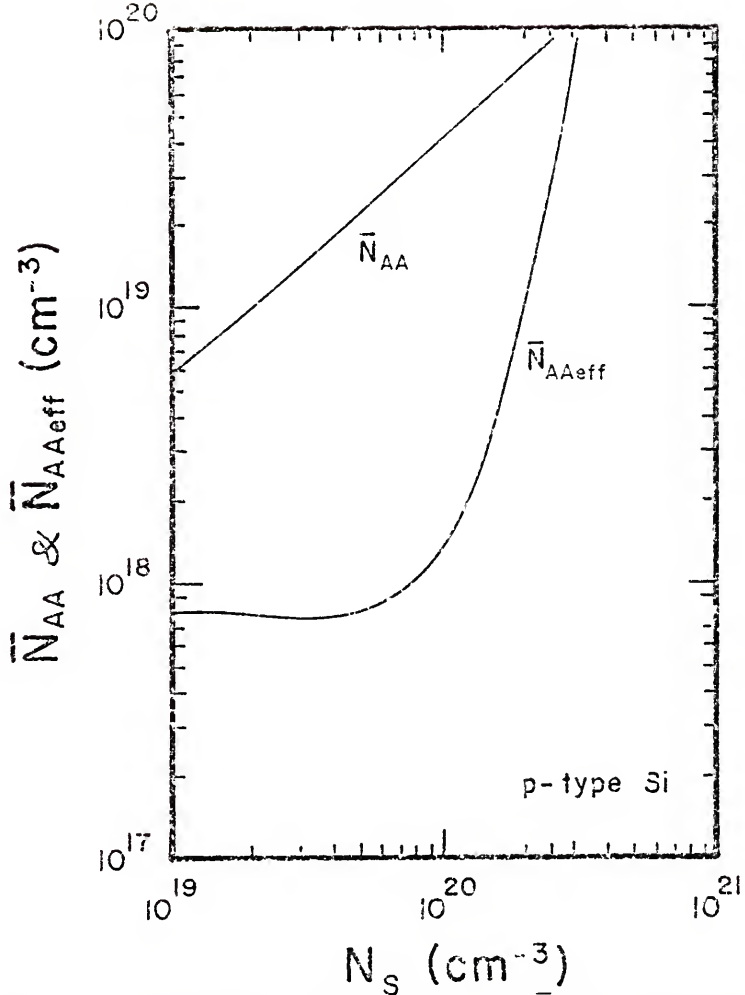

Figure 6.4 The average actual doping density $\bar{N}_{AA}$ and the average effective doping density $\bar{N}_{DDeff}$ versus the surface impurity concentration N_S for P-type silicon. Lanyon-Tuft model of energy-bandgap narrowing and Fermi-Dirac statistics are included.

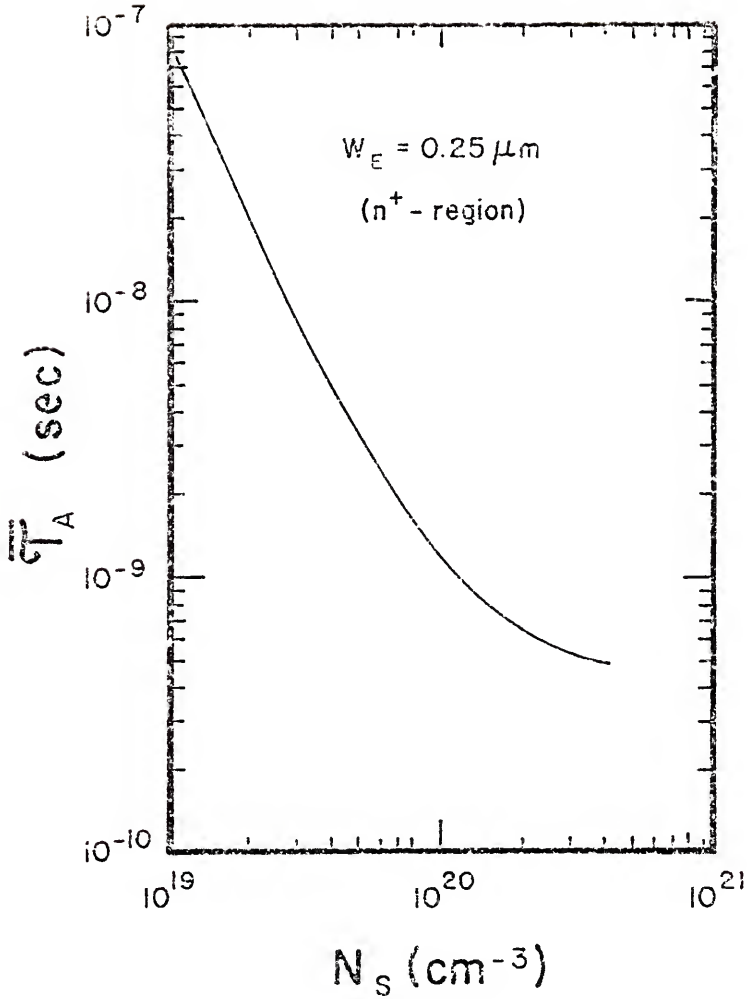

Figure 6.5 The average Auger lifetime $\bar{\tau}_A$ (calculated by computer-aided analysis) versus N_S for N-type silicon

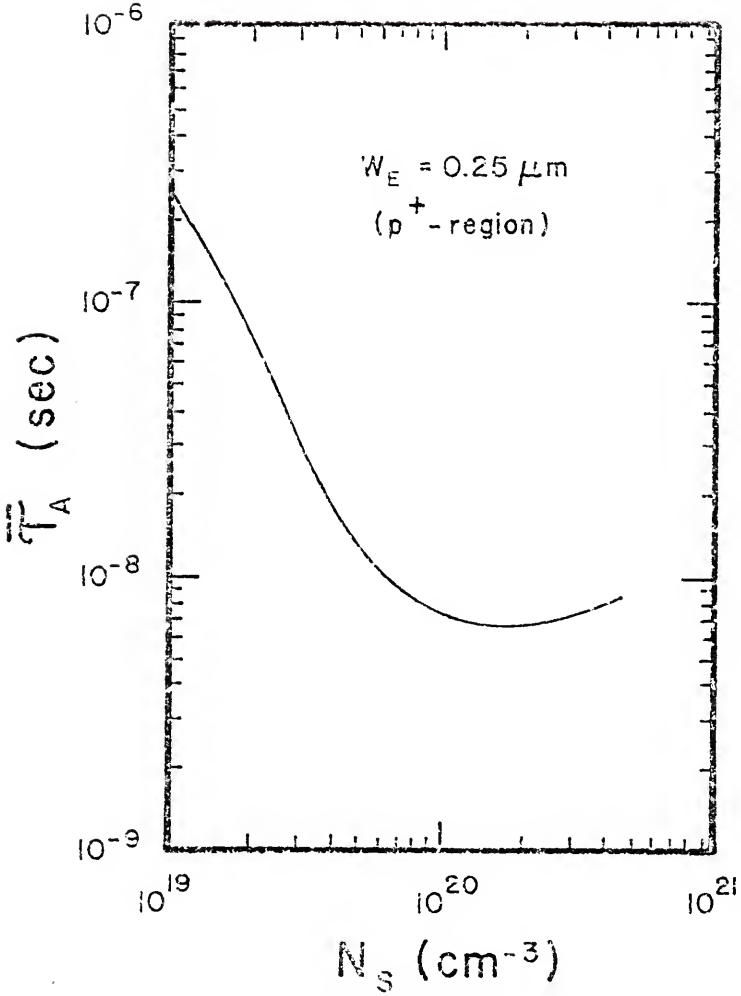

Figure 6.6 The average Auger lifetime $\bar{\tau}_A$ (calculated by computer-aided analysis) versus N_S for P-type silicon

as a function of the surface impurity concentration. Sample results of the computer-aided analysis are presented and discussed in Appendix E.

In Figures 6.7 and 6.8, we plot the minority-carrier saturation currents (and their surface and bulk components), J_{NO} in a P^+-emitter and J_{PO} in an N^+-emitter, as functions of S_N and S_P, respectively, for $N_S = 10^{20}$ cm^{-3} and $W_E = 0.25$ μm. The curves are derived from our computer-aided analysis and the points are derived from calculations using the first-order model as described earlier in this chapter. Note the good agreement between the results of the first-order model and those of the computer-aided analysis.

In Tables III, IV, and V, we compare values of the minority-carrier saturation current obtained from the first-order model and the numerical analysis for N^+- and P^+-emitters having $N_S = 10^{19}$ cm^{-3} (Table III), 10^{20} cm^{-3} (Table IV), and 4×10^{20} cm^{-3} (Table V). Note that good agreement is obtained for $N_S = 10^{19}$ cm^{-3} and 10^{20} cm^{-3} in both N^+- and P^+-emitters. For $N_S = 4 \times 10^{20}$ cm^{-3}, fair agreement is obtained for the N^+-emitter, but poor agreement is obtained for the P^+-emitter. The inadequacy of the first-order model for this latter case can be explained by noting the differences between Figures 6.1 and 6.2 In Figure 6.1 (N^+-emitter), the range of flatness of N_{DDeff} extends up to about $N_{DD} = 4 \times 10^{20}$ cm^{-3}, whereas in Figure 6.2 (P^+-emitter) the flatness of N_{AAeff} extends up to only about $N_{AA} = 2 \times 10^{20}$ cm^{-3}. Hence, at about $N_S = 4 \times 10^{20}$ cm^{-3}, the first-order model does not give accurate results for P^+-regions, although it gives

Figure 6.7 The electron saturation current J_{NO} and its surface and Auger components (J_{NSO} and J_{NAO}) versus the electron surface recombination velocity S_N for a P^+-emitter. Solid curves are for the numerical solution and the points are for first-order model.

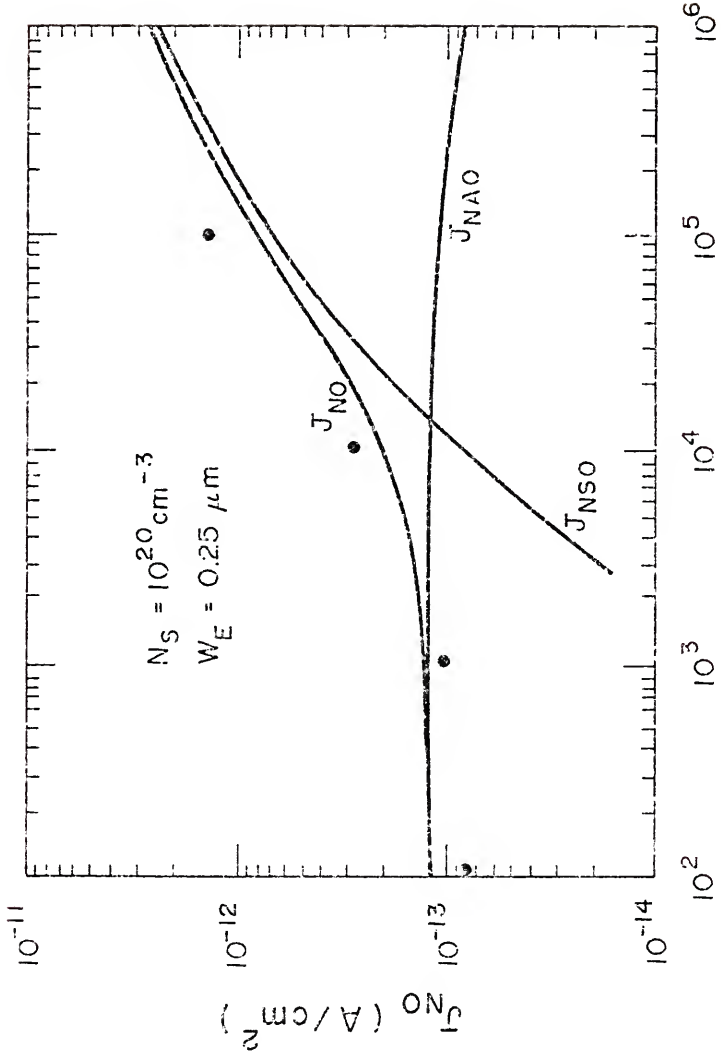
$N_S = 10^{20} cm^{-3}$
$W_E = 0.25\ \mu m$
J_{NO}
J_{NAO}
J_{NSO}
10^{-11}
10^{-12}
10^{-13}
10^{-14}
10^2
10^3
10^4
10^5
10^6
S_N (cm / sec)
σ_{NO} (A/cm^2)

Figure 6.8 The hole saturation current J_{P0} and its surface and Auger components (J_{PS0} and J_{PA0}) versus the hole surface recombination velocity S_p for an N^+-emitter. Solid curves are for the numerical solution and the points are for first-order model.

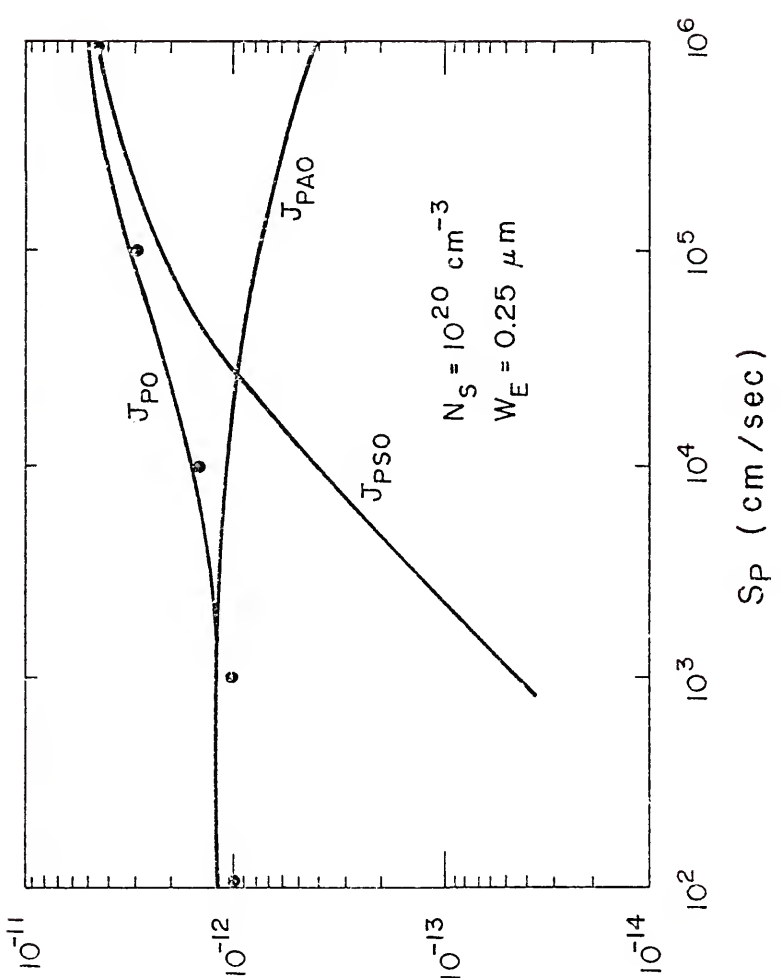
J_{PO}
J_{PAO}
J_{PSO}
$N_S = 10^{20}$ cm^{-3}
$W_E = 0.25$ μm
J_{PO} (A/cm^2)
10^{-11}
10^{-12}
10^{-13}
10^{-14}
10^2
10^3
10^4
10^5
10^6
S_P (cm/sec)

TABLE III

COMPARISON OF EMITTER SATURATION CURRENT CALCULATED FROM FIRST-ORDER MODEL AND COMPUTER-AIDED ANALYSIS FOR $N_S = 10^{19}$ cm^{-3}--EXCELLENT AGREEMENT IS OBTAINED FOR BOTH N^+P AND P^+N DEVICES.

W_E= 0.25 μm	$N_S = 10^{19}$ cm^{-3}			
	N^+P: J_{P0}A/cm^2		P^+N: J_{N0}A/cm^2	
S (cm/sec)	Numerical Solution	First-Order Model	Numerical Solution	First-Order Model
10^2	1.9×10^{-14}	1.9×10^{-14}	8.2×10^{-15}	8.6×10^{-15}
10^3	6.3×10^{-14}	6.7×10^{-14}	4.4×10^{-14}	5.0×10^{-14}
10^4	4.5×10^{-13}	4.7×10^{-13}	3.8×10^{-13}	4.1×10^{-13}
10^5	2.3×10^{-12}	2.3×10^{-12}	2.6×10^{-12}	2.9×10^{-12}
10^6	3.8×10^{-12}	3.4×10^{-12}	6.1×10^{-12}	6.3×10^{-12}
10^7	4.1×10^{-12}	4.0×10^{-12}	7.0×10^{-12}	7.2×10^{-12}

TABLE IV

COMPARISON OF EMITTER SATURATION CURRENT CALCULATED FROM FIRST-ORDER MODEL AND COMPUTER-AIDED ANALYSIS FOR $N_S = 10^{20}$ cm^{-3}--GOOD AGREEMENT IS OBTAINED FOR BOTH N^+P AND P^+N DEVICES.

W_E = 0.25 μm	$N_S = 10^{20}$ cm^{-3}			
	N^+P: $J_{PO}A/cm^2$		P^+N: $J_{NO}A/cm^2$	
S (cm/sec)	Numerical Solution	First Order Model	Numerical Solution	First-Order Model
10^2	1.2×10^{-12}	9.9×10^{-13}	1.2×10^{-13}	8.2×10^{-14}
10^3	1.2×10^{-12}	1.0×10^{-12}	1.3×10^{-13}	1.0×10^{-13}
10^4	1.6×10^{-12}	1.4×10^{-12}	2.0×10^{-13}	3.1×10^{-13}
10^5	3.2×10^{-12}	3.0×10^{-12}	8.0×10^{-13}	1.6×10^{-12}
10^6	5.1×10^{-12}	4.5×10^{-12}	2.7×10^{-12}	3.4×10^{-12}
10^7	5.4×10^{-12}	4.4×10^{-12}	3.8×10^{-12}	3.8×10^{-12}

TABLE V

COMPARISON OF EMITTER SATURATION CURRENT
FROM FIRST-ORDER MODEL AND COMPUTER-AIDED
NUMERICAL ANALYSIS FOR $N_S = 4 \times 10^{20}$--FOR THIS CASE
FAIR ACCURACY IS OBTAINED FOR N^+P BUT
POOR ACCURACY IS OBSERVED FOR P^+N.

$W_E = 0.25$ μm	$N_S = 4 \times 10^{20}$ cm^{-3}			
	N^+P: J_{P0}A/cm^2		P^+N: J_{N0}A/cm^2	
S (cm/sec)	Numerical Solution	First-Order Model	Numerical Solution	First-Order Model
10^2	1.9×10^{-12}	6.5×10^{-13}	6.9×10^{-14}	1.9×10^{-16}
10^3	1.9×10^{-12}	6.6×10^{-13}	6.9×10^{-14}	2.4×10^{-16}
10^4	2.0×10^{-12}	2.3×10^{-13}	6.9×10^{-14}	7.2×10^{-16}
10^5	2.0×10^{-12}	1.0×10^{-12}	6.8×10^{-14}	3.9×10^{-15}
10^6	2.2×10^{-12}	1.3×10^{-12}	6.8×10^{-14}	8.4×10^{-15}
10^7	2.3×10^{-12}	1.3×10^{-12}	6.8×10^{-14}	9.6×10^{-15}

reasonably accurate results for N^+-regions. The physical reason for the differences in Figures 6.1 and 6.2 is that the onset of degeneracy in P^+-emitters occurs at a lower doping density than for N^+-emitters; N_{AAeff} rises sharply due to degeneracy of the charge-carriers at a lower doping density than that at which N_{DDeff} rises.

6.6 Experimental Support

There are limited experimental data that support the first-order model. These data [29], given in Table II, indicate that a reduction in the emitter surface recombination velocity for a variety of silicon solar cells increases the open-circuit voltage. The emitter currents predicted by the first-order model, and verified by the computer-aided analysis, yield values of V_{OC} in rough agreement with these experimental data. We will consider these data further in the next chapter.

6.7 Summary and Conclusions

In this chapter, we established a first-order engineering-design model for heavily doped silicon devices and solar cells that accounts for fundamental heavy-doping mechanisms. After developing the model and discussing its assumptions, we related the emitter design parameters to the parameters of the first-order model. We then verified the accuracy of the first-order model for both N^+- and P^+-emitters by using results of a rigorous computer-aided analysis. We found that the first-order model is valid for surface concentrations up to about 2×10^{20} cm^{-3} for P^+-emitters and up to about

4×10^{20} cm^{-3} for N^+-emitters. The difference in the range of validity of the first-order model between N^+- and P^+- emitters is attributed to the onset of degeneracy in P^+- regions occurring at a lower impurity concentration than in N^+-regions.

The first-order model is useful in the design of heavily doped silicon bipolar devices and solar cells. The model provides a simple, but sufficiently accurate, evaluation of the emitter recombination current that can be effectively used in such designs.

CHAPTER VII

COMPUTER-AIDED STUDY OF V_{OC} IN N^+P AND P^+N SILICON SOLAR CELLS

7.1 Introduction

In this chapter, we present the results of a rigorous computer-aided numerical analysis of the heavily doped emitter in silicon solar cells. The purpose of this treatment is to study the dependence of V_{OC} on the design parameters of the emitter in N^+P and P^+N silicon solar cells.

We include the following fundamental heavy-doping mechanisms: bandgap narrowing, Fermi-Dirac statistics, and Auger recombination. We also include a finite surface recombination velocity at the emitter surface. We assume low-level injection in the heavily doped emitter; this assumption does not significantly limit the applicability of the analysis.

7.2 Dependence of V_{OC} on the Emitter Design Parameters in N^+P and P^+N Silicon Solar Cells

The open-circuit voltage V_{OC} is given by

$$V_{OC} \simeq \frac{kT}{q} \ln \frac{J_{SC}}{J_{BO} + J_{EO}} \tag{7.1}$$

where J_{SC} is the short-circuit current density and J_{BO} and J_{EO} are the base and emitter saturation current densities. In this treatment, both

J_{SC} and J_{BO} are determined by experimental measurements [1,66], and J_{EO} is characterized from our computer-aided analysis (see Appendix E).

In studying the dependence of V_{OC} on J_{EO}, we assume that J_{SC} and J_{BO} do not change. This is a reasonable assumption since variations in the emitter design do not affect J_{BO} and do not change J_{SC} enough to cause considerable changes in V_{OC}. We let J_{SC} = 23 mA/cm^2 [1] and $J_{BO} = 6.2 \times 10^{-14}$ A/cm^2 for an N^+P cell and 3.1×10^{-14} A/cm^2 for a P^+N cell, which correspond to a diffusion length in the base of about 80 μm [66] and a doping density of about 5×10^{17} cm^{-3} for N-type and P-type substrates. Note that our assumed value of J_{SC} is not essential for this study and any experimentally measured value can be incorporated into our results below by adjusting the values of V_{OC} in this chapter accordingly.

7.2A Dependence of V_{OC} on W_E

We have studied the dependence of V_{OC} on W_E for several values of the surface recombination velocity S, in both N^+- and P^+-emitters. Two values of the surface impurity concentration, $N_S = 10^{19}$ cm^{-3} and $N_S = 10^{20}$ cm^{-3}, have been used. The impurity profile in all cases considered is Gaussian.

In Figures 7.1 and 7.2, we plot V_{OC} versus W_E for values of S ranging from 10^2 to 10^7 cm/sec for $N_S = 10^{19}$ cm^{-3}. These curves, for N^+P and P^+N cells, imply the following:

A. The surface recombination velocity significantly affects V_{OC} in both N^+P and P^+N cells. Thus,

Figure 7.1 The open-circuit voltage V_{OC} for an N^+P silicon solar cell versus the emitter quasi-neutral region width W_E for several values of the surface recombination velocity S_P

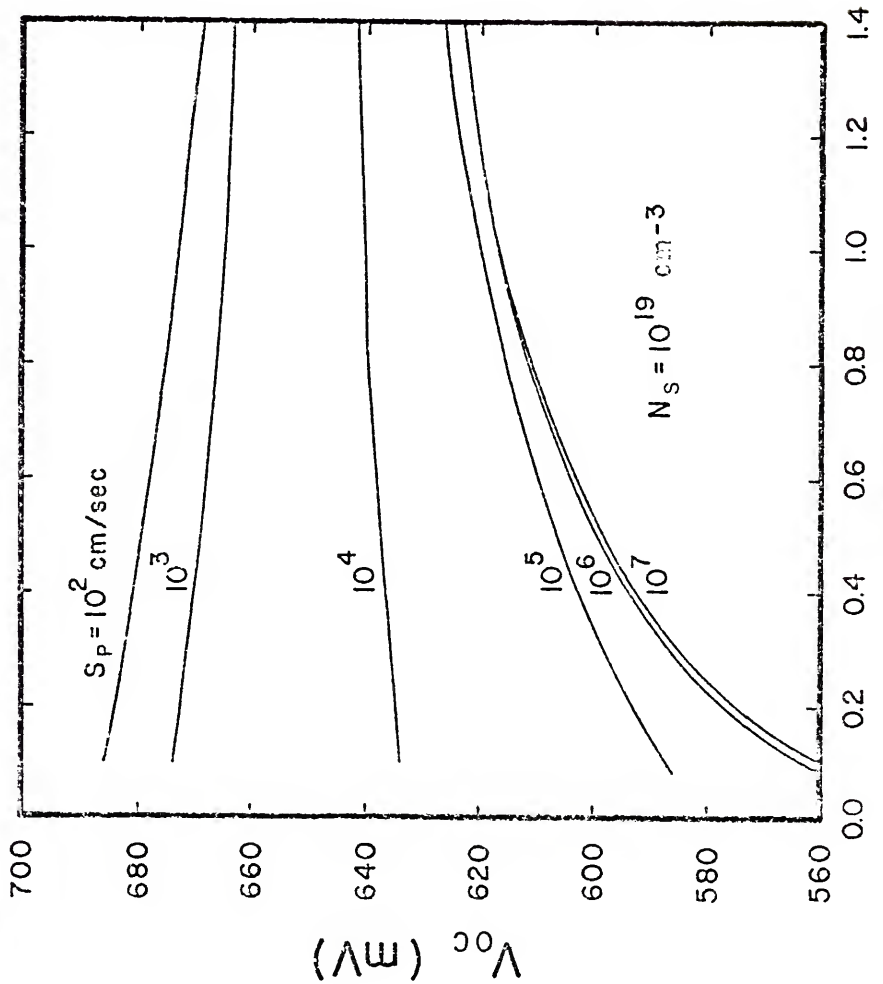
V_{oc} (mV)
700
680
660
640
620
600
580
560
0.0
0.2
0.4
0.6
0.8
1.0
1.2
1.4
W_E (μm)
$S_p = 10^2$ cm/sec
10^3
10^4
10^5
10^6
10^7
$N_s = 10^{19}$ cm^{-3}

Figure 7.2 The open-circuit voltage V_{OC} for a P^+N silicon solar cell versus the emitter quasi-neutral region width W_E for several values of the surface recombination velocity S_N

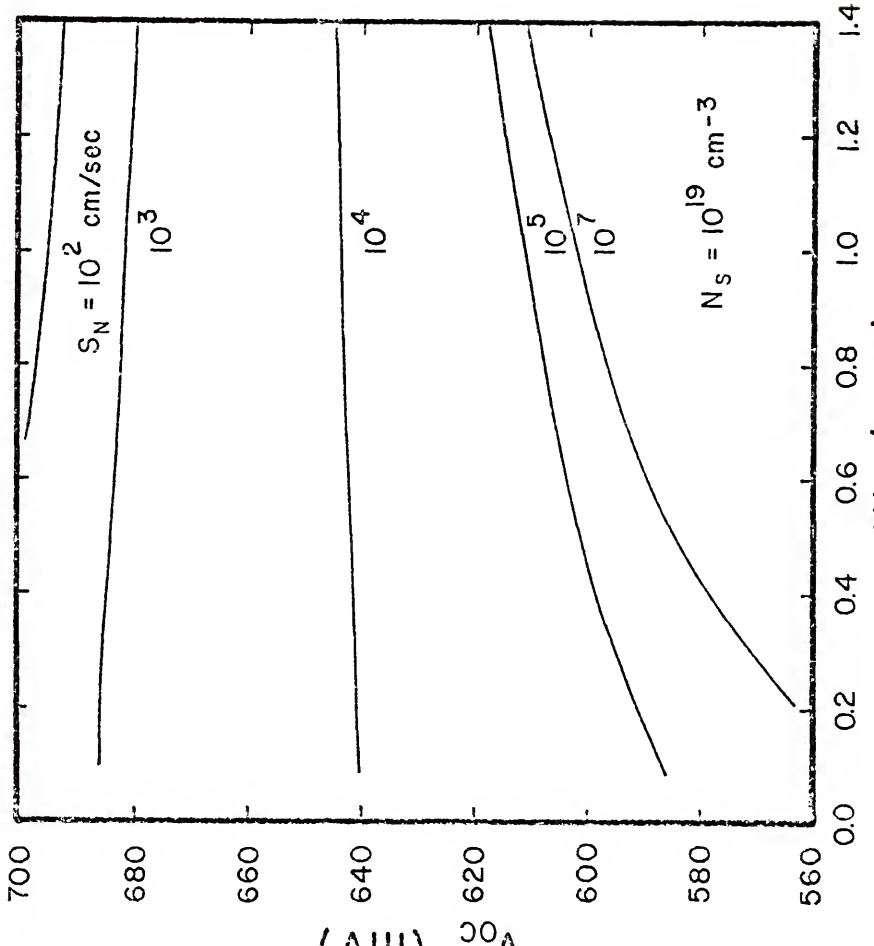
$S_N = 10^2$ cm/sec
10^3
10^4
10^5
10^7
$N_S = 10^{19}$ cm^{-3}
V_{OC} (mV)
700
680
660
640
620
600
580
560
0.0
0.2
0.4
0.6
0.8
1.0
1.2
1.4
W_E (μm)

for low surface concentrations, a low surface recombination velocity will result in a high value of V_{OC}.

B. The range of the surface recombination velocity that significantly affects V_{OC} is $10^2 \leq S \leq 10^7$ cm/sec. Reducing S below 10^2 cm/sec does not significantly affect V_{OC}.

C. In the range of S described above, S affects V_{OC} more in P^+N cells than in N^+P cells. That is, the spread in values of V_{OC} due to different S, for any value of W_E, is larger in P^+N cells than in N^+P cells.

D. Except for $S > 10^5$ cm/sec, V_{OC} is nearly insensitive to variations in W_E. For $S > 10^5$ cm/sec, V_{OC} increases with W_E.

E. Even when $W_E > 1$ μm, V_{OC} is affected by variations in S for both N^+P and P^+N cells.

The main conclusion suggested by Figures 7.1 and 7.2 is that for low emitter doping concentrations (less than or equal to 10^{19} cm^{-3}), the most important design parameter is the surface recombination velocity. By reducing S, V_{OC} can be increased.

The dependence of V_{OC} on W_E for $N_S = 10^{20}$ cm^{-3} is shown in Figures 7.3 and 7.4 for N^+P and P^+N cells, respectively. These results imply:

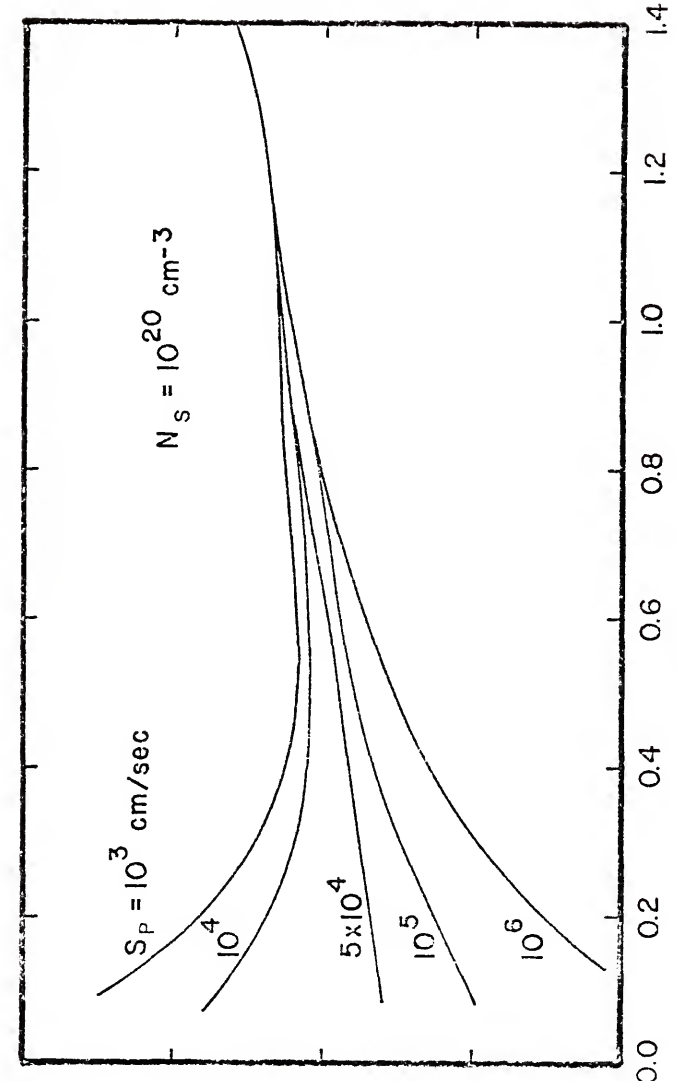

Figure 7.3 The open-circuit voltage V_{OC} for an N^+P silicon solar cell versus the emitter quasi-neutral region width W_E for several values of the surface recombination velocity S_P

Figure 7.4 The open-circuit voltage V_{OC} for a P^+N silicon solar cell versus the emitter quasi-neutral region width W_E for several values of the surface recombination velocity S_N

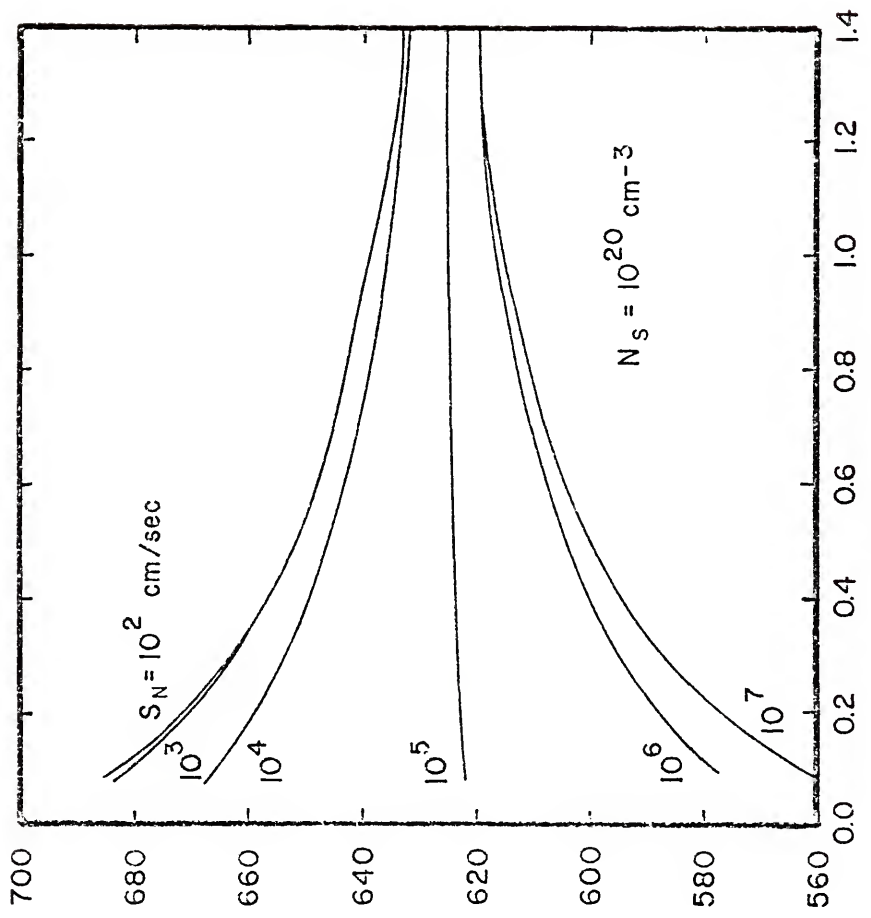
V_{oc} (mV)
700
680
660
640
620
600
580
560
0.0
0.2
0.4
0.6
0.8
1.0
1.2
1.4
W_E (μm)
$S_N = 10^2$ cm/sec
10^3
10^4
10^5
10^6
10^7
$N_S = 10^{20}$ cm^{-3}

A. Variations of S in the range $10^2 \leq S \leq 10^7$ cm/sec affect V_{OC}, for both N^+P and P^+N cells, but less significantly than for the cells having $N_S = 10^{19}$ cm^{-3}.

B. There is a considerable difference in the effect of S in N^+-emitters compared to P^+-emitters. In N^+P cells S affects V_{OC} considerably if W_E is less than 0.5 μm, while in P^+N cells, S affects V_{OC} appreciably if W_E is less than 1 μm.

C. The spread in V_{OC} due to variations of S in the range $10^2 \leq S \leq 10^7$ cm/sec, at low values of W_E, is larger in P^+N cells than in N^+P cells. For example, if W_E = 0.2 μm, the spread in V_{OC} is about 100 mV for P^+N cells compared to about 50 mV for N^+P cells.

D. For both N^+P and P^+N cells, V_{OC} is sensitive to variations in W_E for low and high values of S, but is nearly insensitive to variations in W_E for S in the range 10^4-10^5 cm/sec.

E. For large values of W_E(> 0.5 μm in N^+P cells and 1 μm in P^+N cells), V_{OC} saturates at about 630 mV for P^+N cells and 610 mV for N^+P cells.

We will discuss the significance and the physical interpretation of the above results later in this chapter.

7.2B Dependence of V_{OC} on N_S

We have studied the variation of V_{OC} as a function of N_S for several values of S in N^+P and P^+N cells. The width of the emitter quasi-neutral region for these studies was assumed to be 0.25 μm. We plot in Figures 7.5 and 7.6 V_{OC} versus N_S for N^+P and P^+N silicon solar cells. We observe that:

A. Surface recombination velocity affects V_{OC} if N_S is less than 4×10^{20} cm^{-3} for N^+P and P^+N cells. The sensitivity to S is most pronounced at the lowest surface doping concentrations.

B. For high values of S ($> 10^4$ cm/sec), all the curves of V_{OC} versus N_S have minima at about $N_S = 5 \times 10^{19}$ cm^{-3}, and V_{OC} increases (slowly for N^+P cells and rapidly for P^+N cells) as N_S increases above 5×10^{19} cm^{-3}.

C. For high values of N_S ($> 4 \times 10^{20}$ cm^{-3}), V_{OC} saturates, independently of S, at about 680 mV for P^+N cells and at 600 mV for N^+P cells.

7.2C Dependence of V_{OC} on S

In Figure 7.7, for both N^+P and P^+N structures, we compare quantitatively the dependence of V_{OC} on S for $N_S = 10^{20}$ cm^{-3} and $W_E = 0.25$ μm. As observed before, variation in S affects V_{OC} more in P^+N cells than in N^+P cells. Note that V_{OC} versus S curves saturate at low S ($< 10^4$ cm/sec). For the P^+N cell, V_{OC} saturates at about 670 mV, while for the N^+P cell, V_{OC} saturates at about 610 mV.

Figure 7.5 The open-circuit voltage V_{OC} for an N^+P silicon solar cell versus the surface impurity concentration N_S for several values of the surface recombination velocity S_P

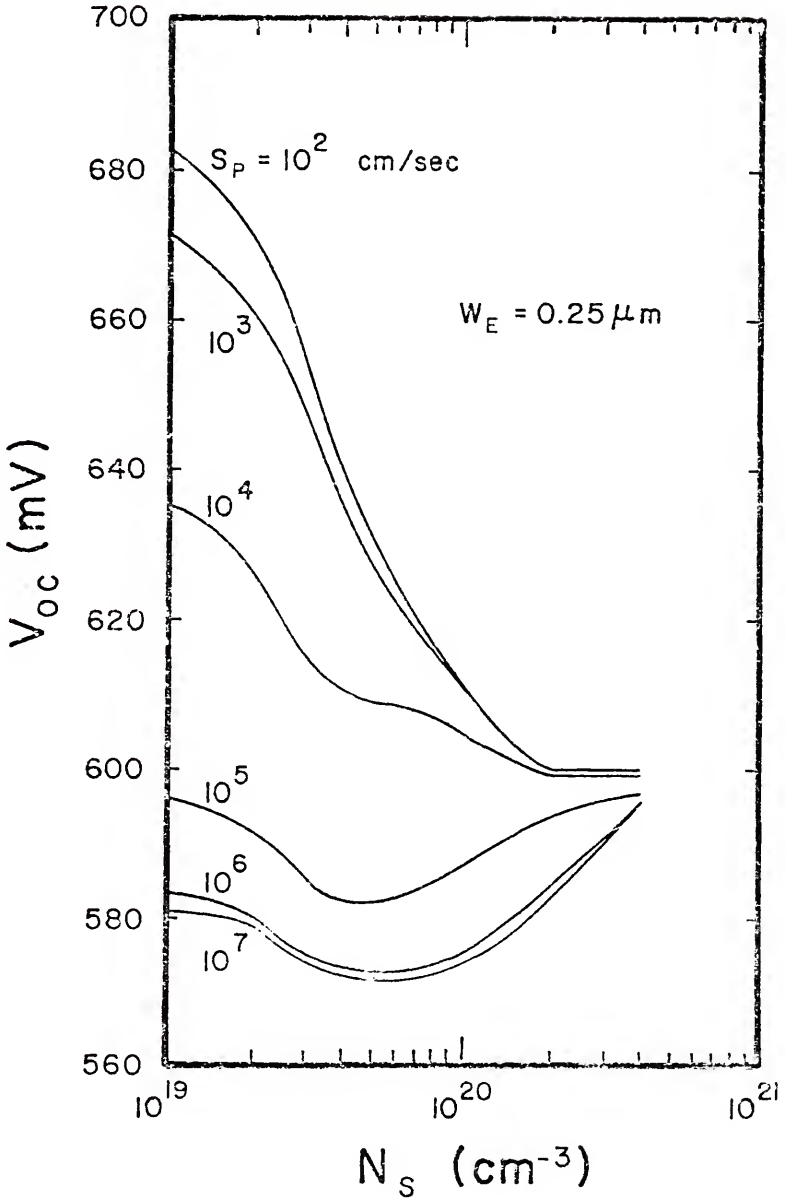
700
680
660
640
620
600
580
560
$S_P = 10^2$ cm/sec
$W_E = 0.25\,\mu m$
10^3
10^4
10^5
10^6
10^7
V_{OC} (mV)
10^{19}
10^{20}
10^{21}
N_S (cm^{-3})

Figure 7.6 The open-circuit voltage V_{OC} for a P^+N silicon solar cell versus the surface impurity concentration for several values of the surface recombination velocity S_N

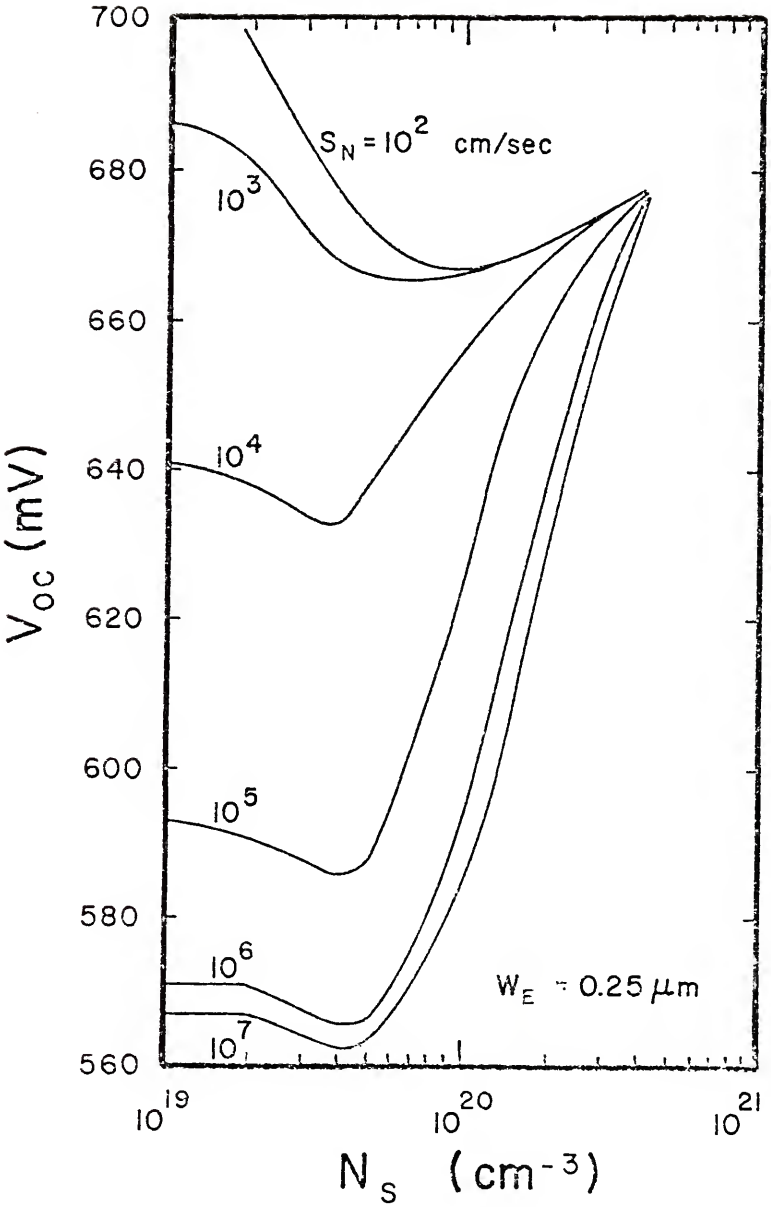
700
680
660
640
620
600
580
560
V_{OC} (mV)
$S_N = 10^2$ cm/sec
10^3
10^4
10^5
10^6
10^7
$W_E = 0.25\,\mu m$
10^{19}
10^{20}
10^{21}
N_S (cm^{-3})

Figure 7.7 The open-circuit voltage V_{OC} for P^+N and N^+P silicon solar cells versus the emitter surface recombination velocity S

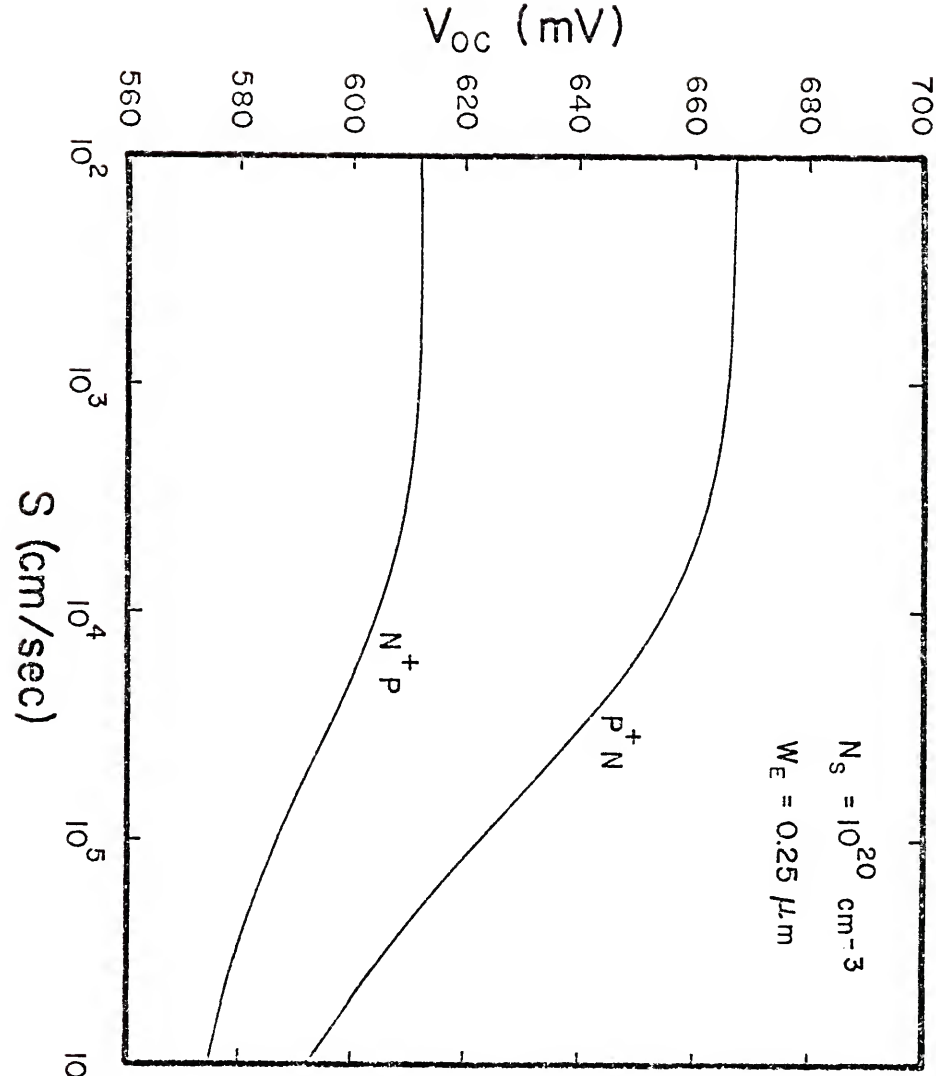
V_{OC} (mV)
700
680
660
640
620
600
580
560
10^2
10^3
10^4
10^5
10^6
S (cm/sec)
$N_S = 10^{20}$ cm^{-3}
$W_E = 0.25$ μm
P^+N
N^+P

7.3 Discussion

From our computer-aided numerical analysis, we deduce two main conclusions:

1. V_{OC} depends strongly on S for moderate surface impurity concentrations (i.e., for $N_S < 4 \times 10^{20}$ cm^{-3})
2. There is a considerable difference in the values of V_{OC} for N^+P and P^+N cells having identical structures.

Because the above results are derived from a rigorous computer-aided analysis that incorporates fundamental heavy-doping effects, they are inherent in the device structure and material and are independent of the fabrication process for the cell. Actual devices may not show the theoretically predicted values for V_{OC} if process-induced effects are important. For example, if deep traps, induced by the processing or due to residual impurities like gold, dominate the recombination process, then our predicted dependence of V_{OC} on design parameters will not be consistent with experiment.

Physically, the strong dependence of V_{OC} on S in both N^+P and P^+N cells implies that the emitter in these devices is transparent to the injected minority carriers. In that case, the analytical study of Chapter V is applicable. From our computer-aided analysis, we verified that the emitter is transparent for low surface impurity concentrations ($< 4 \times 10^{20}$ cm^{-3}) and high S ($> 10^4$ cm/sec). For $N_S \simeq 10^{19}$ cm^{-3}, the emitter is transparent for S larger than 10^3 cm/sec.

The difference in the theoretically predicted values of V_{OC} for N^+P and P^+N cells, with similar structures, is due to three factors:

1. The Auger lifetime of minority carriers is larger in P^+-silicon than in N^+-silicon having the same impurity concentration. That is,

$$(\tau_A)_{P+} > (\tau_A)_{N+} \tag{7.2}$$

because, as experimentally determined [36], the Auger coefficient in P-type silicon is smaller than that in N-type silicon.

2. The onset of degeneracy of the charge carriers in P^+-silicon occurs at a lower impurity concentration than in N^+-silicon. This is due to the lower effective density of states in the valence band than in the conduction band. Degeneracy of the charge carriers tends to decrease the emitter current, as discussed in Chapter V, thus increasing V_{OC}. Note that V_{OC} in P^+N cells is higher than that in N^+P cells of similar structure (see Figures 7.5 and 7.6).

3. The mobility and diffusivity of the minority carriers in the base region of (silicon) N^+P cells are larger than those in P^+N cells. Hence the base current of N^+P cells is larger than that of P^+N cells, if both cells have the same substrate doping

concentration and the same diffusion length. In our calculations, we had

$$(J_{BO})_{N^+P} \simeq 2\ (J_{BO})_{P^+N} \tag{7.3}$$

The effects of bandgap-narrowing and degeneracy of the majority charge-carriers can be seen in Figures 7.5 and 7.6. As N_S increases above 10^{19} cm^{-3} (for $S > 10^4$ cm/sec), V_{OC} decreases in magnitude, reaching a minimum at $N_S \simeq 5 \times 10^{19}$ cm^{-3}. The decrease in V_{OC} with increasing N_S is mainly attributed to bandgap narrowing which increases the emitter current. Above $N_S \simeq 5 \times 10^{19}$ cm^{-3}, degeneracy of the majority charge-carriers effectively compensates for bandgap narrowing; thus V_{OC} increases with increasing N_S. By compensating the effect of bandgap narrowing, degeneracy enhances the built-in electric field due to the impurity concentration gradient. This forces the minority carriers away from the surface, and, as a consequence, V_{OC} becomes less sensitive to S. With the minority carriers located mainly in the low-impurity-concentration region (compared to the surface region) next to the emitter space-charge region, the effective Auger lifetime is not so short, and the emitter current is decreased further. At still higher values of N_S (about 4×10^{20} cm^{-3}), V_{OC} saturates, that is, increases in W_E or S do not affect V_{OC}. In this case, the confinement of the minority carriers away from the surface is complete.

Referring back to Figures 7.5 and 7.6, it is important to point out that the effect of degeneracy may be exaggerated in our treatment. The reason for this is fundamentally related to the density

of states in heavily doped semiconductors. This is discussed in Appendix F briefly. A full treatment of this is beyond the scope of this dissertation and is suggested for future research.

7.4 Experimental Support

Limited experimental data indicating the increase in V_{OC} in typical silicon solar cells as S is decreased [29] are consistent with our theoretical results. Furthermore, our analysis indicates that V_{OC} in silicon solar cells can be in the range of values observed experimentally (typically 600 mV or less) because of heavy doping in the emitter.

7.5 Conclusions

In this chapter, we presented results of a parametric study of V_{OC} in silicon N^+P and P^+N solar cells based on a rigorous computer-aided analysis of the minority-carrier transport in the emitter. The emitter current is influenced by heavy-doping mechanisms that consequently limit V_{OC} in silicon solar cells.

There are two main design-oriented conclusions of this chapter. First, it is beneficial to have a low emitter surface impurity concentration only if S is low (about 10^2 to 10^3 cm/sec). That is, V_{OC} can be increased toward its limit value of 700 mV by moderately doping the emitter and making it thin and transparent to the minority carriers if the surface recombination velocity is below 10^3 cm/sec. Second, it is easier to suppress the emitter current, and thus optimize V_{OC}, in P^+-emitters than in N^+-emitters. This second conclusion is in agreement with experimental observations [69,71].

The physical reasons behind our second conclusion are (a) the Auger lifetime in the P^+-emitter is longer than that in the N^+-emitter, (b) the onset of degeneracy occurs at a lower impurity concentration in P-type silicon than in N-type silicon, and (c) the mobility and diffusivity of electrons in the base of N^+P cells are larger than the mobility and diffusivity of holes in the base of P^+N cells, meaning that the dark base current in N^+P cells is larger than that in P^+N cells.

Limited experimental data and our theoretical results are consistent. This consistency supports the validity and accuracy of the first-order model described in Chapter VI since the computer-aided analysis is in agreement with the first-order model.

CHAPTER VIII

SUMMARY, CONCLUSIONS, AND RECOMMENDATIONS

8.1 Summary

In this dissertation, we investigated the device physics of heavily doped silicon devices and used the results of this investigation to establish engineering models for design.

In Chapter I, we specified the origin of the research problem: the excessive recombination current observed experimentally in heavily doped regions of silicon pn-junction devices. This observation is in conflict with the predictions of classical pn-junction theory. The excessive current is due either to a large excess minority-carrier charge in the emitter or to a short minority-carrier lifetime or to a combination of these causes. Various heavy-doping mechanism were then examined to determine the simplest physical model for heavily doped regions in silicon that is consistent with the observed excessive recombination current.

In Chapter II, we evaluated a rigorous analytic model for a diffused emitter that included Auger recombination only, i.e., a model that neglected other heavy-doping effects. We found that such a model cannot give the low values of V_{OC} in silicon solar cells and of the common-emitter current gain in silicon bipolar transistors. Thus we concluded that other heavy-doping mechanisms, in addition to Auger recombination, must be included in the analysis of these devices.

In Chapter III, we discussed recombination via a position-dependent defect density. We pointed out that such a recombination cannot yield low values of V_{OC} in silicon solar cells and the experimentally observed sensitivity of V_{OC} to surface treatment. We then concluded, considering also the results of Chapter II, that the excessive recombination current is not only due to short lifetimes, but also to an excess minority-carrier charge storage. The excess charge storage is due to an excess intrinsic carrier density n_{ie}^2 in the heavily doped region (or deficit impurity concentration N_{eff}).

In Chapter IV, we showed that the magnitude of n_{ie}^2 and N_{eff} needed to predict the excessive recombination current cannot be due to deionization of impurities as described in the recent models of Heasell [25] and Popovic [45]. This deionization does not remove the need for an effective bandgap narrowing to obtain agreement between theory and experiment.

In Chapter V, we presented and discused the transparent-emitter model in which the minority carriers injected into the emitter recombine mainly at the surface rather than in the bulk. We showed, via a self-consistency test, that the transparency of the emitter prevails despite Auger recombination in the bulk provided that the surface recombination velocity is high (above 10^4 cm/sec), W_E is less than 0.5 μm, and N_S is less than 4×10^{20} cm^{-3}. Furthermore, we verified that for an N^+P silicon solar cell, with emitter parameters consistent with the above values, the transparent-emitter model can explain the experimentally observed value of V_{OC} of about 600 mV.

In Chapter VI, we presented a first-order emitter model that can accurately predict the emitter recombination current. The key assumption involved is a zero net effective drift field, that is, the assumption that the quasi-electric field cancels the built-in field. The first-order model was verified quantitatively by comparing its results to results of a rigorous computer solution of the minority-carrier transport problem in a heavily doped emitter. Limited experimental support for the first-order model was briefly considered in Chapters VI and VII.

A parametric study of V_{OC} in heavily doped N^+P and P^+N silicon solar cells, based on our computer-aided analysis, was also presented in Chapter VII. The study reveals the dependence of V_{OC} in silicon solar cells (both N^+P and P^+N) on the emitter design parameters, and led to conclusions that are important to design.

8.2 Accomplishments

In this dissertation, we accomplished the following:

A. Identified the important heavy-doping mechanisms and showed that:

   1. Auger recombination alone cannot explain the experimentally observed values of V_{OC} in silicon solar cells and the common-emitter current gain in silicon bipolar transistors
   2. Inclusion of Fermi-Dirac statistics is important, and it tends to compensate the effects of bandgap narrowing

3. Deionization of impurities, as described by the recent models of Heasell and Popovic, is not an important mechanism in heavily doped silicon

B. Modified the semiconductor transport equations (in Appendix A) in heavily doped silicon incorporating asymmetry of bandgap narrowing and degeneracy of charge-carriers. We

1. Modified Shockley's auxiliary relations to include asymmetry and degeneracy
2. Showed that n_{ie}^2 depends on the total bandgap narrowing, and on the asymmetry in bandgap narrowing
3. Developed an expression for the minority-carrier current in a heavily doped region that accounts for asymmetry in bandgap narrowing and Fermi-Dirac statistics
4. Presented a new approximation of Fermi-Dirac integrals of order 1/2 (in Appendix C)

C. Established a first-order engineering model for heavily doped regions in silicon pn-junction devices (particularly solar cells) and verified its accuracy

D. Established an efficient computer program that solves the minority-carrier transport problem in heavily doped silicon devices with the fundamental heavy-doping mechanisms included

E. Studied the dependence of V_{OC} on the emitter design parameters in N^+P and P^+N silicon solar cells. We concluded that:

1. For $N_S < 4 \times 10^{20}$ cm^{-3}, surface recombination is important
2. The emitter current can more easily be suppressed in P^+N than in N^+P cells but is more sensitive to S in P^+N cells
3. At high N_S (above about 4×10^{20} cm^{-3}), V_{OC} saturates, that is, it becomes independent of S and W_E, at about 680 mV for P^+N cells and at about 600 mV for N^+P cells
4. Our theoretical results are consistent with available experimental data

8.3 Scope and Limitations

The discussion of the physics underlying the heavy-doping effect has been limited in this work mainly because many aspects of heavy doping have not yet been fully understood. A complete theoretical study of the physics in heavily doped semiconductors is beyond the scope of this dissertation. We considered only what we believe are fundamental first-order heavy-doping effects and neglected or roughly approximated other second-order effects (such as the dependence of the density-of-states effective mass on the doping concentration).

One of the main assumptions is the rigid-band approximation, that is, the assumption that the change in the energy bandgap does not

alter the shape of the density-of-states function from its conventional square-root dependence on energy. Although the real density of states in heavily doped semiconductors is not parabolic, experimental measurements of the differential conductance in heavily doped N-type and P-type metal-silicon tunnel diodes indicate that the rigid-band approximation is good for P-type silicon and is fair for N-type silicon [72]. Other experimental measurements in heavily doped silicon, including the electronic specific heat [56] and nuclear magnetic resonance [57], indicate that the density of states in the vicinity of the Fermi level is well approximated by a parabolic function.

Other approximations made in our study are:

1. The density-of-states effective mass for electrons and holes is independent of impurity concentration
2. Average values are used for the mobility and the diffusion coefficient in the transport equations
3. Low-level injection prevails in the heavily doped emitter
4. The phosphorus or boron atoms are completely ionized for doping levels above 10^{18} cm^{-3}
5. One-dimensional models adequately represent the solar cell
6. A Gaussian Profile adequately approximates actual emitter doping profiles

8.4 Recommendations for Future Research

Some of the approximations listed above deserve further consideration. In addition, we have several other recommendations for future research:

A. Problems pertaining to electronic characterization in heavily doped silicon of the density of states, energy-bandgap narrowing, and electron affinity. These can be explored directly by experiments involving measurements of differential conductance in heavily doped metal-silicon tunnel diodes, magneto-absorption, and photoemission in heavily doped silicon. In addition extensive electrical measurements of the emitter current, as in [22], for N^+P and P^+N diodes, with the use of our theoretical characterization of the emitter current can provide an average value for n_{ie}^2 in an inhomogeneous emitter.

B. A new model to calculate deionization. We propose, for future investigations, a model for the impurity energy levels in heavily doped silicon formed by integrating the experimental results of Pearson and Bardeen [47] with the theoretical results of Morgan [73] pertaining to the impurity band. In the proposed model, the impurity density-of-states function is Gaussian. Its median value, which is the value at which the Gaussian fucntion has its peak, is a function of the impurity concentration as given by the experimental model of Pearson and Bardeen [47] rather than being fixed at the impurity level. We anticipate that such a model may agree well not only with the

results of Pearson and Bardeen, but also with other experimental results discussed in Chapter IV.

C. Extension of our analysis to high-low junctions. Our analysis and modeling can be extended to study the highly doped side of high-low junctions in back-surface-field (BSF) and high-low-emitter (HLE) silicon solar cells.

D. Fabrication of special device structures. Experimental measurements on special devices that are carefully designed and fabricated to explore particular mechanisms (for example, surface recombination) together with our theoretical modeling can provide significant understanding of the physics underlying silicon device operation and performance. One such design that deserves study is a pn-junction with an epitaxial emitter on a low-resistivity substrate. The emitter is fabricated by epitaxy so as to control the shape of the impurity profile. The impurity profile in the structure is a "reversed" profile; that is, it has its highest value near the junction and its lowest value at the emitter surface. Such a device would have an emitter current that is very sensitive to the surface recombination velocity since the impurity profile aids the injected minority

carriers in reaching the emitter surface. The surface recombination velocity can be varied, for example, by growing thin thermal SiO_2, then removing it and depositing Si_3N_4, as in [29].

E. Experimental comparison between P^+N and N^+P devices having identical structures and doping levels. Experiments to provide data in addition to the limited experimental data presented in this dissertation are needed to further corroborate our theoretical conclusion that P^+-emitters can yield lower emitter currents than N^+-emitters.

APPENDICES

APPENDIX A

EXTENSION OF SHOCKLEY'S AUXILIARY RELATIONS FOR HEAVILY DOPED PN-JUNCTION DEVICES

Analysis of semiconductor devices is most often based on Shockley's differential equations [11]: the current density equations,

$$\vec{J}_n = qD_N\nabla n + q\mu_N n\vec{E} \tag{A.1}$$

$$\vec{J}_p = -qD_P\nabla p + q\mu_P p\vec{E} \tag{A.2}$$

the continuity equations,

$$\frac{\partial n}{\partial t} = \nabla \cdot \vec{J}_n + q(G - U) \tag{A.3}$$

$$\frac{\partial p}{\partial t} = -\nabla \cdot \vec{J}_p + q(G - U) \tag{A.4}$$

Poisson's equation,

$$\nabla \cdot \vec{E} = \nabla^2 E_I/q = \frac{q}{\varepsilon}(p - n + N_{DD} - N_{AA}) \tag{A.5}$$

and the auxiliary relations,

$$n = n_i \exp\left(\frac{E_{FN} - E_I}{kT}\right) \tag{A.6}$$

$$p = n_i \exp\left(\frac{E_I - E_{FP}}{kT}\right) \tag{A.7}$$

which relate the carrier concentrations to the corresponding quasi-Fermi levels. The symbols used above have their usual meanings and are defined explicitly in [19].

The auxiliary relations (A.6) and (A.7) provide a useful connection between the electron and hole densities internal to the device and the voltages at the device terminals [19]. This connection has been exploited in device analysis, particularly in computer-aided numerical analyses [17,74-82].

For devices with heavily doped regions--for example, the emitter regions in bipolar transistors and solar cells--experiment and theory have been brought into agreement by accounting for the effect of energy-bandgap narrowing [29,83]. This is done by substituting n_{ie}^2 for n_i^2 in the np product; n_{ie}^2 is proportional to $\exp(\Delta E_G/kT)$ [83], in which ΔE_G is referred to as the bandgap narrowing.

Papers that have accounted for bandgap narrowing in computer-aided numerical analysis [17,80-82] have not defined the pre-exponential factors that appear in the general forms of the auxiliary relations valid for heavily doped semiconductors.

In this appendix, we demonstrate that bandgap narrowing is not properly accounted for by exchanging n_{ie} for n_i in (A.6) and (A.7), as was done in [81,82], except for an uncommon special case. This special case is that of symmetric bandgap narrowing, for which the shifts in the conduction- and valance-band edges are equal in magnitude--which rarely occurs [84]--and for which Boltzmann statistics describe the distribution of the majority carriers--which is often a poor approximation. In this appendix, we also derive the appropriate pre-exponential

factors in the generalizations of (A.6) and (A.7) by accounting for asymmetric bandgap narrowing and Fermi-Dirac statistics. The resulting modified auxiliary relations are shown to be consistent in form with the expressions for minority-carrier current used previously in analytical treatments of heavily doped regions [16,83] in which the drift component is influenced by a quasi-electric field resulting from a spatial dependence of the bandgap narrowing. Furthermore, we show that, for a degenerately doped semiconductor, n_{ie}^2, the square of the effective intrinsic carrier concentration, depends on the asymmetry in bandgap narrowing. This dependence of n_{ie}^2 on asymmetry complicates the interpretation of experimental measurements of n_{ie}^2 and of ΔE_G in degenerately doped semiconductors.

Asymmetric bandgap narrowing in heavily doped regions is due to several physical mechanisms: impurity-band widening [73], band tailing [15,85], electron-electron interaction [86], and screening effects [12, 13]. These mechanisms produce unequal shifts in the intrinsic conduction- and valence-band edges because they affect electrons and holes differently. As an illustrative example, consider impurity-band widening in a heavily doped semiconductor region where discrete energy levels in the bandgap spread into a band of impurity levels. If we consider an uncompensated semiconductor, the impuriry band is formed in the vicinity of the majority-carrier band edge. The impurity band thus effectively shifts the intrinsic majority-carrier band edge and leaves the intrinsic minority-carrier band edge

essentially unchanged. So, in this example, bandgap narrowing resulting from impurity-band widening is due primarily to a shift in only one of the band edges.

To begin the derivation of the modified auxiliary relations, consider an intrinsic or a lightly doped semiconductor. The intrinsic Fermi level is given by

$$E_I = \frac{E_C + E_V}{2} + \frac{1}{2} kT \ln \frac{N_V}{N_C} \tag{A.8}$$

where E_C and E_V are the conduction and valence band edges as shown in Figure A-1, and N_C and N_V are the electron and hole effective densities of states. For this case, the general forms of the auxiliary relations simplify to (A.6) and (A.7), in which E_{FN} and E_{FP} are the electron and hole quasi-Fermi levels.

In a heavily doped semiconductor, we assume that the intrinsic conduction and valence band edges, E_C and E_V, shift to E_C' and E_V', as illustrated in Figure (A-1). In general, we can relate E_C and E_V to E_C' and E_V' as follows:

$$E_C' = E_C - A\Delta E_G \tag{A.9}$$

$$E_V' = E_V + (1 - A)\Delta E_G \tag{A.10}$$

where ΔE_G is the total bandgap narrowing, comprised of a component due to the conduction-band shift $A\Delta E_G$, and a component due to the valence-band shift $(1 - A)\Delta E_G$; A is a factor between zero and one, whose value depends on the physical mechanisms underlying the bandgap

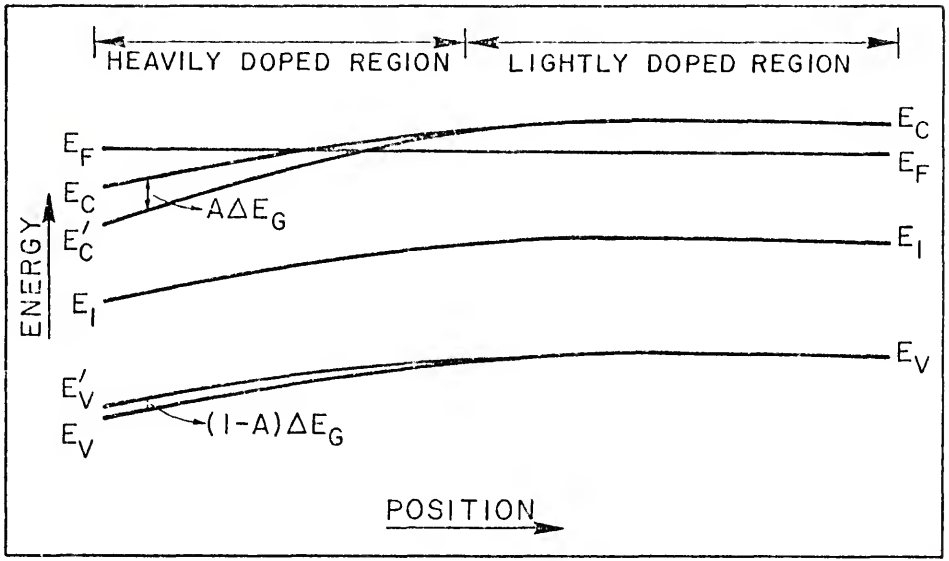

Figure A-1 Energy band edges in a heavily and inhomogeneously doped semiconductor and the two components of the energy-bandgap narrowing ΔE_G: the conduction-band component $A\Delta E_G$ and the valence-band component $(1 - A)\Delta E_G$

narrowing. For example, in an N-type heavily doped semiconductor, if bandgap narrowing were due mainly to impurity-band widening, then $A \simeq 1$.

Consider now an N-type heavily doped semiconductor with an inhomogeneous impurity concentration; a similar derivation applies for a P-type semiconductor. Even for conditions of non-equilibrium, we can assume that the electrons (majority carriers) obey Fermi-Dirac statistics, while the holes (minority carriers) follow, to a good approximation, Maxwell-Boltzmann statistics, provided the injection level is low [11]. For a parabolic density of states in the conduction and valence bands (rigid-band approximation), we have

$$n = N_C F_{1/2}\left(\frac{E_{FN} - E'_C}{kT}\right) \tag{A.11}$$

and

$$p = N_V \exp\left(\frac{E'_V - E_{FP}}{kT}\right) \tag{A.12}$$

In (A.11), $F_{1/2}$ is the Fermi-Dirac integral of order 1/2. Combining (A.9), (A.10, (A.11), and (A.12), we obtain

$$pn = N_C N_V F_{1/2}\left(\frac{E_{FN} - E_C + A\Delta E_G}{kT}\right) \exp\left(\frac{E_V + (1 - A)\Delta E_G - E_{FP}}{kT}\right) \tag{A.13}$$

We now use an analytic approximation for $F_{1/2}(\eta)$ (see Appendix C)

$$F_{1/2}(\eta) \simeq \frac{\exp(\eta)}{1 + C(\eta)\exp(\eta)} \tag{A.14}$$

where $C(\eta)$ is a function of η described in Figure (C-1). Analytic approximations for $C(\eta)$, for $-4 \leq \eta \leq +12$, which introduces errors of less than 2.5%, are given in Appendix C. Use of (A.14) in (A.13) yields

$$pn = \frac{n_i^2 \exp\left(\frac{\Delta E_G}{kT}\right) \exp\left(\frac{E_{FN} - E_{FP}}{kT}\right)}{1 + C(\eta_C) \exp(\eta_C)} \tag{A.15}$$

where

$$\eta_C = \frac{E_{FN} - E_C + A\Delta E_G}{kT} \tag{A.16}$$

If we now <u>define</u> n_{ie}^2 by

$$pn \equiv n_{ie}^2 \exp\left(\frac{E_{FN} - E_{FP}}{kT}\right) \tag{A.17}$$

we get, from (A.15) and (A.17)

$$n_{ie}^2 = \frac{n_i^2 \exp\left(\frac{\Delta E_G}{kT}\right)}{1 + C(\eta_C) \exp(\eta_C)} \tag{A.18}$$

for an N-type semiconductor. When both electrons and holes follow Maxwell-Boltzmann statistics, n_{ie}^2 reduces to the result given by DeMan [83]

$$n_{ie}^2 = n_i^2 \exp\left(\frac{\Delta E_G}{kT}\right) \tag{A.19}$$

From (A.10) and (A.12), we can write

$$p = n_i \exp\left(\frac{(1 - A)\Delta E_G}{kT}\right) \exp\left(\frac{E_I - E_{FP}}{kT}\right) \tag{A.20}$$

If we <u>define</u> n_{ip} by

$$n_{ip} \equiv n_i \exp\left(\frac{(1 - A)\Delta E_G}{kT}\right) \tag{A.21}$$

we then have

$$p = n_{ip} \exp\left(\frac{E_I - E_{FP}}{kT}\right) \tag{A.22}$$

where n_{ip} can be thought of as an <u>effective</u> intrinsic carrier density for holes. From (A.17) and (A.20), we get

$$n = \frac{n_{ie}^2}{n_{ip}} \exp\left(\frac{E_{FN} - E_I}{kT}\right) \tag{A.23}$$

We therefore <u>define</u> n_{in} by

$$n_{in} \equiv \frac{n_{ie}^2}{n_{ip}} \tag{A.24}$$

so that

$$n = n_{in} \exp\left(\frac{E_{FN} - E_I}{kT}\right) \tag{A.25}$$

where n_{in} can be thought of as an <u>effective</u> intrinsic carrier density for electrons.

From (A.18), (A.21), and (A.24), notice that $n_{in} \neq n_{ip} \neq \overline{n_{ie}^2}$. Equations (A.22) and (A.25) are the modified Shockley auxiliary relations for heavily doped N-type regions.

If the electrons and holes are non-degenerate, n_{in} and n_{ip} reduce to

$$n_{in} = n_i \exp\left(\frac{A\Delta E_G}{kT}\right) \tag{A.26}$$

and

$$n_{ip} = n_i \exp\left(\frac{(1 - A)\Delta E_G}{kT}\right) \tag{A.27}$$

Thus, even for non-degenerate carrier concentrations, asymmetric bandgap narrowing gives different pre-exponential factors in the auxiliary relations (A.22) and (A.25). This is contrary to the conclusiions of [35]. Note that the pre-exponential factors are equal only if both electrons and holes are non-degenerate and if bandgap narrowing is symmetric (A = 1/2). (The bandgap narrowing is symmetric when the shift in the conduction band edge is equal to the shift in the valence band edge.)

By differentiating (A.22) and using (A.23) with the assumption that $(dE_{FN}/dx) \simeq 0$ in the (N-type) heavily doped region, we find that

$$\mu_p p \frac{dE_{FP}}{dx} = q\mu_p p \frac{kT}{q}\left(\frac{1}{n_{ie}^2} \cdot \frac{dn_{ie}^2}{dx} - \frac{1}{n} \cdot \frac{dn}{dx}\right) - qD_p \frac{dp}{dx} \tag{A.28}$$

The right-hand side of (A.28) is the hold current density in a heavily doped N-type region [16,83], including an effective drift component dependent on $n_{ie}^2(x)$ and $n(x)$ (see Appendix B). Thus, (A.28) is consistent with

$$J_p = \mu_p p \frac{dE_{FP}}{dx} \tag{A.29}$$

which is the conventional Shockley expression for the hole current in terms of the quasi-Fermi level. Note that the hole current density as described in (A.28) depends on n_{ie}^2 as given by (A.18), and not on the factors n_{ip} and n_{in}. Thus when Maxwell-Boltzmann statistics are applicable for both electrons and holes, the minority-carrier current in (A.28) depends on the total bandgap narrowing irrespective of asymmetry, as noted in [35]. However, if the electrons or holes are degenerate, the minority-carrier current, via its dependence on n_{ie}^2 in (A.28), depends not only on the total bandgap narrowing but also on the asymmetry in bandgap narrowing, contrary to the conclusion in [35].

We have shown that degeneracy of electrons or holes and energy-bandgap narrowing in a semiconductor requires that n_{ie}^2 depend on the total bandgap narrowing and on the asymmetry in bandgap narrowing. This result is particularly important in interpreting experimental measurements of n_{ie}^2 and of ΔE_G in degenerately doped semiconductors. In (A.18), the term $(1 + C(\eta_C))$, where η_C is given in (A.16) for an N-type semiconductor, can be considerably larger than unity for a degenerate semiconductor. If this term is neglected, the magnitude of bandgap narrowing deduced from experimental measurements will be smaller than the true shrinkage (in the rigid-band

model) of the bandgap. Further complication in interpreting experimental measurements of n_{ie}^2 arises from the dependence of n_C, in (A.16), on asymmetry in bandgap narrowing. Therefore, detailed interpretation of experimental measurements of n_{ie}^2 and of ΔE_G in degenerately doped semiconductors requires a knowledge of the asymmetry in energy-bandgap narrowing.

APPENDIX B

QUASI-ELECTRIC FIELDS IN HEAVILY DOPED SEMICONDUCTORS

In this appendix, we show that the minority-carrier (hole) current in a heavily doped, quasi-neutral N-type region, for low-level injection, is given by

$$j_p = q\mu_p p \left\{ \frac{kT}{q} \left[\frac{1}{n_{ie}^2} \cdot \frac{dn_{ie}^2}{dx} - \frac{1}{n} \cdot \frac{dn}{dx} \right] \right\} - qD_p \frac{dp}{dx} \tag{B.1}$$

We also show that the effective electric field acting on the minority carriers is composed of two components--one related to the position dependence of n_{ie}^2, and a second related to the majority-carrier concentration gradient.

In thermal equilibrium, the principle of detailed balance requires that

$$j_p = q\mu_p p_0 E_p - qD_p \frac{dp_0}{dx} = 0 \tag{B.2}$$

and

$$j_n = q\mu_N n_0 E_N + qD_N \frac{dn_0}{dx} = 0 \tag{B.3}$$

where E_p and E_N are phenomenological effective electric fields acting on holes and electrons. These effective electric fields can be expressed, via (B.2) and (B.3), as

$$E_P = \frac{D_P}{\mu_P} \cdot \frac{1}{p_0} \cdot \frac{dp_0}{dx} \tag{B.4}$$

and

$$E_N = - \frac{D_N}{\mu_N} \cdot \frac{1}{n_0} \cdot \frac{dn_0}{dx} \tag{B.5}$$

For non-equilibrium, but low-level-injection conditions, if we assume full impurity ionization in a heavily doped, quasi-neutral N-type region, then

$$n \simeq n_0 \simeq N_{DD} \tag{B.6}$$

Using (B.6) and the thermal-equilibrium condition

$$p_0 n_0 = n_{ie}^2(x) \tag{B.7}$$

in (B.4) and (B.5), we obtain

$$E_P = \frac{D_P}{\mu_P} \left[\frac{1}{n_{ie}^2} \cdot \frac{dn_{ie}^2}{dx} - \frac{1}{N_{DD}} \cdot \frac{dN_{DD}}{dx} \right] \tag{B.8}$$

and

$$E_N = - \frac{D_N}{\mu_N} \cdot \frac{1}{N_{DD}} \cdot \frac{dN_{DD}}{dx} \tag{B.9}$$

Note that the expressions for E_P and E_N given in (B.8) and (B.9) hold for low-injection as well as for equilibrium conditions. In (B.8) and (B.9), we see that E_P is not equal to E_N. Note that E_N depends on

the space variation of N_{DD}, while E_P depends on the space variation of N_{DD} and n_{ie}^2. The position dependence of n_{ie}^2 is due to the position dependence of ΔE_G and of η_C as given in (A.18).

The relation between E_P and E_N is found by combining (B.8) and (B.9). This yields

$$E_P = \frac{D_P}{\mu_P}\left[\frac{1}{n_{ie}^2}\cdot\frac{dn_{ie}^2}{dx} + \frac{\mu_N}{D_N}\cdot E_N\right] \tag{B.10}$$

Note that for N^+ material $D_N/\mu_N > D_P/\mu_P = kT/q$ because of the degeneracy of electrons [70,87].

If we substitute (B.8) into the non-equilibrium form of (B.2) obtained by using (B.6), we get (B.1).

APPENDIX C

INCLUSION OF DEGENERACY IN THE ANALYSIS OF HEAVILY DOPED SEMICONDUCTOR DEVICES

Fermi-Dirac integrals of order 1/2 defined by [26]

$$F_{1/2}(\eta) = \frac{1}{\sqrt{\pi}} \int_0^\infty \frac{E^{1/2} dE}{1 + \exp(E - \eta)} \tag{C.1}$$

appear in the theory of metals and semiconductors because the charge carriers obey Fermi-Dirac statistics and because an $E^{1/2}$ dependence is used to describe their density of states. For metals and semiconductors, values of $F_{1/2}(\eta)$ are used to calculate the Fermi energy ($= kT\eta$) from the concentrations of electrons or holes. Often Maxwell-Boltzmann statistics, which reduce (C.1) to

$$F_{1/2}(\eta) \simeq \exp(\eta) \tag{C.2}$$

are used for semiconductors because electron and hole concentrations are not as high as in metals. However, for heavily doped semiconductor regions, as in the emitter of bipolar transistors and solar cells, (C.2) introduces a large error and (C.1) must be used.

The Fermi-Dirac integral in (C.1) only can be evaluated numerically; values of $F_{1/2}(\eta)$ are given in Tables [26,88,39] for η typically in the range of -4 to +10. Several analytic approximations for $F_{1/2}(\eta)$ are found in the literature [24,26,90-96]. Most of these

approximations require short intervals of η over which different expressions are used to approximate $F_{1/2}(\eta)$. This makes the evaluation of $F_{1/2}(\eta)$ tedious and inconvenient in computer-aided analysis and in analytic treatments of heavily doped semiconductor devices and possibly also in other problems in physics.

Recent approximations of $F_{1/2}(\eta)$ [95,96] yielded simple and fairly accurate expressions for the reduced Fermi energy η in terms of the charge-carrier concentration. However, these approximations do not give simple expressions for $F_{1/2}(\eta)$ itself, which is used not only to calculate the Fermi energy, but also in the expression for the square of the effective intrinsic carrier concentration n_{ie}^2 in a heavily doped semiconductor. The square of the effective intrinsic carrier concentration, which enters into most of the expressions of the electrical parameters in heavily doped regions, is defined by

$$n_{ie}^2 \equiv N_0 P_0 = N_C N_V F_{1/2}(\eta_C) F_{1/2}(\eta_V) \tag{C.3}$$

where N_0 and P_0 are the equilibrium concentrations of electrons and holes in the semiconductor, N_C and N_V are the effective density of states for electrons and holes, and

$$\eta_C = \frac{E_F - E_C}{kT} \tag{C.4}$$

and

$$\eta_V = \frac{E_V - E_F}{kT} \tag{C.5}$$

In this appendix we present a simple analytic empirical approximation for the Fermi-Dirac integrals of order 1/2, and use this approximation to derive a simple analytic expression for the effective intrinsic carrier concentration n_{ie}^2 in a heavily doped semiconductor having energy-bandgap narrowing and degenerate majority-carrier distribution.

As in [91], we express $F_{1/2}(\eta)$ by

$$F_{1/2}(\eta) \simeq \frac{\exp(\eta)}{1 + C(\eta)\exp(\eta)} \tag{C.6}$$

where $C(\eta)$ is a function of η given graphically in [91]. In Figure C-1, we have calculated $C(\eta)$ from tabulated values of $F_{1/2}(\eta)$ [26]. Our Figure C-1 is similar to Figure 4 in [91] except that we have extended the range of η from -4 to an upper bound of +12.

By curve-fitting techniques, we found the following analytic expressions for $C(\eta)$:

$$C(\eta) = -4.4 \times 10^{-2}\eta + 3.1 \times 10^{-1} \quad \text{for } -4 \leq \eta \leq +2 \tag{C.7}$$

and

$$C(\eta) = \exp(8.6 \times 10^{-3}\eta^2 - 3.2 \times 10^{-1}\eta - 8.8 \times 10^{-1})$$

$$\text{for } +2 < \eta \leq +12 \tag{C.8}$$

These expressions for $C(\eta)$ provide values of $F_{1/2}$ over the range $-4 \leq \eta \leq +12$ with less than 2.5% error. We have reported an expression similar to (C.4) in a previous paper [24]. In this note the accuracy

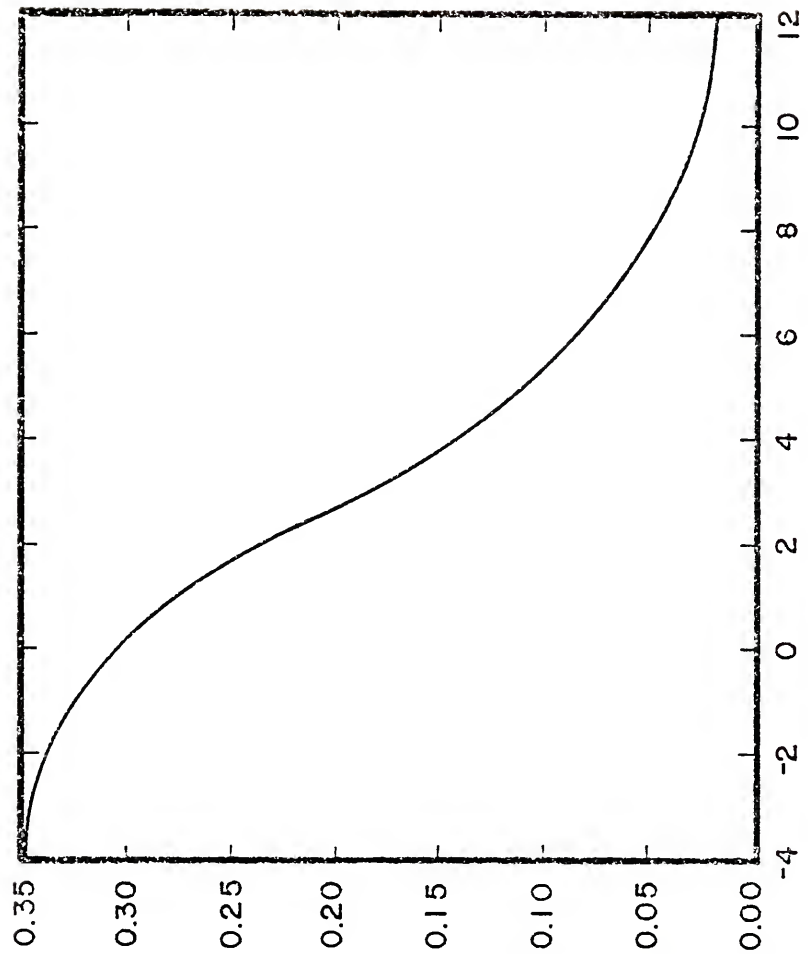

Figure C-1. C(η) versus η

of (C.7) is increased over the counterpart in [24] so that the error in the range $-4 \leq \eta \leq +2$ is less than 1%. For the expression in (C.8), the largest error lies in the range $+2 < \eta < 2.5$ and is about 2.2%. For values of $\eta > 2.5$, the expression in (C.8) yields an error in $F_{1/2}(\eta)$ less than 1%.

In Table C-I, we present values of $F_{1/2}(\eta)$ for several values of η in the range $-4 \leq \eta \leq +12$. Exact values of $F_{1/2}(\eta)$ are taken from tables in [26], and approximate values are calculated using (C.6), (C.7), and (C.8). The percentage error is shown in the fourth column of Table C-I. Note that the error is less than 1%; the largest error is in the range $+2 < \eta < +2.5$ and is about 2.2%.

If we use (C.6) in (C.3), we get

$$n_{ie}^2 = \frac{N_C N_V \exp(-E_G/kT)}{[1 + C(\eta_C) \exp(\eta_C)] \cdot [1 + C(\eta_V) \exp(\eta_V)]} \tag{C.9}$$

where η_C and η_V are given in (C.4) and (C.5), and E_G is the energy-bandgap of the heavily doped semiconductor,

$$E_G = E_{GO} - \Delta E_G \tag{C.10}$$

In (C.10), E_{GO} is the energy-bandgap of the intrinsic (pure) semiconductor, and ΔE_G is the bandgap narrowing due to high impurity concentrations in the doped semiconductor. Equations (C.9) and (C.10) can be combined with the definition of n_i^2 [11] to give

$$n_{ie}^2 = \frac{n_i^2 \exp(\Delta E_G/kT)}{[1 + C(\eta_C) \exp(\eta_C)] \cdot [1 + C(\eta_V) \exp(\eta_V)]} \tag{C.11}$$

In (C.11), we have derived a simple analytic expression for n_{ie}^2 that provides physical insight into the effects of bandgap narrowing and degeneracy of the charge carriers on n_{ie}^2. Note that, for the most part, the effect of energy-bandgap narrowing is included in the numerator of the right-hand side of (C.11), while degeneracy is incorporated in the denominator of the right-hand side of (C.11) (for a more rigorous analysis of the dependence of n_{ie}^2 on degeneracy and bandgap narrowing, see Appendix A). From (C.11), it is clear that energy-bandgap narrowing increases n_{ie}^2, while degeneracy of the charge carriers decreases n_{ie}^2 by increasing the terms in the denominator.

If only one type of carrier is degenerate, as is usually the case for the majority carriers in heavily doped semiconductor regions, (C.11) reduces to

$$n_{ie}^2 = \frac{n_i^2 \exp(\Delta E_G/kT)}{1 + C(n_C) \exp(n_C)} \tag{C.12}$$

for an N-type region, and

$$n_{ie}^2 = \frac{n_i^2 \exp(\Delta E_G/kT)}{1 + C(n_V) \exp(n_V)} \tag{C.13}$$

for a P-type region. Furthermore, if both kinds of carriers are non-degenerate, (C.11) reduces to [83]:

$$n_{ie}^2 = n_i^2 \exp(\Delta E_G/kT) \tag{C.14}$$

In conclusion, we presented a simple analytic approximation of the Fermi-Dirac integral of order 1/2 that is suitable for analysis

of heavily doped semiconductor devices. We used our new approximation to derive simple analytic expressions for n_{ie}^2, the square of the effective intrinsic carrier concentration, in the heavily doped semiconductor.

TABLE C-I

COMPARISON BETWEEN EXACT AND APPROXIMATE VALUES OF $F_{1/2}(\eta)$

η	Exact $F_{1/2}(\eta)$ [26]	Approximate $F_{1/2}(\eta)$ Using (C.6), (C.7), and (C.8)	Percentage Error
-4	1.82×10^{-2}	1.82×10^{-2}	0.2
-3	4.89×10^{-2}	4.88×10^{-2}	0.3
-2	1.29×10^{-1}	1.29×10^{-1}	0.5
-1	3.28×10^{-1}	3.27×10^{-1}	0.2
0	7.65×10^{-1}	7.69×10^{-1}	0.5
1	1.58	1.59	0.1
2	2.82	2.81	0.9
3	4.49	4.49	0.1
4	6.51	6.57	0.9
5	8.84	8.92	0.8
6	1.14×10^{1}	1.15×10^{1}	0.6
7	1.43×10^{1}	1.44×10^{1}	0.4
8	1.74×10^{1}	1.74×10^{1}	0.6
9	2.06×10^{1}	2.08×10^{1}	0.7
10	2.41×10^{1}	2.42×10^{1}	0.6
11	2.77×10^{1}	2.78×10^{1}	0.2
12	3.15×10^{1}	3.13×10^{1}	0.7

APPENDIX D

LISTING OF THE COMPUTER PROGRAM

The computer program we developed for our analysis is listed below. Parts of the program are from the Harwell Subroutine Library, Harwell, England.

```
C THIS COMPUTER PROGRAM 'SOLAR' SOLVES A ONE-DIMENSIONAL CONTINUITY      00001000
C EQUATION FOR ELECTRONS OR HOLES IN A HEAVILY-DOPED SEMICONDUCTOR       00002000
C REGION WITH SPECIFIED BOUNDARY CONDITIONS.                             00003000
C IN THE CONTINUITY EQUATION A POSITION-DEPENDENT GENERATION AND         00004000
C RECOMBINATION RATES CAN BE CONSIDERED.                                 00005000
C THE CONTINUITY EQUATION IS PUT IN THE FORM OF A SECOND-ORDER LINEAR    00006000
C NONHOMOGENOUS DIFFERENTIAL EQUATION WITH VARIABLE COEFFICIENTS :       00007000
C              Y'' + F(X)*Y' + G(X)*Y = H(X)                             00008000
C THE ABOVE EQUATION IS THEN DISCRETIZED BY A UNIFORMLY-SPACED MESH OF   00009000
C POINTS OVER WHICH VALUES OF F(X),G(X),AND H(X) ARE SUPPLIED IN THE     00010000
C MAIN PROGRAM BY THE USER.                                              00011000
C THE METHOD OF SOLUTION IS BY RELAXATION WITH CORRECTIONS TO THE        00012000
C THIRD AND FOURTH DIFFERENCES.  THE LIMIT OF ACCURACY OF                00013000
C THE SOLUTION, YA , AND THE NUMBER OF TIMES THE CORRECTION TERMS ARE    00014000
C TO BE APPLIED, LIM , ARE SPECIFIED BY THE USER.                        00015000
C THE CALCULATIONS ARE IN DOUBLE PRECISION AND FORTRAN-IV G-COMPILER     00016000
C IS USED .                                                              00017000
C MIXED BOUNDARY CONDITIONS AT THE END REGIONS CAN BE USED AND ARE       00018000
C SPECIFIED BY THE USER .                                                00019000
C A POSITION DEPENDENT GENERATION RATE ( GEN(X) ) CAN BE INCLUDED IN     00020000
C H(X) :      H(X) = GEN(X) / DP                                         00021000
C                                                                        00022000
C IN ITS PRESENT FORM , THE PROGRAM SOLVES THE CONTINUITY EQUATION       00023000
C FOR HOLES  FOR A POSITION-DEPENDENT RECOMBINATION RATE AND NO          00024000
C GENERATION (H(X) IS SET TO ZERO).                                      00025000
C LANYON-TUFT MODEL OF BANDGAP NARROWING IS IMPLEMENTED, AND FERMI-      00026000
C DIRAC STATISTICS ARE INCLUDED BY THE ANALYTIC APPROXIMATION OF         00027000
C SHIBIB ( RELATIVE ERROR IS LESS THAN  2.5% )                           00028000
C                                                                        00029000
C REQUIRED CONSTANTS ARE SPECIFIED                                       00030000
C DND(I) IS THE ACTUAL IMPURITY PROFILE                                  00031000
C WE IS THE WIDTH OF THE REGION, AND HD IS THE SPACING INTERVAL          00032000
```

```
C DNEF(I) IS THE EFFECTIVE IMPURITY PROFILE                                    00033000
C BOUNDARY CONDITIONS ARE SPECIFIED IN : YO(1) AND YN(I) I=1 OR 2 OR 3         00034000
      IMPLICIT REAL*8(A-H,O-Z)                                                 00035000
C THE COMMON AREA SIZE IS 61 X 8 = 488                                         00036000
      COMMON W(488)                                                            00037000
C THE NUMBER OF EQUALLY-SPACED MESH POINTS IS 61                               00038000
      DIMENSION  F(61),G(61),H(61),Y(61),YO(3),YN(3),E(61),DNEF(61),DND(       00039000
     C61)                                                                      00040000
       Q=1.6D-19                                                               00041000
       B1=22.5D-12                                                             00042000
       B2=162.D-03/(1.D+20)**(1./6.)                                           00043000
       QPO=0.D+00                                                              00044000
       DNI2=2.26D+20                                                           00045000
       WE=0.25D-04                                                             00046000
       DP=4.D+00                                                               00047000
       UKT=0.0259                                                              00048000
       DNS=1.D+20                                                              00049000
       DNO=1.D+18                                                              00050000
       DL=WE/(2.*DSQRT(-DLOG(DNO/DNS)))                                        00051000
       SP=1.D+07                                                               00052000
       CA=2.8D-31                                                              00053000
       HD=WE/60.                                                               00054000
       DOS=2.8D+19                                                             00055000
       AA=8.61D-03                                                             00056000
       BB=-3.17D-01                                                            00057000
       DD=-8.83D-01                                                            00058000
       RTO=-6.D+00                                                             00059000
       DO 365 I=1,61                                                           00060000
       X=(I-1)*HD                                                              00061000
       DND(I)=DNS*DEXP(-(WE-X)**2/(4.*DL**2))                                  00062000
       G(1)=-(CA/DP)*DND(I)**2                                                 00063000
       H(1)=0.                                                                 00064000
```

```
      DN=DND(I)                                                          00065000
      CALL FOCUS(RTO,DN,DDS,Z)                                           00066000
      RTO=Z                                                              00067000
      IF(Z-3.0D+00)5,6,6                                                 00068000
    5 CED=-0.044*Z+0.31                                                  00069000
      GO TO 100                                                          00070000
    6 CFD=DEXP(AA*Z**2+BB*Z+DD)                                          00071000
  100 IF(DND(I)-4.0D+19)101,102,102                                      00072000
  101 DNEF(I)=DND(I)*(1.D+00+CFD*DEXP(Z))*DEXP(-B1*DSQRT(DND(I))/UKT)    00073000
      GO TO 105                                                          00074000
  102 DNEF(I)=DND(I)*(1.D+00+CFD*DEXP(Z))*DEXP(-B2*DND(I)**(1.D+00/6.D+00)00075000
     C0)/UKT)                                                            00076000
  105 PRINT 80 ,X,DNEF(I),DND(I),Z                                       00077000
   80 FORMAT(5X,'X=',D13.6,5X,'DNEF=',D13.6,5X,'DND=',D13.6,5X,'Z=',D13.00078000
     C6)                                                                 00079000
  365 CONTINUE                                                           00080000
      DO 95 I=1,60                                                       00081000
   95 F(I)=-(1./DNEF(I))*((DNEF(I+1)-DNEF(I))/HD)                        00082000
      F(61)=F(60)                                                        00083000
      XO=0.                                                              00084000
      XN=WE                                                              00085000
      YO(1)=0.                                                           00086000
      YO(2)=1.                                                           00087000
      YO(3)=DNI2                                                         00088000
      YN(1)=DP                                                           00089000
      YN(2)=SP                                                           00090000
      YN(3)=0.                                                           00091000
      LIM=4                                                              00092000
      YA=1.1D+11                                                         00093000
      CALL DD01AD(Y,XO,XN,61,YO,YN,F,G,H,E,LIM,YA,NUM)                   00094000
      PRINT 70,XO,XN                                                     00095000
   70 FORMAT(10X,'XO=',D13.6,10X,'XN=',D13.6)                            00096000
```

```
      PRINT 60                                                          00097000
      PRINT 72,LIM                                                      00098000
   72 FORMAT(10X,'LIM=',I6)                                             00099000
      PRINT 60                                                          00100000
      PRINT 73,YA                                                       00101000
   73 FORMAT(10X,'YA=',D13.6)                                           00102000
      PRINT 60                                                          00103000
      PRINT 74,NUM                                                      00104000
   74 FORMAT(10X,'NUM=',I6)                                             00105000
      PRINT 60                                                          00106000
      DJPA=0.D+00                                                       00107000
      DO 90 I=2,60,2                                                    00108000
      QPO=QPO+(Y(I-1)/DNEF(I-1)+4.*Y(I)/DNEF(I)+Y(I+1)/DNEF(I+1))*HD*Q/300109000
     C.                                                                 00110000
      DJPA=DJPA+Q*(HD/3.)*CA*(Y(I-1)*DND(I-1)**2/DNEF(I-1)+4.*Y(I)*DND(I00111000
     C)**2/DNEF(I)+Y(I+1)*DND(I+1)**2/DNEF(I+1))                        00112000
   90 CONTINUE                                                          00113000
      DJP1=-Q*DP*(1./DNEF(1))*(Y(2)-Y(1))/HD                            00114000
      PRINT 97,DJP1                                                     00115000
   97 FORMAT(10X,'DJPO FROM DIFF. APROX. =',D13.6)                      00116000
      PRINT 60                                                          00117000
      DJPS=Q*SP*(Y(61)/DNEF(61))                                        00118000
      DJPO=DJPA+DJPS                                                    00119000
      TP=QPO/DJPO                                                       00120000
      TPS=QPO/DJPS                                                      00121000
      TPA=QPO/DJPA                                                      00122000
      PRINT 91,QPO                                                      00123000
   91 FORMAT(10X,'QPO=',D13.6)                                          00124000
      PRINT 60                                                          00125000
      PRINT 92,DJPS,DJPA,DJPO                                           00126000
   92 FORMAT(10X,'DJPS=',D13.6,10X,'DJPA=',D13.6,10X,'DJPO=',D13.6)     00127000
      PRINT 60                                                          00128000
```

```
      PRINT 93,TPS,TPA,TP                                                    00129000
   93 FORMAT(10X,'TPS=',D13.6,10X,'TPA=',D13.6,10X,'TP=',D13.6)              00130000
   60 FORMAT(///)                                                            00131000
      STOP                                                                   00132000
      END                                                                    00133000
      SUBROUTINE DD01AD(Y,XO,XN,NPT,YO,YN,F,G,H,E,LIM,YA,NUM)                00134000
C                                                                            00135000
C     DD01AD   SOLVES A 2 POINT BOUNDARY VALUE PROBLEM OF THE FORM:-         00136000
C              Y" + F(X)*Y' + G(X)*Y = H(X)                                  00137000
C              BY A FINITE DIFFERENCE APPROXIMATION                          00138000
C                                                                            00139000
C     Y . . . THE FIRST NPT ELEMENTS OF THIS ARRAY ARE THE SOLUTION          00140000
C              ON RETURN                                                     00141000
C     XO. . . THE LOWER LIMIT OF X                                           00142000
C     XN. . . THE UPPER LIMIT OF X                                           00143000
C     NPT . . THE NUMBER OF POINTS WHERE THE VALUE OF Y IS REQUIRED          00144000
C              (INCLUDING XO AND XN)                                         00145000
C     YO. . . THE BOUNDARY CONDITION AT XO IS GIVEN BY:-                     00146000
C              YO(1)*Y' + YO(2)*Y = YO(3)                                    00147000
C     YN. . . THE BOUNDARY CONDITION AT XN IS GIVEN BY:-                     00148000
C              YN(1)*Y' + YN(2)*Y = YN(3)                                    00149000
C              YO AND YN ARE BOTH ARRAYS OF DIMENSION AT LEAST 3.            00150000
      IMPLICIT REAL*8 (A-H,O-Z)                                              00151000
C                                                                            00152000
C     F). . . ( ARE ALL ARRAYS OF DIMENSION AT LEAST NPT.THE FIRST           00153000
C     G). . . ( NPT ELEMENTS CONTAINING THE VALUES OF F(X),G(X),&            00154000
C     H). . . ( H(X) AT XO.....XN.                                           00155000
C     E . . . AN ARRAY OF AT LEAST NPT SET TO THE DIFFERENCE BETWEEN THE     00156000
C              INITIAL APPROXIMATION AND THE CORRECTED SOLUTION.I.E. THE     00157000
C              EFFECT OF THE THIRD AND FOURTH DIFFERENCES.                   00158000
C     LIM . . SET BY THE USER TO THE MAXIMUM NUMBER OF TIMES THE             00159000
C              DIFFERENCE CORRECTIONS ARE TO BE APPLIED.IF CORRECTIONS       00160000
```

```
C             ARE NOT TO BE APPLIED SET LIM=0                                   00161000
C     YA. . . SET BY THE USER TO THE MAXIMUM ABSOLUTE DIFFERENCE              00162000
C             BETWEEN THE LAST TWO APPROXIMATIONS TO Y.IF THIS IS               00163000
C             LESS THAN YA THE ROUTINE RETURNS.                                 00164000
C     NUM . . SET BY THE ROUTINE TO THE NUMBER OF TIMES THE                   00165000
C             CORRECTION TERMS ARE APPLIED.IF AFTER LIM CORRECTIONS             00166000
C             HAVE BEEN APPLIED THEY ARE STILL GREATER THAN YA NUM IS           00167000
C             SET TO -1                                                         00168000
C     W . . . THE FIRST 8*NPT WORDS OF COMMON ARE USED AS WORKING             00169000
C             SPACE.                                                            00170000
      COMMON W(488)                                                           00171000
      DIMENSION  F(61),G(61),H(61),Y(61),YO(3),YN(3),E(61),DNEF(61),DND(00172000
     C61)                                                                     00173000
C                                                                             00174000
C      EXISTS IF THERE ARE NO BOUNDARY CONDITIONS AT XO OR XN.                00175000
C     IF LIM IS NEGATIVE THEN MOD(LIM) CORRECTIONS ARE APPLIED TO             00176000
C     THE INITIAL APPROXIMATION IN W(3*NPT+1) TO W(4*NPT).                    00177000
C                                                                             00178000
C      THIS IS ONLY FOR USE AFTER A PREVIOUS CALL OF DD01AD IN THE            00179000
C     SAME PROGRAM,OTHERWISE SEVERAL ARRAY SUBSCRIPTS WILL BE                 00180000
C     UNDEFINED.THE RESULT WILL BE IN Y                                       00181000
      IF(LIM)10,30,30                                                         00182000
   10 LIM = -LIM                                                              00183000
      DO 20 IE = 1,NPT                                                        00184000
      Y(IE)=0.0D0                                                             00185000
   20 CONTINUE                                                                00186000
      GO TO 110                                                               00187000
   30 IF(DABS(YO(1)) + DABS(YO(2)))40,40,60                                   00188000
   40 PRINT 50                                                                00189000
   50 FORMAT(37H NO BOUNDARY CONDITION AT XO IN DD01A)                        00190000
      CALL EXIT                                                               00191000
   60 IF(DABS(YN(1)) + DABS(YN(2)))70,70,90                                   00192000
```

```
   70 PRINT 80                                                          00193000
   80 FORMAT (37H NO BOUNDARY CONDITION AT XN IN DD01A)                 00194000
      CALL EXIT                                                         00195000
C                                                                       00196000
C     INITIALISE THE FOLLOWING FOR USE AS ARRAY SUBSCRIPTS.             00197000
   90 NP = NPT                                                          00198000
      NP2 = NP + NP                                                     00199000
      NP3 = NP2 + NP                                                    00200000
      NP4 = NP3 + NP                                                    00201000
      NP5 = NP4 + NP                                                    00202000
      NP6 = NP5 + NP                                                    00203000
      NP7 = NP6 + NP                                                    00204000
      N = NP - 1                                                        00205000
      NL = NP - 2                                                       00206000
      DX = (XN - X0)/N                                                  00207000
      ZA=DX**2*0.5D0                                                    00208000
C                                                                       00209000
C      SETS UP W FOR THE EQUATIONS GIVING THE FIRST APPROXIMATION TO    00210000
C     THE SOLUTION.W(2) TO W(3*NPT-1) CONTAINS THE LEFT HAND SIDE       00211000
C     MATRIX,AND W(3*NPT+1) TO W(4*NPT) CONTAINS THE RIGHT HAND         00212000
C     SIDE VECTOR,IN A FORM SUITABLE FOR USE IN MA07AD.                 00213000
      W(NP + 1) = -Y0(1) + DX*Y0(2) + ZA*(G(1)*Y0(1) - F(1)*Y0(2))      00214000
      W(NP2+1) = Y0(1)                                                  00215000
      W(NP3+1) = DX*Y0(3) + ZA*(H(1)*Y0(1) - F(1)*Y0(3))                00216000
      W(NP) = YN(1)                                                     00217000
      W(NP2) = -YN(1) - DX*YN(2) + ZA*(G(NP)*YN(1) - F(NP)*YN(2))       00218000
      W(NP4) = -DX*YN(3) + ZA*(H(NP)*YN(1) - F(NP)*YN(3))               00219000
      Y(1)=0.0D0                                                        00220000
      E(1)=0.0D0                                                        00221000
      Y(NP)=0.0D0                                                       00222000
      E(NP)=0.0D0                                                       00223000
      DO 100 IB = 2,N                                                   00224000
```

```
      Y(IB)=0.0D0                                                       00225000
      E(IB)=0.0D0                                                       00226000
      Z = 0.5*DX*F(IB)                                                  00227000
      W(IB) = 1 - Z                                                     00228000
      M1 = NP + IB                                                      00229000
      M2 = NP2 + IB                                                     00230000
      M3 = NP3 + IB                                                     00231000
      W(M1) = DX**2*G(IB) - 2                                           00232000
      W(M2) = 1 + Z                                                     00233000
      W(M3) = DX**2*H(IB)                                               00234000
  100 CONTINUE                                                          00235000
      NPHRT=NP3+1                                                       00236000
C                                                                       00237000
C     MA07AD PRODUCES THE INITIAL SOLUTION IN W(3*NPT+1) TO W(4*NPT)    00238000
      CALL MA07AD(W,W(NPHRT),NP,NP,3,1,1)                               00239000
  110 DO 220 J = 1,LIM                                                  00240000
C                                                                       00241000
C      ALTERS Y TO THE LATEST SOLUTION,AND E TO THE AMOUNT OF THE       00242000
C     DIFFERENCE CORRECTIONS SO FAR APPLIED.                            00243000
      DO 130 IC = 1, NP                                                 00244000
      NC = NP3 + IC                                                     00245000
      Y(IC) = Y(IC) + W(NC)                                             00246000
      IF(J-1)130,130,120                                                00247000
  120 E(IC) = E(IC) + W(NC)                                             00248000
  130 CONTINUE                                                          00249000
C                                                                       00250000
C      IF LIM IS ZERO RETURNS BEFORE APPLING ANY CORRECTIONS,           00251000
C     SETTING NUM TO ZERO.                                              00252000
      IF(LIM)140,140,150                                                00253000
  140 NUM = 0                                                           00254000
      RETURN                                                            00255000
  150 NPHRT=NP3+1                                                       00256000
```

```
C                                                                       00257000
C     TA03AD FINDS THE CENTRAL DIFFERENCES OF EVEN ORDER UP TO FOUR.    00258000
      CALL TA03AD(W(NPHRT),NP,1,1,NP,4,0)                               00259000
C                                                                       00260000
C      SETS THE COEFFICIENTS IN THE MATRIX EQUATION TO FIND THE         00261000
C     CORRECTION DUE TO THE HIGHER ORDER DIFFERENCES.                   00262000
      W(NP7+2) = W(NP7+3)                                               00263000
      W(NP6+2) = W(NP6+3) - W(NP7+2)                                    00264000
      NA = NP7 + N                                                      00265000
      W(NA) = W(NA-1)                                                   00266000
      NB = NP6 + N                                                      00267000
      W(NP7) = W(NA) + W(NB)                                            00268000
      DO 190 J2 = 2,N                                                   00269000
      IF(F(J2))170,160,170                                              00270000
  160 CA=0.0D0                                                          00271000
      GO TO 180                                                         00272000
  170 NC = NP6 + J2 + I                                                 00273000
      CA = -(W(NC-1) + W(NC))/12                                        00274000
  180 NE = NP7 + J2                                                     00275000
      CB = -W(NE)/12                                                    00276000
      NF = NP3 + J2                                                     00277000
      W(NF) = -(CB + CA*DX*F(J2))                                       00278000
  190 CONTINUE                                                          00279000
      W(NP3+1) = YO(1)*(4*W(NP6+2) + 3*W(NP7+2))/24                     00280000
      W(NP4) = YN(1)*(W(NA-1) - 4*W(NP7))/24                            00281000
      NPHRT=NP3+1                                                       00282000
C                                                                       00283000
C     MA07AD SOLVES THE EQUATION AND PUTS THE CORRECTION TERMS IN       00284000
C     W(3*NPT+1) TO W(4*NPT).                                           00285000
      CALL MA07AD(W,W(NPHRT),NP,NP,J,I,0)                               00286000
C                                                                       00287000
C      CHECKS IF ANY DIFFERENCE CORRECTIONS ARE GREATER THAN YA.IF NOT  00288000
```

```
C     IT APPLIES THE CORRECTION,ALTERS E,SETS NUM AND RETURNS.                00289000
      DO 200 ID = 1,NP                                                        00290000
      NG = NP3 + ID                                                           00291000
      IF(DABS(W(NG)) - YA)200,200,220                                         00292000
  200 CONTINUE                                                                00293000
      DO 210 JJ = 1,NP                                                        00294000
      NH = NP3 + JJ                                                           00295000
      E(JJ) = E(JJ) + W(NH)                                                   00296000
      Y(JJ) = Y(JJ) + W(NH)                                                   00297000
  210 CONTINUE                                                                00298000
      NUM = J                                                                 00299000
      RETURN                                                                  00300000
  220 CONTINUE                                                                00301000
C                                                                             00302000
C      NO SOLUTION OF THE PROBLEM WITHIN THE DESIRED ACCURACY HAS             00303000
C     BEEN FOUND AFTER LIM APPLICATIONS OF THE CORRECTION TERMS.              00304000
      NUM = -1                                                                00305000
      RETURN                                                                  00306000
      END                                                                     00307000
      SUBROUTINE MA07AD (A,B,MO,NO,NW,NR,NL)                                  00308000
      IMPLICIT REAL*8(A-H,O-Z)                                                00309000
C     SOLVES SETS OF LINEAR EQUATIONS OF THE FORM A*X=B, WHERE A IS A         00310000
C     SQUARE MATRIX OF ORDER NO AND X,B ARE MATRICES EACH WITH NO ROWS        00311000
C     AND NR COLUMNS.   THE SOLUTION X OVERWRITES THE RHS B.   THE ONLY       00312000
C     NON ZERO ELEMENTS OF A APPEAR IN A BAND OF WIDTH NW CENTRED ON THE      00313000
C     DIAGONAL.                          THE ELEMENTS IN THE I TH ROW         00314000
C     AND J TH COLUMN OF A AND B MUST BE WRITTEN INTO A(I,J-I+(NW+1)/2)       00315000
C     AND B(I,J) RESPECTIVELY AND THE FIRST DIMENSION OF THE ARRAYS A,B       00316000
C     MUST BE MO IN THE CALLING ROUTINE.   NL MUST BE NON ZERO UNLESS         00317000
C     THE SAME LHS IS TO BE USED REPEATEDLY IN WHICH CASE SPEED CAN BE        00318000
C     GAINED AFTER THE INITIAL ENTRY TO THE SUBROUTINE BY LEAVING THE         00319000
C     ARRAY A IN THE FORM PRODUCED BY THE INITIAL ENTRY AND SETTING NL        00320000
```

```
C     TO ZERO FOR SUBSEQUENT ENTRIES.                                   00321000
      DIMENSION A(MO,1),B(MO,1)                                         00322000
      M=(NW+I)/2                                                        00323000
      MM1=M-1                                                           00324000
      I=NO                                                              00325000
      DO 14 L1=1,NO                                                     00326000
      IF(NL)1,4,1                                                       00327000
 1    A(I,M)=1.0/A(I,M)                                                 00328000
      J=MM1                                                             00329000
      DO 3 L2=1,MM1                                                     00330000
      IF(I+J-M)4,4,2                                                    00331000
 2    A(I,J)=A(I,J)*A(I,M)                                              00332000
      J=J-1                                                             00333000
 3    CONTINUE                                                          00334000
 4    DO 5 L=1,NR                                                       00335000
      B(I,L)=B(I,L)*A(I,M)                                              00336000
 5    CONTINUE                                                          00337000
      IF(I-1)13,13,6                                                    00338000
 6    DO 12 K=1,MM1                                                     00339000
      I1=I-K                                                            00340000
      IF(I1)13,13,7                                                     00341000
 7    I2=M+K                                                            00342000
      IF(NL)8,11,8                                                      00343000
 8    J=MM1                                                             00344000
      DO 10 L2=1,MM1                                                    00345000
      IF(I+J-M)11,11,9                                                  00346000
 9    I3=J+K                                                            00347000
      A(I1,I3)=A(I1,I3)-A(I,J)*A(I1,I2)                                 00348000
      J=J-1                                                             00349000
 10   CONTINUE                                                          00350000
 11   DO 12 L=1,NR                                                      00351000
      B(I1,L)=B(I1,L)-B(I,L)*A(I1,I2)                                   00352000
```

```
 12    CONTINUE                                                  00353000
 13    I=I-1                                                     00354000
 14    CONTINUE                                                  00355000
 15    DO 19 I=2,NO                                              00356000
       J=MM1                                                     00357000
       DO 18 L1=1,MM1                                            00358000
       I1=I+J-M                                                  00359000
       IF(I1)19,19,16                                            00360000
 16    DO 17 L=1,NR                                              00361000
       B(I,L)=B(I,L)-B(I1,L)*A(I,J)                              00362000
 17    CONTINUE                                                  00363000
       J=J-1                                                     00364000
 18    CONTINUE                                                  00365000
 19    CONTINUE                                                  00366000
       RETURN                                                    00367000
       END                                                       00368000
       SUBROUTINETA03AD(Y,MU,NL,NS,NU,NO,LO)                     00369000
       IMPLICIT REAL*8(A-H,O-Z)                                  00370000
C  EVALUATES CENTRAL DIFFERENCES                                 00371000
       DIMENSION Y(MU,5)                                         00372000
       LOJ=LO+1                                                  00373000
       NH=NS/2                                                   00374000
       NSH=NS-NH                                                 00375000
       L=NL+NS                                                   00376000
       M=NU                                                      00377000
       DO 11 J=1,NO                                              00378000
       GO TO (1,2,3),LOJ                                         00379000
 1     JA=J+1                                                    00380000
       JB=J                                                      00381000
       GO TO 6                                                   00382000
 2     JA=(J+3)/2                                                00383000
       JB=(J+2)/2                                                00384000
```

```
      GO TO 6                                                          00385000
3     JA=(J+4)/2                                                       00386000
      IF(J-1)5,4,5                                                     00387000
4     JB=1                                                             00388000
      GO TO 6                                                          00389000
5     JB=(J+3)/2                                                       00390000
6     IF(J/2*2-J)9,7,9                                                 00391000
7     L1=L                                                             00392000
      STL=Y(L1,JA)                                                     00393000
      DO 8 I=L,M,NS                                                    00394000
      IA=1                                                             00395000
      IB=I+NSH                                                         00396000
      IC=I-NH                                                          00397000
      Y(IA,JA)=Y(IB,JB)-Y(IC,JB)                                       00398000
8     CONTINUE                                                         00399000
      IF(LO-2)15,12,15                                                 00400000
12    IF(NS-1)15,14,15                                                 00401000
14    Y(M1,JA)=STM                                                     00402000
15    L=L+NS                                                           00403000
      GO TO 11                                                         00404000
9     IC=L-NS                                                          00405000
      WS2=Y(IC,JB)                                                     00406000
      M1=M-NH                                                          00407000
      STM=Y(M1,JA)                                                     00408000
      DO 10 I=L,M,NS                                                   00409000
      IA=I-NH                                                          00410000
      IB=1                                                             00411000
      WS1=WS2                                                          00412000
      WS2=Y(IB,JB)                                                     00413000
      Y(IA,JA)=WS2-WS1                                                 00414000
10    CONTINUE                                                         00415000
      IF(LO-1)18,16,18                                                 00416000
```

```
 16    IF(NS-1)18,13,18                                                  00417000
 13    IF(J-1)17,18,17                                                   00418000
 17    Y(L1,JA)=STL                                                      00419000
 18    M=M-NS                                                            00420000
 11    CONTINUE                                                          00421000
       RETURN                                                            00422000
       END                                                               00423000
       SUBROUTINE FOCUS(RTO,DN,DOS,RT)                                   00424000
C                                                                        00425000
C      SUBROUTINE FOCUS(RTO,DN,DOS,RT) CALCULATES RT FOR ANY DN,DOS,     00426000
C      AND RTO SPECIFIED IN THE MAIN PROGRAM.                            00427000
C      RTO . . INITIAL ESTIMATE OF RT (THE NORMALIZED FERMI ENERGY)      00428000
C      DN . . IMPURITY CONCENTRATION                                     00429000
C      DOS. . EFFECTIVE DENSITY-OF-STATES IN CONDUCTION OR VALENCE BANDS 00430000
C      THE SUBROUTINE CALLS FUNCTION YM, AND IT RETURNS TO THE MAIN      00431000
C      PROGRAM THE VALUE OF RT.                                          00432000
C                                                                        00433000
       IMPLICIT REAL*8(A-H,O-Z)                                          00434000
       RT=RTO                                                            00435000
       DL1=1.D+00                                                        00436000
       DL2=1.D-01                                                        00437000
       DL3=1.D-02                                                        00438000
       IF(YM(RT,DN,DOS))500,501,502                                      00439000
  500  RT=RT-DL1                                                         00440000
       IF(YM(RT,DN,DOS))500,501,503                                      00441000
  502  RT=RT+DL1                                                         00442000
       IF(YM(RT,DN,DOS))503,501,502                                      00443000
  503  IF(YM(RT,DN,DOS))504,501,505                                      00444000
  504  RT=RT-DL2                                                         00445000
       IF(YM(RT,DN,DOS))504,501,506                                      00446000
  505  RT=RT+DL2                                                         00447000
       IF(YM(RT,DN,DOS))506,501,505                                      00448000
```

```
  506 IF(YM(RT,DN,DOS))507,501,509                                  00449000
  507 RT=RT-DL3                                                     00450000
      IF(YM(RT,DN,DOS))507,501,501                                  00451000
  509 RT=RT+DL3                                                     00452000
      IF(YM(RT,DN,DOS))501,501,509                                  00453000
  501 RETURN                                                        00454000
      END                                                           00455000
      FUNCTION YM(RT,DN,DOS)                                        00456000
C                                                                   00457000
C     FUNCTION YM(RT,DN,DOS) CALCULATES THE FERMI-DIRAC INTEGRAL    00458000
C     OF ORDER ONE-HALF FOR ANY VALUE OF RT. THE CALCULATION IS     00459000
C     BASED ON POLYNOMIAL APPROXIMATIONS.                           00460000
C     RT . . IS THE NORMALIZED FERMI ENERGY                         00461000
C     DN . . IS THE IMPURITY CONCENTRATION                          00462000
C     DOS. . IS THE EFFECTIVE DENSITY-OF-STATES                     00463000
C     DN, DOS, AND RT SPECFIED IN SUBROUTINE FOCUSARE INPUT         00464000
C     PARAMETERS. THE FUNCTION RETURNS THE VALUE OF THE FERMI-DIRAC 00465000
C     INTEGRAL OF ORDER 1/2 .                                       00466000
C                                                                   00467000
      IMPLICIT REAL*8(A-H,O-Z)                                      00468000
      DIMENSION A(7),B(8),C(6),D(5),DK(6)                           00469000
      A(1)=-0.35353667                                              00470000
      A(2)=+0.19210895                                              00471000
      A(3)=-0.12236525                                              00472000
      A(4)=0.78991718D-01                                           00473000
      A(5)=-0.43441957D-01                                          00474000
      A(6)=+0.16320377D-01                                          00475000
      A(7)=-0.29297496D-02                                          00476000
      B(1)=+0.76514805                                              00477000
      B(2)=+0.60491025                                              00478000
      B(3)=+0.18990505                                              00479000
      B(4)=+0.20131714D-01                                          00480000
```

```
      B(5)=-0.39688853D-02                                              00481000
      B(6)=-0.76558999D-03                                              00482000
      B(7)=+0.39807837D-03                                              00483000
      B(8)=-0.28395599D-04                                              00484000
      C(1)=+1.0002404                                                   00485000
      C(2)=+1.1981922                                                   00486000
      C(3)=+2.9838285                                                   00487000
      C(4)=-24.984495                                                   00488000
      C(5)=+96.877279                                                   00489000
      C(6)=-156.23522                                                   00490000
      D(1)=+1.0000313                                                   00491000
      D(2)=+1.2248008                                                   00492000
      D(3)=+1.8177898                                                   00493000
      D(4)=-5.0849956                                                   00494000
      D(5)=-3.2409718                                                   00495000
      DK(1)=1.0                                                         00496000
      DK(2)=1.2337005                                                   00497000
      DK(3)=1.0654119                                                   00498000
      DK(4)=9.7015185                                                   00499000
      DK(5)=242.71502                                                   00500000
      DK(6)=11865.691                                                   00501000
    1 IF(RT+2.)9,11,11                                                  00502000
    9 SIGN=+1.                                                          00503000
      SMU=0.D+00                                                        00504000
      DO 10 I=1,12                                                      00505000
      DI=I                                                              00506000
      SM=SIGN*DEXP(DI*RT)/DI**(3./2.)                                   00507000
      SMU=SMU+SM                                                        00508000
      SIGN=SIGN*(-1.)                                                   00509000
   10 CONTINUE                                                          00510000
      YM=DN/DOS-SMU                                                     00511000
```

```
      GO TO 4                                                          00512000
   11 IF(RT)12,13,13                                                   00513000
   12 SUM=0.D+00                                                       00514000
      DO 14 I=1,7                                                      00515000
      S=A(I)*DEXP((I+1)*RT)                                            00516000
      SUM=SUM+S                                                        00517000
   14 CONTINUE                                                         00518000
      YM=DN/DOS-(DEXP(RT)+SUM)                                         00519000
      GO TO 4                                                          00520000
   13 IF(RT-3.0)15,16,16                                               00521000
   15 TUM=0.D+00                                                       00522000
      DO 17 I=1,8                                                      00523000
      T=B(I)*RT**(I-1)                                                 00524000
      TUM=TUM+T                                                        00525000
   17 CONTINUE                                                         00526000
      YM=DN/DOS-TUM                                                    00527000
      GO TO 4                                                          00528000
   16 IF(RT-6.0)18,19,19                                               00529000
   18 YUM=0.D+00                                                       00530000
      DO 20 I=1,6                                                      00531000
      YW=C(I)/RT**(2*(I-1))                                            00532000
      YUM=YUM+YW                                                       00533000
   20 CONTINUE                                                         00534000
      FDI=0.75225278*YUM*(RT**(3./2.))                                 00535000
      YM=DN/DOS-FDI                                                    00536000
      GO TO 4                                                          00537000
   19 IF(RT-12.0)21,23,23                                              00538000
   21 ZUM=0.D+00                                                       00539000
      DO 22 I=1,5                                                      00540000
      ZW=D(I)/RT**(2*(I-1))                                            00541000
      ZUM=ZUM+ZW                                                       00542000
   22 CONTINUE                                                         00543000
```

```
      FDI=0.75225278*ZUM*(RT**(3./2.))                                  00544000
      YM=DN/DOS-FDI                                                     00545000
      GO TO 4                                                           00546000
   23 IF(RT-18.)24,26,26                                                00547000
   24 OUM=0.D+00                                                        00548000
      DO 25 I=1,6                                                       00549000
      O=DK(I)/RT**(2*(I-1))                                             00550000
      OUM=OUM+O                                                         00551000
   25 CONTINUE                                                          00552000
      FDI=0.75225278*OUM*(RT**(3./2.))                                  00553000
      YM=DN/DOS-FDI                                                     00554000
      GO TO 4                                                           00555000
   26 PRINT 27                                                          00556000
   27 FORMAT('RT IS LARGER THAN 18')                                    00557000
    4 RETURN                                                            00558000
      END                                                               00559000
```

APPENDIX E

CHARACTERIZATION OF THE EMITTER CURRENT IN HEAVILY DOPED SILICON DEVICES BY COMPUTER-AIDED NUMERICAL ANALYSIS

In this appendix, we present characterizations of the emitter current as a function of design parameters: surface impurity concentration, surface recombination velocity, and the width of the quasi-neutral emitter region. This study is based on our rigorous computer-aided analysis of the minority-carrier transport in a heavily doped semiconductor region. A listing of the computer program is given in Appendix D.

In Figures E-1 and E-2, we plot the variations of the emitter saturation currents J_{PO} (for an N^+-emitter) and J_{NO} (for a P^+-emitter), including both the surface and the Auger (bulk) components, as functions of S. For values of S lower than 10^4 cm/sec, the emitter current is mostly due to the Auger (bulk) component, while for values higher than 10^4 cm/sec, the emitter current is almost entirely due to surface recombination.

Figures E-3 and E-4 show the dependencies on S of $\bar{\tau}_p$ and $\bar{\tau}_N$, the effective average hole and electron lifetimes in N^+- and P^+-emitters defined by the charge-control relation

$$\bar{\tau}_E = \frac{Q_E}{J_E} \tag{E.1}$$

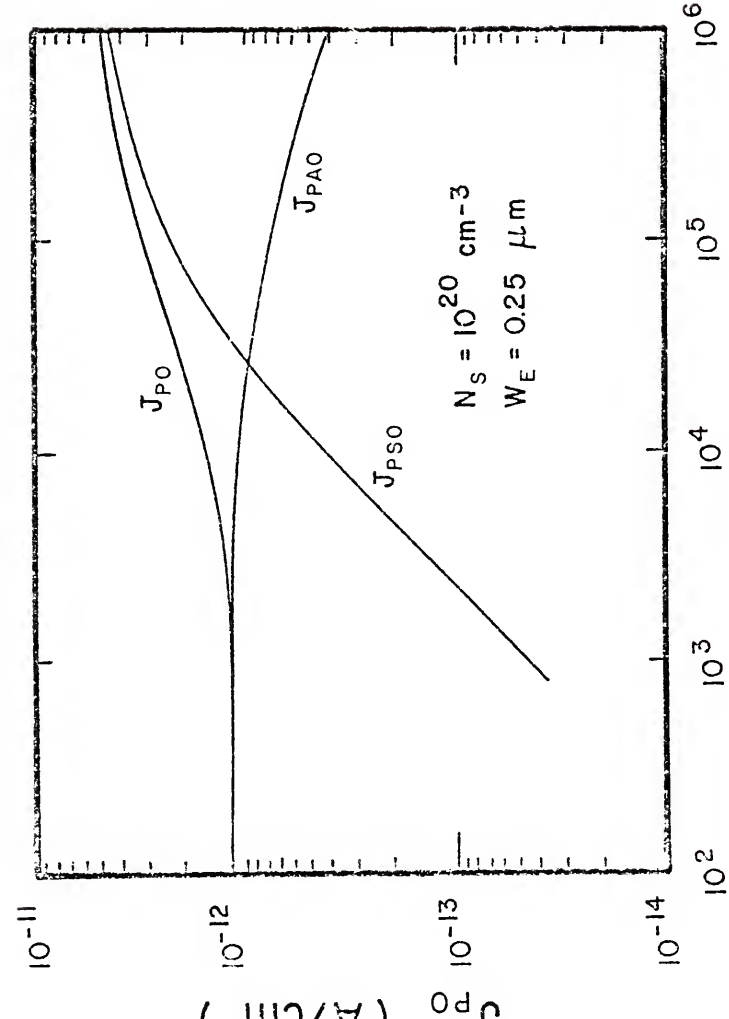

Figure E-1 The hole saturation current density J_{PO} and its surface and Auger components J_{PSO} and J_{PAO}, in an N^+-emitter versus the hole surface recombination velocity S_P

Figure E-2 The electron saturation current density J_{NO} and its surface and Auger components, J_{NSO} and J_{NAO} in a P^+-emitter versus the electron surface recombination velocity S_N

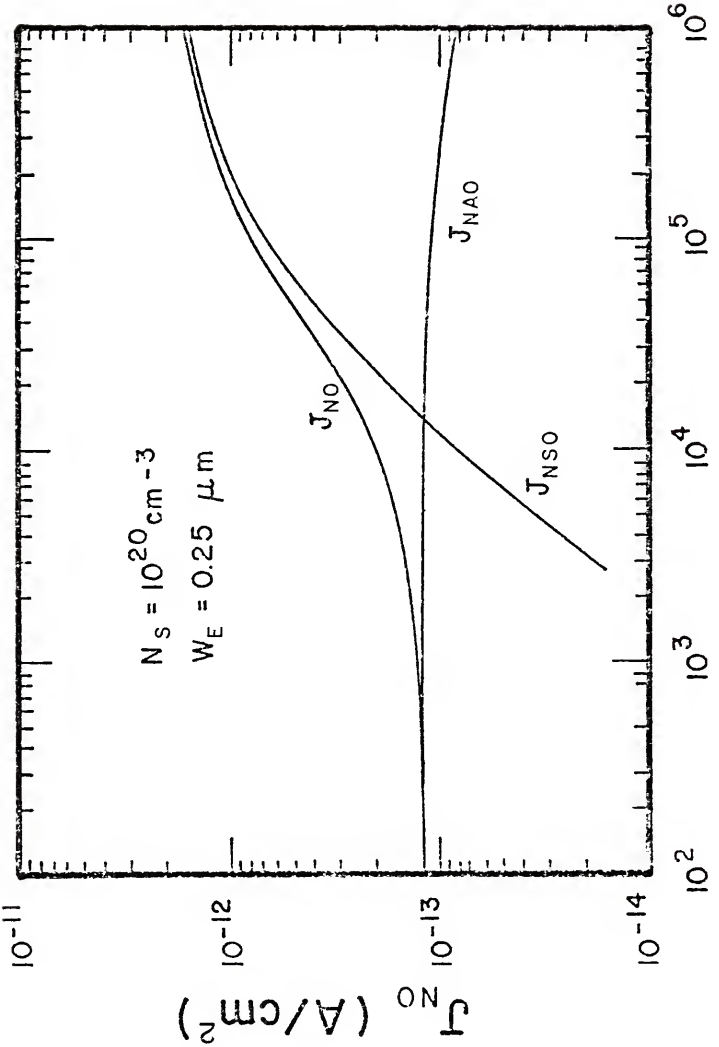
J_{NO} (A/cm^2)
10^{-11}
10^{-12}
10^{-13}
10^{-14}
$N_S = 10^{20}$ cm^{-3}
$W_E = 0.25$ μm
J_{NO}
J_{NAO}
J_{NSO}
10^2
10^3
10^4
10^5
10^6
S_N (cm/sec)

Figure E-3 The effective hole lifetime $\bar{\tau}_p$, the transit time τ_t, and the average Auger lifetime $\bar{\tau}_A$ in an N^+-emitter versus the hole surface recombination velocity Sp

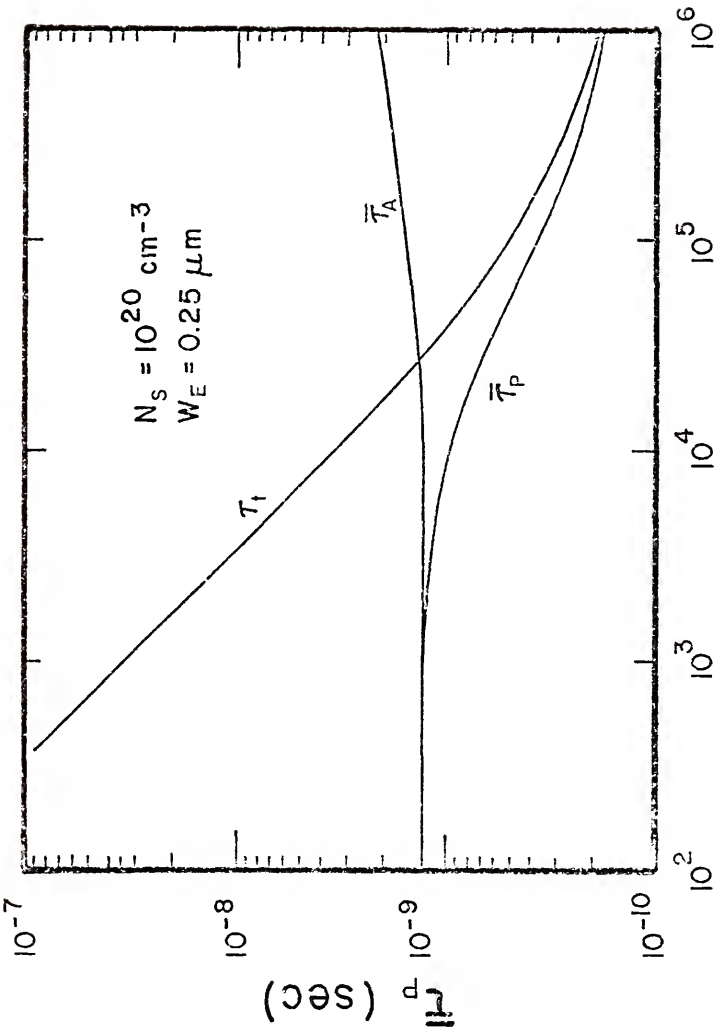
$N_S = 10^{20}$ cm^{-3}
$W_E = 0.25\ \mu$m
τ_t
$\bar{\tau}_A$
$\bar{\tau}_P$
$\bar{\tau}_p$ (sec)
10^{-7}
10^{-8}
10^{-9}
10^{-10}
10^2
10^3
10^4
10^5
10^6
S_P (cm/sec)

Figure E-4 The effective electron lifetime $\bar{\tau}_N$, the transit time τ_t, and the average Auger lifetime $\bar{\tau}_A$ in a P^+-emitter versus the electron surface recombination velocity S_N

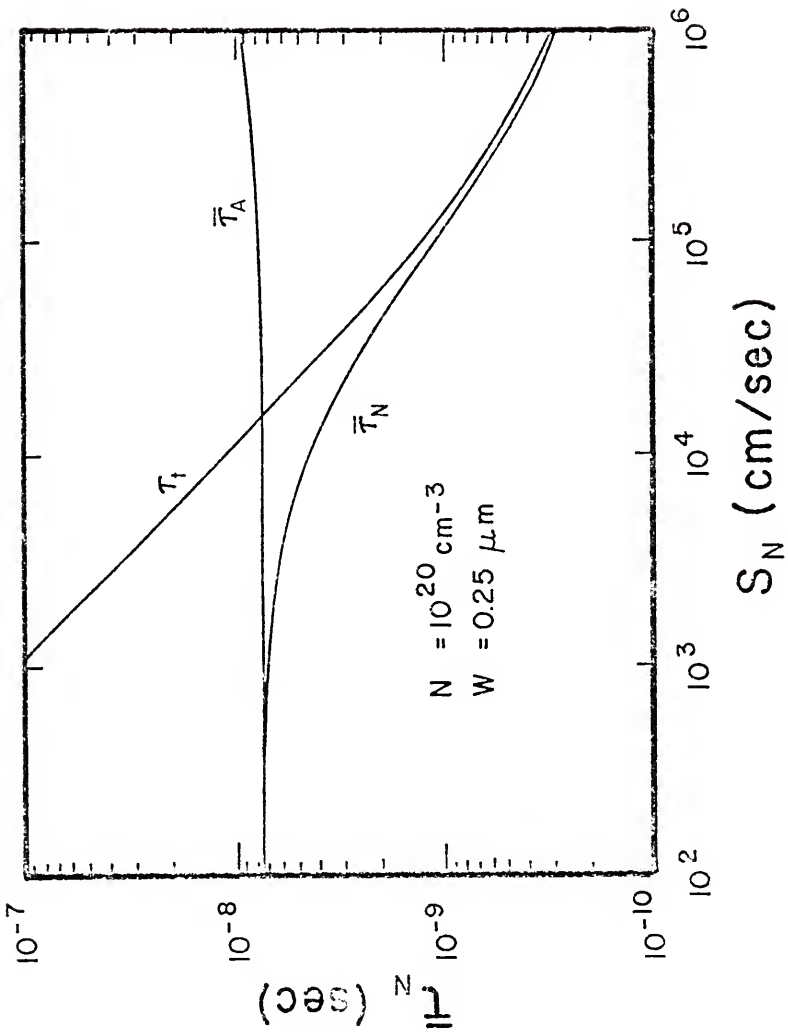
10^{-7}
10^{-8}
10^{-9}
10^{-10}
τ_n (sec)
τ_t
$\bar{\tau}_A$
$\bar{\tau}_N$
N = 10^{20} cm^{-3}
W = 0.25 μm
10^2
10^3
10^4
10^5
10^6
S_N (cm/sec)

where Q_E is the total charge in the emitter, and J_E is the emitter current. From (E.1), we can deduce that

$$\frac{1}{\overline{\tau}_E} = \frac{1}{\tau_t} + \frac{1}{\overline{\tau}_A} \tag{E.2}$$

where τ_t is the minority-carrier transit time, and $\overline{\tau}_A$ is the average Auger (bulk) lifetime for minority carriers. Note that for S larger than 10^4 cm/sec, where $\tau_t < \overline{\tau}_A$, the emitter is transparent to the minority carriers, and for S smaller than 10^4 cm/sec, the emitter is opaque.

In Figures E-5 and E-6, we plot J_{PO} and J_{NO} versus W_E for values of S in the range 10^2-10^7 cm/sec and for $N_S = 10^{19}$ cm^{-3}. Note the strong influence of S on J_{PO} and J_{NO}. Note also the weak dependence of J_{PO} and J_{NO} on W_E. For this case, the emitter saturation current density can be approximately given by the first-order model current expression in (6.7), in which the emitter current is directly proportional to S and is independent of W_E.

Figures E-7 and E-8 are analogous to Figures E-5 and E-6, but with $N_S = 10^{20}$ cm^{-3}. Note the weaker dependence on S and the stronger dependence on W_E of the emitter current compared to the variations of Figures F-5 and F-6. Therefore, we conclude that as N_S increases above 10^{19} cm^{-3}, the emitter current becomes less dependent on S and more dependent on W_E, provided τ_t remains less than $\overline{\tau}_A$.

Furthermore, we see in Figures E-7 and E-8 that the dependencies of J_{PO} and J_{NO} on W_E are altered by variations in S. For low values

Figure E-5 The hole saturation current density J_{PQ} in an N^+-emitter versus the width of the quasi-neutral emitter region W_E for several values of the hole surface recombination velocity S_P

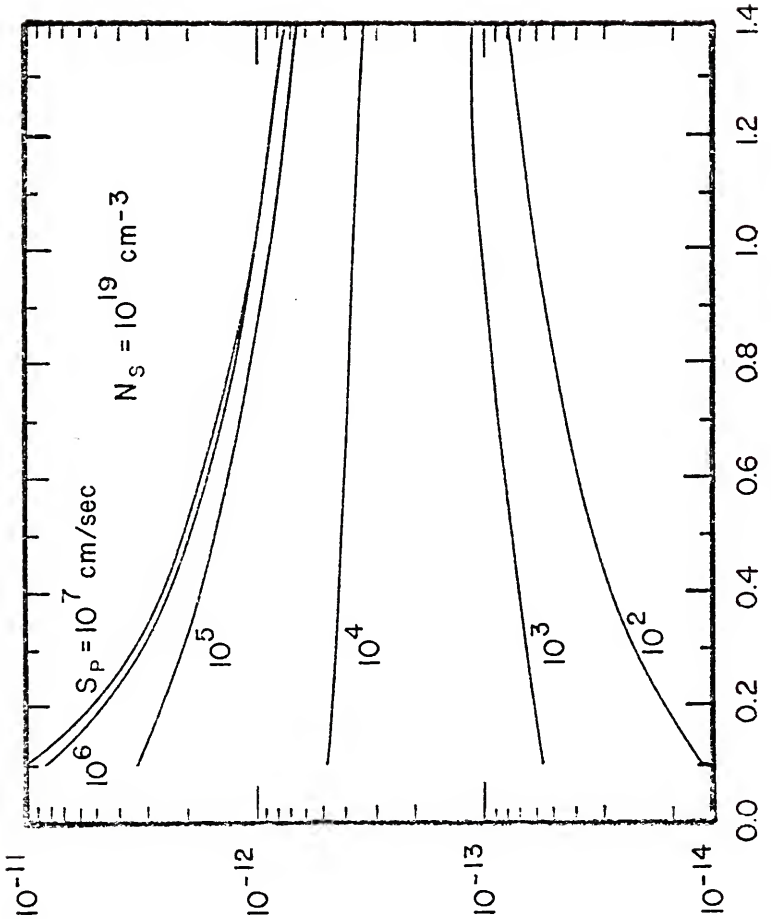
J_{po} (A/cm^2)
10^{-11}
10^{-12}
10^{-13}
10^{-14}
0.0
0.2
0.4
0.6
0.8
1.0
1.2
1.4
W_E (μm)
$S_p = 10^7$ cm/sec
$N_s = 10^{19}$ cm^{-3}
10^6
10^5
10^4
10^3
10^2

Figure E-6 The electron saturation current density J_{NO} in a P^+-emitter versus the width of the quasi-neutral emitter region W_E for several values of the electron surface recombination velocity S_N

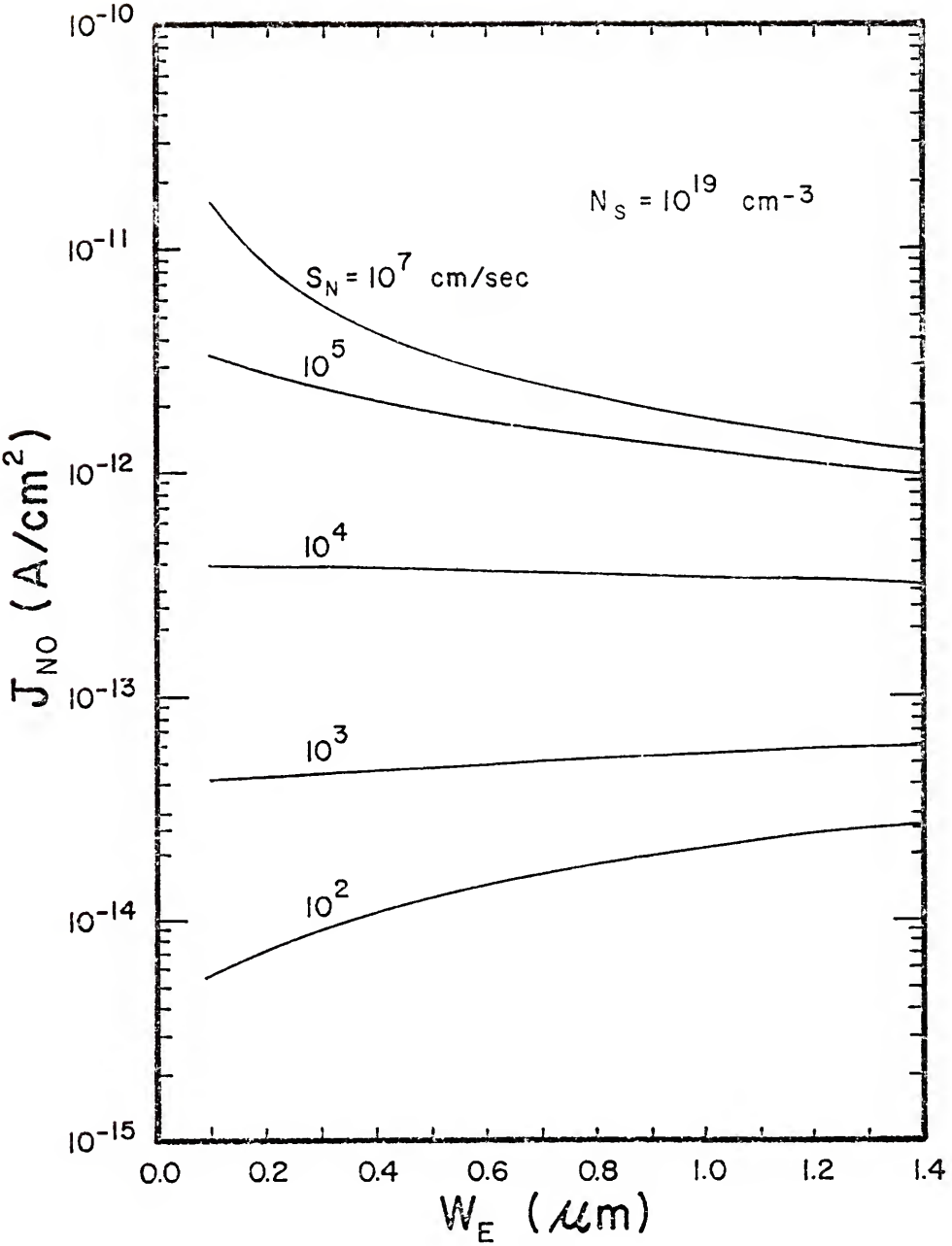
10^{-10}
10^{-11}
10^{-12}
10^{-13}
10^{-14}
10^{-15}
J_{NO} (A/cm^2)
$N_S = 10^{19}$ cm^{-3}
$S_N = 10^7$ cm/sec
10^5
10^4
10^3
10^2
0.0
0.2
0.4
0.6
0.8
1.0
1.2
1.4
W_E (μm)

Figure E-7 The hole saturation current density J_{P0} in an N^+-emitter versus the width of the quasi-neutral emitter region W_E for several values of the hole surface recombination velocity S_p

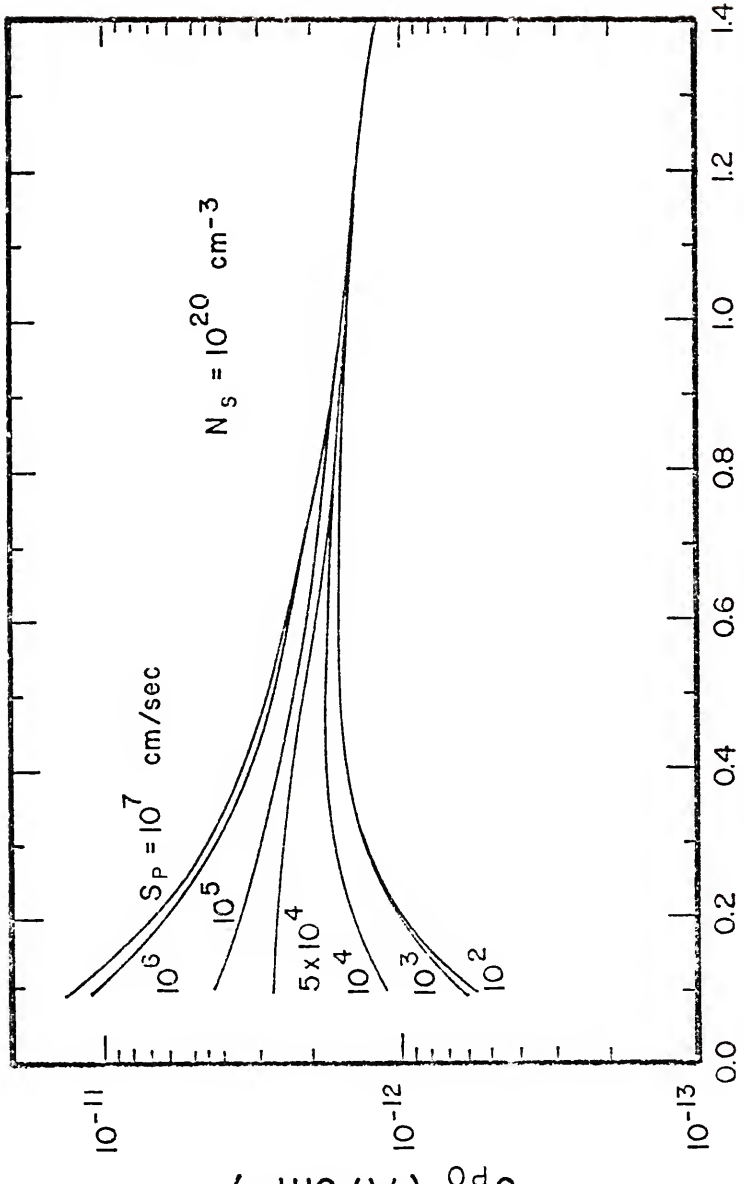
J_{PO} (A/cm^2)
10^{-11}
10^{-12}
10^{-13}
0.0
0.2
0.4
0.6
0.8
1.0
1.2
1.4
W_E (μm)
$N_S = 10^{20}$ cm^{-3}
$S_P = 10^7$ cm/sec
10^6
10^5
5×10^4
10^4
10^3
10^2

Figure E-8 The electron saturation current density J_{NO} in a P^+-emitter versus the width of the quasi-neutral emitter region W_E for several values of the electron surface recombination velocity S_N

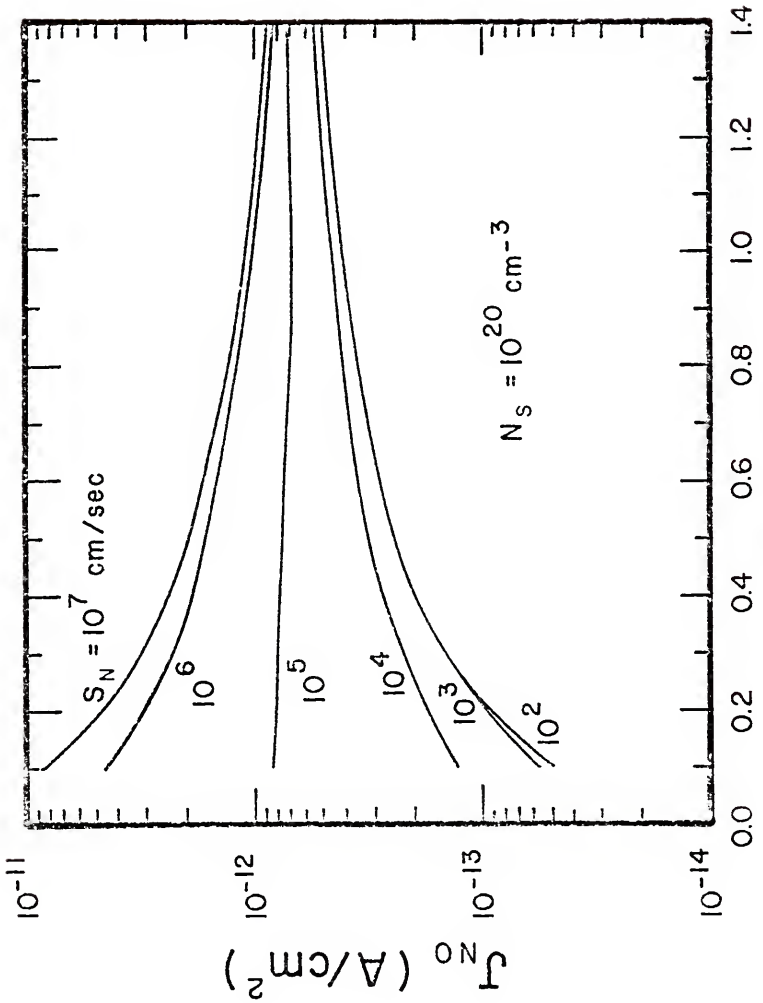
J_{NO} (A/cm^2)
10^{-11}
10^{-12}
10^{-13}
10^{-14}
0.0
0.2
0.4
0.6
0.8
1.0
1.2
1.4
W_E (μm)
$S_N = 10^7$ cm/sec
10^6
10^5
10^4
10^3
10^2
$N_S = 10^{20}$ cm^{-3}

of W_E (less than 0.5 μm for N^+-emitters and less than 1.0 μm for P^+-emitters) J_{PO} and J_{NO} vary as follows:

A. In proportion to W_E for low S

B. Independent of W_E for moderate S, and

C. In inverse proportion to W_E for high S

These dependences of the emitter current on W_E, for different values of S, are consistent with the expressions of the emitter current given by the first-order model expressions (6.5), (6.6), and (6.7).

In this appendix, we have provided plots of theoretical results showing the variations of the emitter saturation current density in N^+- and P^+-emitters as the emitter design parameters vary. These results are used to study the parametric dependence of V_{OC} in N^+P and P^+N silicon solar cells on design parameters in Chapter VII. The results in this appendix can also be used to characterize the emitter injection efficiency of silicon bipolar transistors once the base current is determined.

APPENDIX F

ON THE PARABOLIC DENSITY OF STATES IN HEAVILY DOPED SILICON

In this dissertation, we assume the rigid-band approximation to be valid. That is, we assume a parabolic density of states' dependence on energy, i.e.,

$$g(E) = C_e E^{1/2} \tag{F.1}$$

where C_e is a constant coefficient, independent of E. In this appendix, we discuss the applications of the parabolic density of states to heavily doped semiconductors.

High impurity concentrations (typically above 10^{19} cm^{-3} in silicon) introduce a large number of "excess" available states for the charge carriers. Most of these states are close to the band edge. This increases the density of states in (F.1), although it may not alter the parabolic nature. In other words, the parabolic density of states may still be a good approximation, as suggested from experimental observations [56-57,72], however C_e may be larger than its value in intrinsic material. If C_e increases with doping, the density of states remains parabolic but the concavity of the parabola describing g(E) increases. Hence, there are more available states than in the pure semiconductor at any energy level in the band. This mechanism tends to reduce the effect of carrier degeneracy as considered in our

treatment. We cannot comment quantitatively on this effect without knowing exactly the actual density of states in heavily doped silicon and fitting them into parabolic density of states with appropriate values for C_e.

In any case, degeneracy of the majority carriers would always have a lower threshold in the P^+-emitter compared to the N^+-emitter. Further investigation of the parabolic approximation for the actual density of states is suggested for future research.

REFERENCES

[1] F. A. Lindholm, A. Neugroschel, C. T. Sah, M. P. Godlewski, and H. W. Brandhorst, Jr., "A Methodology for Experimentally Based Determination of Gap Shrinkage and Effective Lifetimes in the Emitter and Base of p-n-Junction Solar Cells and Other p-n-Junction Devices," IEEE Trans. Electron Devices, ED-24, 402-410 (1977).

[2] A. Neugroschel, F. A. Lindholm, and C. T. Sah, "A Method for Determining the Emitter and Base Lifetimes in p-n Junction Diodes," IEEE Trans. Electron Devices, ED-24, 662-671 (1977).

[3] H. W. Brandhorst, Jr., Record of 9th Photovoltaic Specialists Conf., 1 (1972).

[4] W. L. Kauffman and A. A. Bergh, "The Temperature Dependence of Ideal Gain in Double Diffused Silicon Transistors," IEEE Trans. Electron Devices, ED-15, 732-735 (1968).

[5] D. Buhanan, "Investigation of Current-Gain Temperature Dependence in Silicon Transistors," IEEE Trans. Electron Devices, ED-16, 117-124 (1969).

[6] E. O. Johnson and A. Rose, "Simple General Analysis of Amplifier Devices with Emitter, Control, and Collector Functions," Proc. IRE, 47, 407-418 (1959).

[7] R. D. Middlebrook, "A Modern Approach to Semiconductor and Vacuum Device Thoery," IEE Proc., 106B, Suppl. 17, 887-902 (1960).

[8] H. K. Gummel and H. C. Poon, "An Integral Charge Control Model of Bipolar Transistors," Bell System Techn. J., 49, 827-852 (1969).

[9] F. A. Lindholm, S. S. Li, and C. T. Sah, "Fundamental Limitations Imposed by High Doping on the Performance of PN Junction Silicon Solar Cells," Record of the 11th Photovoltaic Specialists Conf., 3-12, 1975.

[10] J. G. Fossum, R. D. Nasby, and S. C. Pao, "Physics Underlying the Performance of Back-Surface-Field Solar Cells," accepted for publication in IEEE Trans. Electron Devices, April 1980.

[11] W. Shockley, "The Theory of p-n Junctions in Semiconductors and p-n Junction Transistors," Bell System Tech. J., 28, 435-489 (1949).

[12] J. R. Hauser, Final Report on NSF Grant GK-1615 (1969).

[13] H. P. D. Lanyon and R. A. Tuft, "Bandgap Narrowing in Moderately to Heavily Doped Silicon," IEEE Trans. Electron Devices, ED-26, 1014-1018 (1979)

[14] D. D. Kleppinger and F. A. Lindholm, "Impurity Concentration Dependent Density of States and Resulting Fermi Level for Silicon," Solid State Electronics, 14, 407-416 (1971).

[15] V. L. Bonch-Bruyevich, The Electronic Theory of Heavily Doped Semiconductors, American Elsevier, Inc., New York, 1966.

[16] R. J. Van Overstraeten, H. J. DeMan, and R. P. Mertens, "Transport Equations in Heavily Doped Silicon," IEEE Trans. Electron Devices, ED-20, 290-298 (1972).

[17] M. S. Mock, "Transport Equations in Heavily Doped Silicon and the Current Gain of a Bipolar Transistor," Solid State Electronics, 16, 1251-1259 (1973).

[18] R. B. Fair, "The Effect of Strain-Induced Band-Gap Narrowing on High Concentration Phosphorus Diffusion in Silicon," J. Appl. Phys., 50, 860-868 (1979).

[19] F. A. Lindholm and C. T. Sah, "Fundamental Electronic Mechanisms Limiting the Performance of Solar Cells," IEEE Trans. Electron Devices, ED-24, 299-304 (1977).

[20] J. W. Slotboom and H. C. DeGraaff, "Measurement of Bandgap Narrowing in Silicon Bipolar Transistors," Solid State Electronics, 19, 857-862 (1976).

[21] H. P. D. Lanyon, A. K. McCurdy, and R. A. Tuft, "Infrared Photoresponse of Silicon Devices at 1.15 Microns," Record of 13th IEEE Photovoltaic Specialists Conf., 60-63 (1978).

[22] A. Neugroschel, P. J. Chen, S. C. Pao, and F. A. Lindholm, "Forward-Bias Capacitance and Current Measurements for Determining Lifetimes and Band Narrowing in p-n Junction Solar Cells," Record of 13th Photovoltaic Specialists Conf., 70-75, 1978.

[23] J. Van Meerbergn, J. Nijs, R. Mertens, and R. Van Overstraeten, "Measurement of Bandgap Narrowing and Diffusion Length in Heavily Doped Silicon," Record of 13th Photovoltaic Specialist Conf., 66-69 (1978).

[24] M. A. Shibib, F. A. Lindholm, and F. Therez, "Heavily Doped Transparent-Emitter Regions in Junction Solar Cells, Diodes, and Transistors," IEEE Trans. Electron Devices, ED-26, 959-965 (1979).

[25] E. L. Heasell, "The Emitter Efficiency of Silicon Bipolar Transistors--An Unperterbed Band Model," IEEE Trans. Electror Devices, ED-26, 919-923 (1979).

[26] J. S. Blakemore, Semiconductor Statistics, Pergamon Press, New York, 1962.

[27] W. Shockley and W. T. Read, "Statistics of the Recombination of Holes and Electrons," Phys. Rev., 87, 835 (1952).

[28] R. N. Hall, "Electron-Hole Recombination in Germanium," Phys. Rev., 87, 387 (1952).

[29] J. G. Fossum, F. A. Lindholm, and M. A. Shibib, "The Importance of Surface Recombination and Energy-Bandgap Narrowing in p-n-Junction Silicon Solar Cells," IEEE Trans. Electron Devices, ED-26, 1294-1298 (1979).

[30] D. Redfield, "Mechanism of Performance Limitations in Heavily Doped Silicon Devices," Appl. Phys. Lett., 33, 531-533 (1978).

[31] H. W. Brandhorst, Jr., "Current Status of Silicon Solar Cell Technology," Tech. Dig. IEDM, 331-334 (1975).

[32] P. M. Dunbar and J. R. Hauser, "Theoretical Effects of Surface Diffused Region Lifetime Models on Silicon Solar Cells," Solid-State Electronics, 20, 697-701 (1977).

[33] E. J. McGrath and D. H. Navon, "Factors Limiting Current Gain in Power Transistors," IEEE Trans. Electron Devices, ED-24, 1255-1259 (1977).

[34] P. Lauwers, J. Van Meerbergen, P. Sulteel, R. Mertens, and R. Van Overstraeten, "Influence of Bandgap Narrowing on the Performance of Silicon n-p Solar Cells," Solid-State Electronics, 21, 747-752 (1978).

[35] M. S. Adler, "Achieveing Accuracy in Transistor and Thyristor Modeling," Invited Paper, Tech. Dig. IEDM, 550-554, 1978.

[36] J. Dziewior and W. Schmid, "Auger in Coefficient for Highly Doped and Highly Excited Silicon," Appl. Phys. Lett., 31, 346-348 (1977).

[37] W. W. Sheng, "The Effect of Auger Recombination on the Emitter Injection Efficiency of Bipolar Transistors," IEEE Trans. Electron Devices, ED-22, 25-27 (1975).

[38] H. T. Weaver and R. D. Nasby, "Evidence for Bandgap Narrowing Effects in Silicon Solar Cell Performance," Tech. Dig. IEDM, 693 1979.

[39] C. T. Sah and C. T. Wang, "Experiments on the Origin of Process Induced Recombination Centers in Silicon," J. Appl. Phys., 46, 1767-1776 (1975).

[40] J. Lindmayer and J. F. Allison, "The Violet Cell: An Improved Silicon Solar Cell," COMSAT Tech. Rev., 3, 1-22 (1973).

[41] M. Klein, "The Injection Efficiency in Double Diffused Transistors," Proc. IRE, 49, 1708 (1961).

[42] D. P. Kennedy and P. C. Murley, "Minority Carrier Injection Characteristics of the Diffused Emitter Junction," IRE Trans. Electron Devices, ED-9, 136-142 (1962).

[43] J. G. Fossum, "Computer-Aided Numerical Analysis of Silicon Solar Cells," Solid-State Electronics, 19, 269-277 (1976).

[44] E. L. Heasell, "Injection Efficiency in Bipolar Devices," Tech. Dig. IEDM, 310-311 (1978).

[45] R. S. Popovic, "On the Apparent Narrowing of the Bandgap in the Base Region of Bipolar Transistors," Solid-State Electronics, 22, 248-349 (1979).

[46] K. Seeger, Semiconductor Physics, Springer-Verlag, New York, 1973.

[47] G. L. Pearson and J. Bardeen, "Electrical Properties of Pure Silicon and Silicon Alloys Containing Boron and Phosphorous," Phys. Rev., 75, 865 (1949).

[48] N. A. Penin, B. G. Zhurkin, and B. A. Volkov, "Influence of Concentration of Donors and Acceptors on the Electrical Conductivity of Heavily Doped n-Type Silicon," Sov. Phys.--Solid State, 7, 2580 (1965-66).

[49] W. R. Thurber, "Ionization of Dopant Density in Silicon," p. 13 in NBS Special Publication 400-19, January 1 to June 30, 1975.

[50] A. A. Vol'fson and V. K. Subashiev, "Fundamental Absorption Edge of Silicon Heavily Doped with Donor or Acceptor Impurities," Sov. Phys.--Semiconductors, 1, 327 (1967).

[51] G. A. Swartz, "Low-Temperature Hall Coefficient and Conductivity in Heavily Doped Silicon," J. Phys. Chem. Solids, 12, 245 (1960).

[52] P. W. Chapman, O. N. Tufte, J. D. Zook and D. Long, "Electrical Properties of Heavily Doped Silicon," J. Appl. Phys., 34, 3291 (1963).

[53] I. Granacher and W. Czaja, "Mobility and Electron Spin Resonance Linewidth in Phosphorous Doped Silicon," J. Phys. Chem. Solids, 28, 231-238 (1967).

[54] C. Yamanouchi, K. Mizuguchi, and W. Sasuki, "Electric Conduction in Phosphorous Doped Silicon at Low Temperatures," J. Phys. Soc. Japan, 22, 859 (1967).

[55] F. Mousty, P. Ostoja, and L. Passari, "Relationship between Resistivity and Phosphorous Concentration in Silicon," J. Appl. Phys., 45, 4576 (1974).

[56] N. Kobayashi, S. Ikehata, S. Kobayashi, and W. Sasaki, "Specific Heat Study of Heavily P Doped Si," Solid-State Commun., 24, 67 (1977).

[57] R. K. Sundfors and D. F. Holcomb, "Nuclear Magnetic Resonance Studies of the Metallic Transitions in Doped Silicon," Phys. Rev., 136, A810-820 (1964).

[58] M. N. Alexander and D. F. Holcomb, "Semiconductor-to-Metal Transition in n-type Group IV Semiconductors," Rev. Mod. Phys., 40, 815 (1968).

[59] C. Kittel, Introduction to Solid State Physics, 4th ed., John Wiley and Sons, Inc., New York, 1971.

[60] L. I. Rosier, "Surface States and Surface Recombination Velocity Characteristics of Si-SiO_2 Interfaces," IEEE Trans. Electron Devices, ED-13, 260-268 (1966).

[61] C. T. Sah and F. A. Lindholm, "Carrier Generation, Recombination, Trapping, and Transport in Semiconductors with Position-Dependent Composition," IEEE Trans. Electron Devices, ED-24, 253-362 (1977).

[62] P. M. Dunbar and J. R. Hauser, "A Study of Efficiency in Low Resistivity Silicon Solar Cells," Solid-State Electronics, 19, 95-102 (1976).

[63] J. R. Hauser and P. M. Dunbar, "Performance Limitations of Silicon Solar Cells," IEEE Trans. Electron Devices, ED-24, 305-321 (1977).

[64] F. A. Lindholm, A. Neugroshel, S. C. Pao, J. G. Fossum, and C. T. Sah, "Design Considerations for Silicon HLE Solar Cells," Record of the 13th Photovoltaic Specialists Conf., 1300-1305 (1978).

[65] A. Neugroshel, F. A. Lindholm, S. C. Pao, and J. G. Fossum, "Emitter Current Suppression in a High-Low-Junction Emitter Solar Cell Using an Oxide-Charge Induced Electron Accumulation Layer," Appl. Phys. Lett., 33, 168-170 (1978).

[66] P. A. Iles and S. I. Soclof, "Effect of Impurity Doping Concentration on Solar Cell Output," Record of 11th Photovoltaic Specialists Conf., 19-24 (1975).

[67] M. Wolf, "The Silicon Solar Cell Design Handbook," Record of the 9th Photovoltaic Specialists Conf., 53-60 (1972).

[68] J. G. Fossum and E. L. Burgess, "High-Efficiency p^+nn^+ Back-Surface-Field Silicon Solar Cells," Appl. Phys. Lett., 33, 238-240 (1978).

[69] J. G. Fossum, R. D. Nasby, and E. L. Burgess, "Development of High-Efficiency p^+nn^+ Back-Surface-Field Silicon Solar Cells," Record of the 13th Photovoltaic Specialists Conf., 1294-1299 (1978).

[70] S. S. Li and F. A. Lindholm, "Alternative Formulation of Generalized Einstein Relation for Degenerate Semiconductors," Proc. IEEE, 56, 1256-1257 (1968).

[71] I. V. Grekhov, N. N. Korobkov, and A. E. Otblesk, "Injection Efficiency of p-n Junctions in Silicon," Sov. Phys.--Semiconductors, 9, 493-494 (1975).

[72] K. P. Abdurakhmanov, Sh. Mirakhmedov, and A. T. Teshabaev, "Characteristics of the Distribution of the Density of States in Heavily Doped Silicon," Sov. Phys.--Semiconductors, 12, 457-459 (1978).

[73] T. N. Morgan, "Broadening of Impurity Bands in Heavily Doped Semiconductors," Phys. Rev., 139, A343-348 (1965).

[74] H. K. Gummel, "A Self-Consistent Iterative Scheme for One-Dimensional Steady State Transistor Calculations," IEEE Trans. Electron Devices, ED-24, 299-305 (1977).

[75] B. V. Gokhale, "Numerical Solutions for a One-Dimensional Silicon n-p-n Transistor," IEEE Trans. Electron Devices, ED-17, 594-602 (1970).

[76] G. D. Hachtel, R. C. Joy, and J. W. Cooley, "A New Efficient One-Dimensional Analysis Program for Junction Device Modeling," Proc. IEEE, 60, 86-98 (1972).

[77] J. W. Slotboom, "Computer Aided Two-Dimensional Analysis of Bipolar Transistors," IEEE Trans. Electron Devices, ED-20, 669-679 (1973).

[78] H. H. Heimeier, "A Two-Dimensional Numerical Analysis of Silicon n-p-n Transistor," IEEE Trans. Electron Devices, ED-20, 708-174 (1974).

[79] O. Manck and M. L. Engl, "Two-Dimensional Computer Simulation for Switching a Bipolar Transistor Out of Saturation," IEEE Trans. Electron Devices, ED-22, 339-347 (1975).

[80] A. Chryssafis and W. Love, "A Computer-Aided Analysis of One-Dimensional Thermal Transients in n-p-n Power Transistors," Solid-State Electronics, 22, 249-256 (1979).

[81] S. P. Gaur, "Performance Limitations of Silicon Bipolar Transistors," IEEE Trans. Electron Devices, ED-26, 415-421 (1979).

[82] A. Phillips, Jr., "Calculations of the Effect of Emitter Compensation on β and f_T of Bipolar Devices," IBM J. Res. Develop., 22, 687-689 (1971).

[83] H. J. DeMan, "The Influence of Heavy Doping on the Emitter Efficiency of a Bipolar Transistor," IEEE Trans. Electron Devices, ED-18, 833-835 (1971).

[84] B. L. H. Wilson, "The Emitter Efficiency of Silicon Transistors," Solid-State Electronics, 20, 71-74 (1977).

[85] E. O. Kane, "Thomas-Fermi Approach to Impure Semiconductor Band Structure," Phys. Rev., 131, 79-88 (1963).

[86] P. A. Wolff, "Theory of Band Structure of Very Degenerate Semiconductors," Phys. Rev., 126, 405-412 (1962).

[87] F. A. Lindholm and R. W. Ayers, "Generalized Einstein Relation for Degenerate Semiconductors," Proc. IEEE, 56, 371-372 (1968).

[88] O. Madelung, Handbuch der Physik, 20, Springer, Berlin, 1957.

[89] J. McDougall and E. C. Stoner, "The Computation of Fermi-Dirac Functions," Phil. Trans., A 237, 67-104 (1938).

[90] W. Ehrenberg, "The Electric Conductivity of Simple Semiconductor," Proc. Phys. Soc., A 63, 75-76 (1950).

[91] P. T. Landsberg, R. W. MacKay and A. D. McRonald, "The Parameters of Simple Excess-Semiconductors," Proc. Phys. Soc., A 476-480 (1950).

[92] R. B. Dingle, "The Fermi-Dirac Integrals," Appl. Sci. Res., 36, 225-239 (1955-57).

[93] R. E. Battocletti, "Polynomial Approximation of Fermi Integrals," Proc. IEEE, 53, 2162-2163 (1965).

[94] E. L. Jones, "Rational Chebyshev Approximation of the Fermi-Dirac Integrals," Proc. IEEE, 4, 708-709 (1966).

[95] W. B. Joyce and R. W. Dixon, "Analytic Approximation for the Fermi Energy of an Ideal Fermi Gas," Appl. Phys. Lett., 31, 354-356 (1977).

[96] N. G. Nilsson, "Empirical Approximations for the Fermi Energy in a Semiconductor with Parabolic Bands," Appl. Phys. Lett., 33, 653-654 (1978).

BIOGRAPHICAL SKETCH

Muhammed Ayman Shibib was born in Damascus, Syria, on February 14, 1953. He completed an advanced high school degree in mathematics and physics at the International College, Beirut, Lebanon, and graduated in June 1972 with high distinction. In June 1975, he received the B.S. degree from the American University of Beirut, Beirut, Lebanon. His major field was in physics, and he was on the American University of Beirut Dean's Honor List. He started graduate studies in electrical engineering at the University of Florida in September 1975, and he graduated in December 1976 with an M.S. and in December 1979 with a Ph.D.

His master's research involved computer-aided analysis of Integrated Injection Logic (I^2L). Since 1976, he has been a graduate research assistant and a graduate research associate.

His research interests are in solar cells, semiconductor and solid-state physics, and semiconductor device modeling.

He is a member of IEEE, the American Physical Society, and the Society of Physics Students.

I certify that I have read this study and that in my opinion it conforms to acceptable standards of scholarly presentation and is fully adequate, in scope and quality, as a dissertation for the degree of Doctor of Philosophy.

Fredrik A. Lindholm, Chairman
Professor of Electrical Engineering

I certify that I have read this study and that in my opinion it conforms to acceptable standards of scholarly presentation and is fully adequate, in scope and quality, as a dissertation for the degree of Doctor of Philosophy.

Jerry G. Fossum, Co-Chairman
Associate Professor of Electrical Engineering

I certify that I have read this study and that in my opinion it conforms to acceptable standards of scholarly presentation and is fully adequate, in scope and quality, as a dissertation for the degree of Doctor of Philosophy.

Arnost Neugroschel
Associate Professor of Electrical Engineering

I certify that I have read this study and that in my opinion it conforms to acceptable standards of scholarly presentation and is fully adequate, in scope and quality, as a dissertation for the degree of Doctor of Philosophy.

Sheng S. Li
Professor of Electrical Engineering

I certify that I have read this study and that in my opinion it conforms to acceptable standards of scholarly presentation and is fully adequate, in scope and quality, as a dissertation for the degree of Doctor of Philosophy.

Charles F. Hooper, Jr.
Professor of Physics

This dissertation was submitted to the Graduate Faculty of the College of Engineering and to the Graduate Council, and was accepted as partial fulfillment of the requirements for the degree of Doctor of Philosophy.

December 1979

L. William Kostiuk
Dean, College of Engineering

Dean, Graduate School